Contents

List of Figures

List of Tables

Abstract

The fixed spectrum regulation policy has been considered as the cause leading to the conflict between the growing demands for spectrum and the inefficient frequency utilization. The Cognitive Radio (CR), as an innovative communication technology, can hopefully improve the utilization efficiency of wireless spectrum in an intelligent and flexible way.

This dissertation investigates the signal detection schemes from two perspectives, non-cooperative detection and cooperative detection, with the goal of solving several problems in spectrum sensing that is the key issue in CR.

Chapter 1 introduces the background of CR and the motivation of the research.

In Chapter 2, the author proposes a low-complexity cyclostationarity feature detection scheme for detect and avoid (DAA) of Ultra-Wideband (UWB) system in order to solve the coexistence issues between UWB system and Long Term Evolution-Advanced (LTE-Advanced) system which can be considered as a practical model of CR. The localized Single-carrier Frequency Division Multiple Access (SC-FDMA) signal utilized in the uplink of LTE-Advanced system is utilized to be detected.

In Chapter 3, a dual-stage detection scheme composed of coarse detection stage and refined detection stage has been proposed. The threshold factor for the probability of indefinite detection is firstly proposed and defined to combine the two stages. The proposed scheme focuses on the integration of two different detection schemes with different complexities in order to reduce total computational complexity. The computer simulation results show that the proposed scheme can make a trade-off between the detection performance and the computational complexity

by setting the probability of indefinite detection.

In Chapter 4, the author discusses the cooperative signal detection problem from a finite Random Matrix Theoretical (RMT) perspective. Specifically, the author employs recently-derived closed-form and exact expressions for the distribution of the Standard Condition Number (SCN) of uncorrelated and semi-correlated random dual central Wishart matrices of finite sizes in the design Hypothesis-Testing algorithms to detect the primary signal.

In particular, two algorithms are designed, with basis on the SCN distribution in the absence and in the presence of primary signal, respectively. It is also shown that the proposed finite RMT-based algorithms outperform all similar alternatives currently known in the literature, at a substantially lower complexity. Several new results on the distributions of eigenvalues and SCNs of random Wishart Matrices are also offered.

Chapter 5 summarizes the results of each chapter and concludes this dissertation.

Chapter 1

General Introduction

In this chapter, Cognitive Radio (CR), being considered as an innovative communication technology to hopefully improve the utilization efficiency of wireless spectrum in an intelligent and flexible way, is described, followed by the introductions of varied conventional signal detection schemes in CR. The system models are described and a specific and practical coexistence model between Ultra-Wideband (UWB) system and International Mobile Telecommunications-Advanced (IMT-Advanced) system is also included to illustrate the non-cooperative signal detection schemes. The motivation of the research and the relation of the associated research are finally presented.

1.1 Cognitive Radio

1.1.1 Background

The fixed frequency assignment policy issued by the by national regulatory bodies like the Federal Communications Commission (FCC) is said to bring the current conflict between the scarcity of spectrum and the inefficient spectrum utilization. There is a large portion of the assigned spectrum, which is sporadically utilized [1, 2].

The growing demands for spectrum due to the rapid development of wireless devices and applications have made the useful frequency to be very rare sources. However, the fact of the current utilization of such rare resource is that the Primary Users (PUs) who are assigned fixed frequency do not use efficiently the exclusive spectrum and the Secondary Users (SUs) who have no spectrum licenses have no

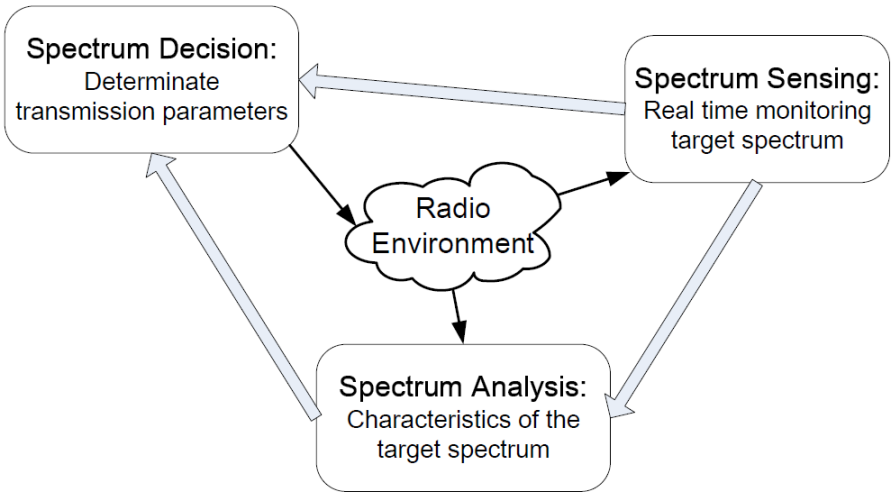

Figure 1.1: Cognitive Radio framework.

rights to access such spectrum.

Based on the current spectrum utilization situation, a new technology named Cognitive Radio [3], has been considered to improve the efficiency of the spectrum usage.

1.1.2 Cognitive Radio Definition and Framework

Cognitive radio is defined as an intelligent wireless communication system that is aware of its environment and uses the methodology of understanding-by-building to learn from the environment and adapt to statistical variations in the input stimuli, with two primary objectives in mind [4]:

- highly reliable communication whenever and wherever needed,
- efficient utilization of the radio spectrum.

The CR framework is shown in Fig. 1.1 [1, 4]. The main functions in CR are the followings:

I. Spectrum Sensing: Real time monitoring the target spectrum bands, gather their information, and decide the "white" [1] spectrum band,

[1]The notation of "white" means the target spectrum band is not occupied by the Primary Users and can be utilized by the Secondary Users

II. Spectrum Analysis: Rapidly decide the characteristics of the gathered "white" spectrum,

III. Spectrum Decision: Determinate the transmission parameters according to the spectrum characteristics and the user requeirements.

The primary and key function in CR is spectrum sensing, which is mainly implemented by the detection of the PUs' signal. Therefore, the so-called spectrum sensing can be equivalently considered as the signal detection. In this thesis, the notation of spectrum sensing will thereafter be replaced by the notation of signal detection.

1.1.3 Current Developments of Cognitive Radio

With the rapid development of cognitive radio technology, there are some standard organizations or research forums such as IEEE DYSPAN Standards Committee (Formerly IEEE Standards Coordinating Committee 41) [5], IEEE 802.22 the Working Group on Wireless Regional Area Networks [6], and Software Defined Radio (SDR) forum [7] to accelerate such developments.

IEEE DYSPAN Standards Committee, formerly IEEE Standards Coordinating Committee 41 (SCC41), is seeking proposals for standards projects in the areas of dynamic spectrum access, cognitive radio, interference management, coordination of wireless systems, advanced spectrum management, and policy languages for next generation radio systems [5].

The IEEE P1900 Standards Committee was founded in 2005 jointly by the IEEE Communications Society (ComSoc) and the IEEE Electromagnetic Compatibility (EMC) Society. It aims to develop supporting standards dealing with new technologies and techniques being developed for next generation radio and advanced spectrum management. The work of the IEEE 1900.x Working Groups continues under SCC41.

There are main 6 parts of IEEE 1900.x, from IEEE 1900.1 to IEEE 1900.6, in which IEEE 1900.6 is working on Spectrum Sensing Interfaces and Data Structures for Dynamic Spectrum Access and other Advanced Radio Communication Systems [5].

IEEE 802.22 is a standard for Wireless Regional Area Network (WRAN) using white spaces in the TV frequency spectrum [6]. The development of the IEEE

802.22 WRAN standard is aimed at using cognitive radio techniques to allow sharing of geographically unused spectrum allocated to the Television Broadcast Service, on a non-interfering basis, to bring broadband access to hard-to-reach, low population density areas, typical of rural environments, and is therefore timely and has the potential for a wide applicability worldwide. It is the first worldwide effort to define a standardized air interface based on CR techniques for the opportunistic use of TV television bands on a non-interfering basis [6].

IEEE 802.22 WRANs are designed to operate in the TV broadcast bands while assuring that no harmful interference is caused to the incumbent operation, i.e., digital TV and analog TV broadcasting, and low power licensed devices such as wireless microphones. This standard is supposed to work in the United States, however, the feature remains under investigation as mandatory in other parts of the world including Europe, Japan and China.

The SDR Forum, established in 1996, is now the Wireless Innovation Forum, which is a non-profit mutual benefit corporation dedicated to driving technology innovation in commercial, civil, and defense communications worldwide. Members bring a broad base of experience in Software Defined Radio (SDR), Cognitive Radio (CR) and Dynamic Spectrum Access (DSA) technologies in diverse markets and at all levels of the wireless value chain to address emerging wireless communications requirements [7].

The above mentioned standard committees or research organization have issued plenty of standards or technique reports based on a mass of research papers to stimulate the development of cognitive radio. Within such technique articles and research papers, the spectrum sensing issues take a large portion since such issue is the key point in cognitive radio.

The signal detection is the main tool to implement spectrum sensing function. Therefore, this dissertation mainly discusses signal detection problems.

1.1.4 Detect and Avoid Mechanism

The coexistence model between the Ultra-Wideband system and the IMT-Advanced system can be deemed as a practical cognitive radio prototype, in which the UWB system works as the secondary user system and the IMT-Advanced system works as the primary user system. The UWB system takes a "Spectrum Underlay" way to access the licenced spectrum [8] and a detect and avoid mechanism to peacefully

operate with the spectrum holder such as the IMT-Advanced system and avoid the harmful interference [9, 10].

In DAA, there are two types of detection operations, initial detection and continuous detection [9]. The initial detection is used to sense the victim signal of the target frequency band initially, and the continuous detection is utilized to monitor regularly the target band. In the continuous detection operation, the signal level of the victim system is sensed continuously [9].

There are some standard committees such as IEEE 802.19 Wireless Coexistence Working Group (WG) [11] and the European Computer Manufacturers Association (ECMA) [12] are working on the coexistence issues in the UWB system.

In order to avoid the harmful interference to the IMT-Advanced system, the primary task of the UWB system is to detect the primary user signal. The IMT-Advanced system, which will be implemented and occupy 3.4∼3.6GHz band in the near future [9, 10, 13]. The 3rd Generation Partnership Project (3GPP) LTE-Advanced system can fully reach or even surpass the requirements on IMT-Advanced system within the ITU-R time plan [14, 15]. Therefore, the Long Term Evolution-Advanced (LTE-Advanced) system is supposed to be the victim system for the UWB system and the coexistence issues between these two systems should be investigated.

The LTE-Advanced transmission included the downlink and the uplink should be detected and protected by the UWB system with the DAA mechanism. In 3.4∼3.6GHz band, the LTE-Advanced system takes the Time Division Duplex (TDD) mode for the downlink and the uplink [16]. In this case, detecting the uplink is adequate since the downlink also uses the same band. On the other hand, detecting the uplink is relatively easier than detecting the downlink since the UWB device is closer to the User Equipment (UE) than to the Base Station (BS) [17].

The Single-carrier Frequency Division Multiple Access (SC-FDMA) system has been selected as the uplink of LTE-Advanced system. The 3GPP standards such as [16, 18–21] describe SC-FDMA uplink system from different views.

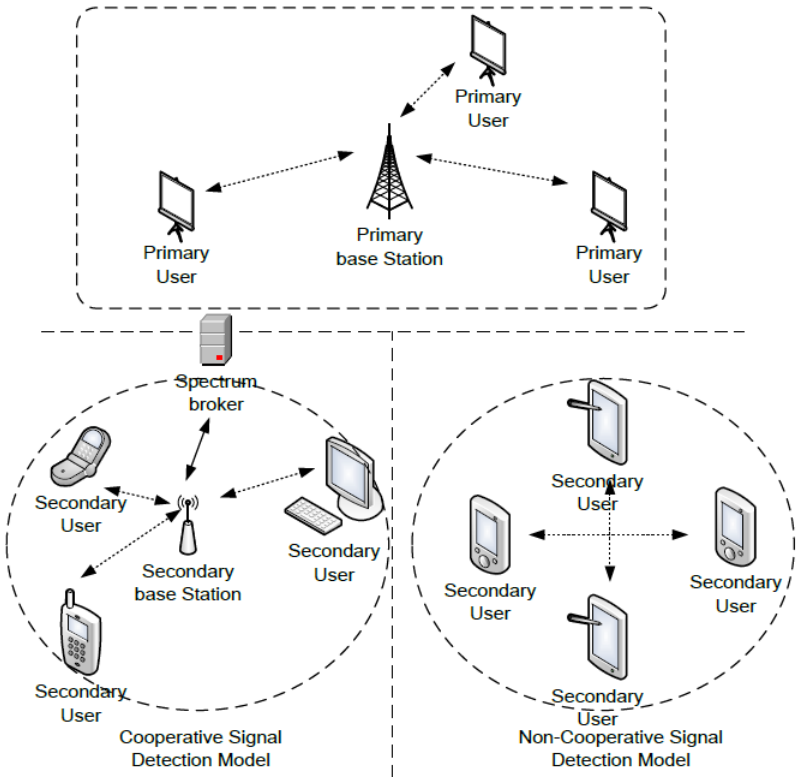

Figure 1.2: Cognitive Radio system model.

1.2 Signal Detection Schemes

1.2.1 System Models

Figure 1.2 indicates the CR system model, which includes the primary system, the non-cooperative secondary system and the cooperative secondary system [5]. In the non-cooperative mode, SUs monitor the target frequency band assigned to PUs and take communications using such spectrum. There are no secondary base station and spectrum broker in this mode. SUs operating in the cooperative mode receive the information of "white" spectrum from the secondary base station. The detectors fitted in SUs also detect PU signal and transfer individual detection result to the secondary base station. The spectrum broker gathers and transfers the information of the target frequency band.

The non-cooperative detection means that there is no cooperation between the distributed detectors or there is not the fusion center to deal with detection information from individual detector. The main detection schemes in non-cooperative detection such as energy detection and cyclostationarity feature detection are dis-

cussed.

In order to improve the detection performance, many researchers have proposed cooperative detection scheme, in which a fusion center is used to gather detection information from distributed detectors. Of course, the non-cooperative detection method can also be used by the distributed detector in the cooperative detection system. However, the limitations of individual detection scheme still affect detection performance of the cooperative detection scheme.

1.2.2 Non-cooperative Signal Detection Schemes

1.2.2.1 SC-FDMA Uplink System

SC-FDMA uplink system has been described in [20, 22]. Figure 1.3 presents the structures of the UE transmitter and the Base Station (BS) receiver. The M input symbols $s[m](m = 0, ..., M-1)$ are transformed into frequency domain $S[l]$

$$S[l] = \sum_{m=0}^{M-1} s[m] \cdot \exp(-j\frac{2\pi ml}{M}), l = 0, ..., M-1. \tag{1.1}$$

Each of the DFT outputs $\mathbf{S} = [S[0], ..., S[M-1]]^T$ is then mapped to one of the N orthogonal subcarriers. The localized mapping way is supported by 3GPP [20,21]. The localized mapping way can be defined as

$$X[k] = \begin{cases} S[l], & k = D + N_{\text{Sub}} \cdot \Delta(\lfloor l/N_{\text{Sub}} \rfloor) + l \bmod N_{\text{Sub}} \\ 0, & k = others, \end{cases}$$

where D is band margin and N_{Sub} is the number of the subcarriers per Resource Block (RB). $\lfloor \alpha \rfloor$ indicates the largest interger that does not exceed α. $\Delta(\lfloor l/N_{\text{Sub}} \rfloor)$ is a random integer, which belongs to $[0, N_{\text{RB}} - 1]$ and N_{RB} is the total number of RBs.

A RB distribution example of the localized SC-FDMA signal is shown in Fig. 1.4. The example is based on a practical SC-FDMA uplink system with 10 MHz channel bandwidth (BW) [19,20]. In this figure, the number of subcarriers N, the number of RBs ,N_{RB} and the number of subcarriers in one RB, N_{Sub} are set to be 1024, 50 and 12, respectively. The margin D is $(N - N_{\text{RB}} \cdot N_{\text{Sub}})/2 = 212$. In time domain, the transmission time unit is the time slot, which is 0.5 ms. 7 SC-FDMA symbols make up one time slot. Note that the same slot structure is taken in the

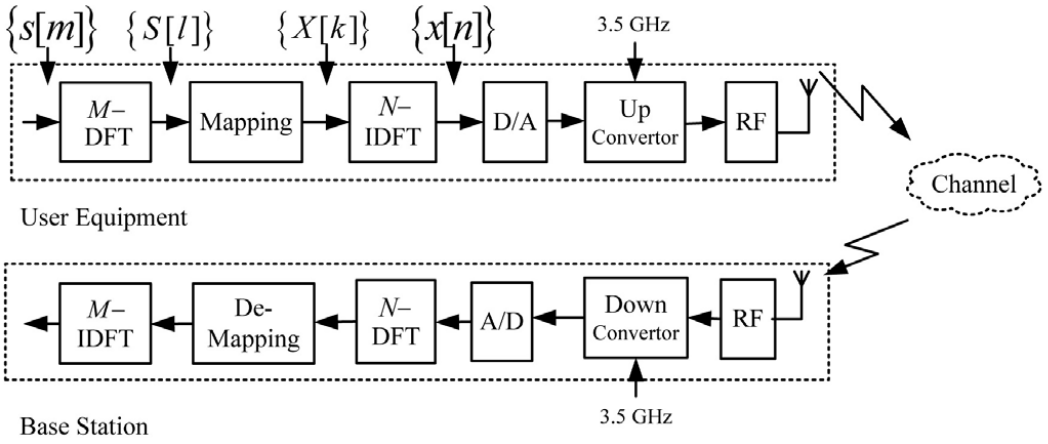

Figure 1.3: SC-FDMA uplink system structure.

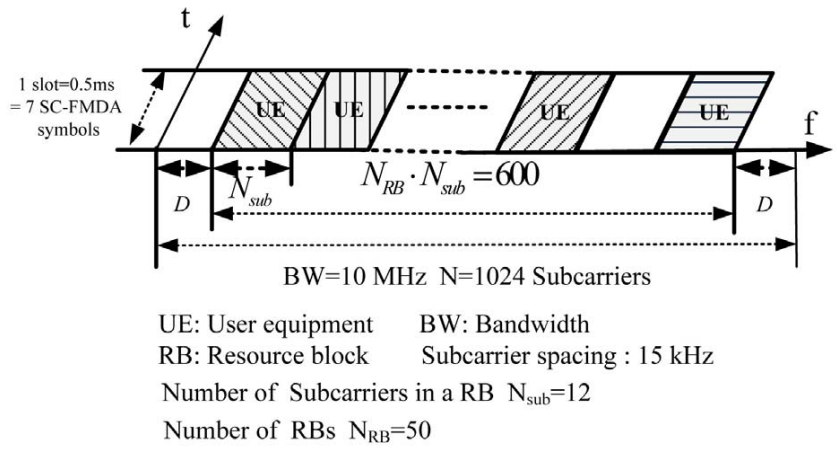

Figure 1.4: SC-FDMA signal distribution in frequency.

FDD mode and the TDD mode [20]. It means that the distribution ways of RBs in the FDD mode and the TDD mode are the same in a specific slot.

The output signal $x[n]$ expressed in time domain is generated by N-point inverse DFT (IDFT).

$$x[n] = \frac{1}{N} \sum_{k=0}^{\mathrm{N}-1} X[k] \cdot \exp(j\frac{2\pi nk}{N}), n = 0, 1, ..., \mathrm{N}-1. \tag{1.2}$$

The receiver does the inverse action of the transmitter to receive the transmitted SC-FDMA signal tainted from a non-ideal channel.

SC-FDMA signal utilizes 180 KHz RB shown in Fig. 1.4, which contains 12 subcarriers with 15 KHz per subcarrier. Compared with the WiMAX signal, it is

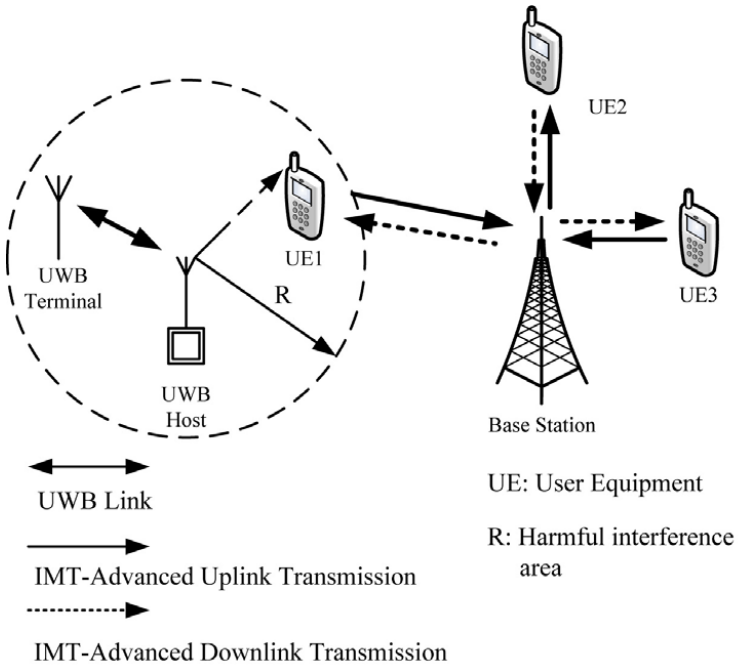

Figure 1.5: A coexistence model between UWB system and IMT-Advanced system.

more difficult for the detector in [17] to detect SC-FDMA signal especially when high detection performance is required. Notice that such a detector can also reuse some components of the UWB receiver.

Both energy detection (ED) and Cyclostationarity Feature Detection (CFD) can be implemented with this detector structure. Note that ED is built in time domain and located after A/D component without the DFT block while CFD is in frequency domain.

1.2.2.2 Non-cooperative Signal Detection Model-A Practical Coexistence Model

The author will illustrate non-cooperative signal detection schemes in a practical coexistence model between a UWB system and an IMT-Advanced system. The UWB system can be regarded as a secondary system and the IMT-Advanced system can be considered as a primary system. DAA is essential for the UWB system to coexist with the IMT-Advanced system, which will be implemented and occupy 3.4∼3.6GHz band in the near future [9, 10, 13]. 3GPP LTE-Advanced system can fully reach or even surpass the requirements on IMT-Advanced system within the ITU-R time plan [14, 15]. Therefore, the LTE-Advanced system is supposed to be

the victim system for the UWB system and the coexistence issues between these two systems should be investigated.

The coexistence issues between the WiMAX system and the UWB system have been discussed in [17]. The detection of the transmitted signal of the victim system is prerequisite for DAA. Comparing with WiMAX signal detection, the minimum bandwidth of the LTE-Advanced signal is narrower and more sophisticated detection scheme is required.

1.2.2.3 Binary Hypothesis Test

In order to detect the SC-FDMA uplink signal, a binary hypothesis test is given as follows,

$$\begin{aligned} \mathcal{H}_0 &: x[m] = w[m], \\ \mathcal{H}_1 &: x[m] = \frac{1}{P}\sum_{p=0}^{P-1} h[p]s[m-p] + w[m], \end{aligned} \tag{1.3}$$

where P is the number of multipath, $x[m]$ and $s[m;p]$ are the m-th samples of the received signal, the transmitted SC-FDMA signal affected by the p-th path fading. Here, $w[m]$ is assumed to be an i.i.d. variate such that $w[m] \sim \mathcal{N}_{\mathbb{C}}(0,1)$ in which $\mathcal{N}_{\mathbb{C}}(0,1)$ denotes the circularly symmetric complex standard normal distribution and the symbol $\sim$ indicates that the variate on the lefthand-side follow the distribution on the righthand-side.

The hypothesis $\mathcal{H}_1$ indicates the presence of the target signal, whereas the hypothesis $\mathcal{H}_0$ reveals that the target frequency band is available. The factor h indicates the impulse response of the channel. For Additive White Gaussian Noise (AWGN) channel, the parameter P is set to 1 and only $h[0]$ is included, denoting the linear time-invariant channel gain. Nevertheless, for multipath fading channel, $h[p]$ is a complex random variable denoting the channel fading on the p-th path. JTC94 Indoor Office B channel is utilized to simulate the multipath Rayleigh fading channel model in the coexistence model [23]. Suppose the AWGN $w[m]$, the transmitted signal $x[m]$ and the parameter $h[p]$ are independent of each other.

1.2.2.4 Hypothesis Test Logic and Detection Parameters

Before the discussion of specific detection schemes, the author should emphasize the importance of cumulative distribution function (CDF) and its derivative prob-

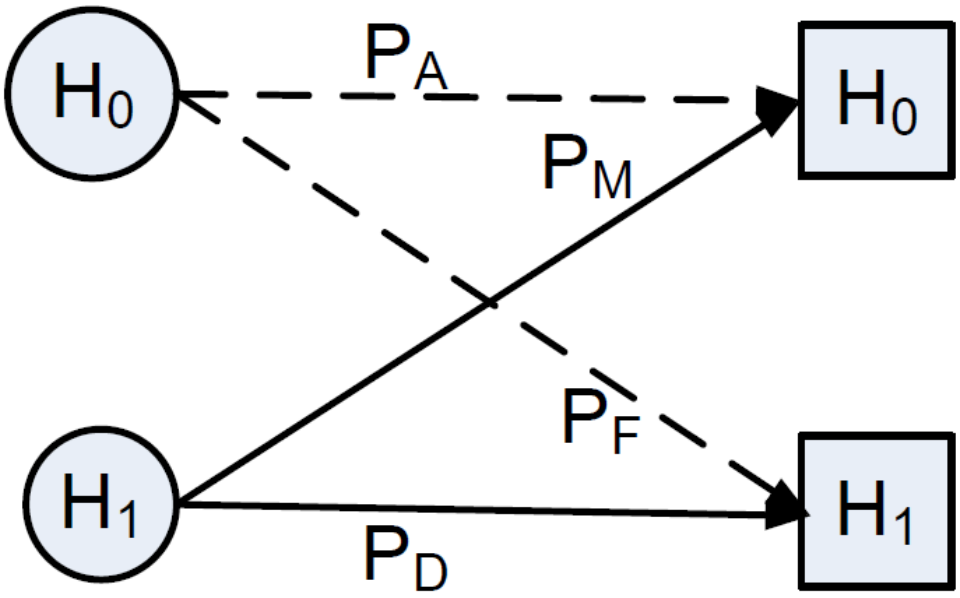

Figure 1.6: Binary hypothesis test sketch.

ability density function (PDF) in the researches of cognitive radio. The author also should make some detection logics be clear and define some statistic parameters.

The signal detection schemes are based on binary hypothesis test simply indicated in Fig. 1.6, in which there are two hypotheses in left circles denoted by $\mathcal{H}_0$ and $\mathcal{H}_1$ and two results in right squares.

In this figure $\mathcal{H}_0$ and $\mathcal{H}_1$ indicate that the absence and presence of the target signal, respectively. P_D is the probability of detection, denoting the probability that the detector detects the target signal when the hypothesis is the presence of such signal. On the contrary, P_M means that the probability that the detector misses the target signal. According to the similar story, P_F is the probability of false alarm and P_A is the probability of acquisition which means the target frequency band is not occupied by the primary users and can be accessed by the secondary systems.

Figure 1.7 indicates the binary test decided by the threshold γ. Functions f_1 and f_0 denote the PDFs of the detector distributions under the conditions of the presence and absence of the target signal, respectively. The threshold γ is decided

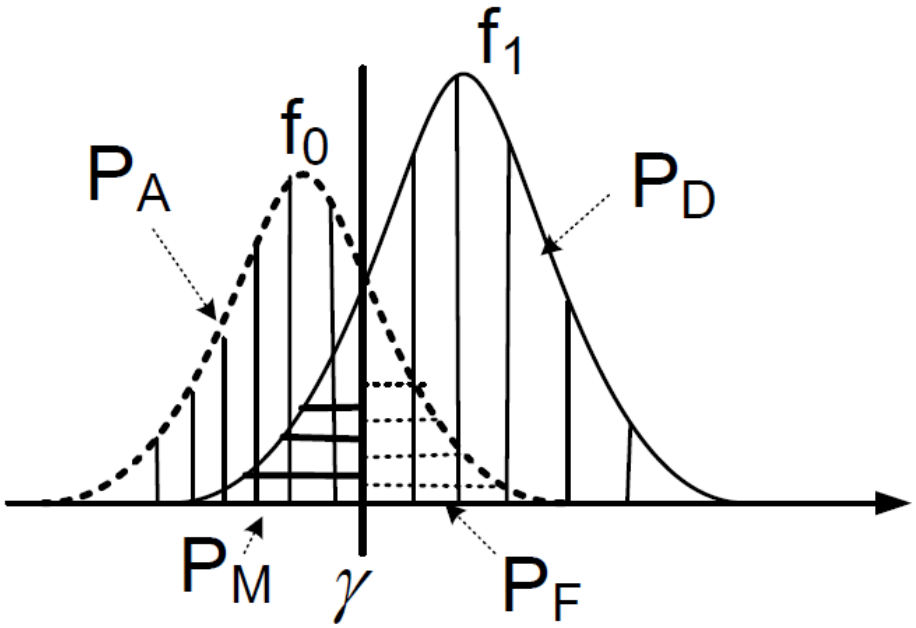

Figure 1.7: Binary hypothesis test and PDFs.

by the required probability of false alarm P_F, which is the small area left side of γ under f_0. It is not difficult to calculate P_D when the PDFs of f_0 and f_1. However, the calculation is not straightforward since the integral operations are required if we want to get those detection results. Therefore the CDFs of the detector under two hypotheses cases are required.

If the CDFs of the detector under two hypotheses are known, the calculations become clear and easy. Figure 1.8 indicates this case. Function F_1 denotes the CDF of the detector when the target signal is present and and F_0 denotes the CDF of the detector when the target signal is absent, respectively. We can directly decide the threshold γ and consequently other parameters.

Therefore the CDF and PDF are very important in the research of signal detection. In this dissertation, the author focuses on the CDF and PDF of several statistic schemes.

1.2.2.5 Energy Detection

An energy detector for N received signal $y[n]$ in time domain is defined as

$$D_{\mathrm{E}} = \sum_{n=0}^{N-1} (|y[n]|)^2. \tag{1.4}$$

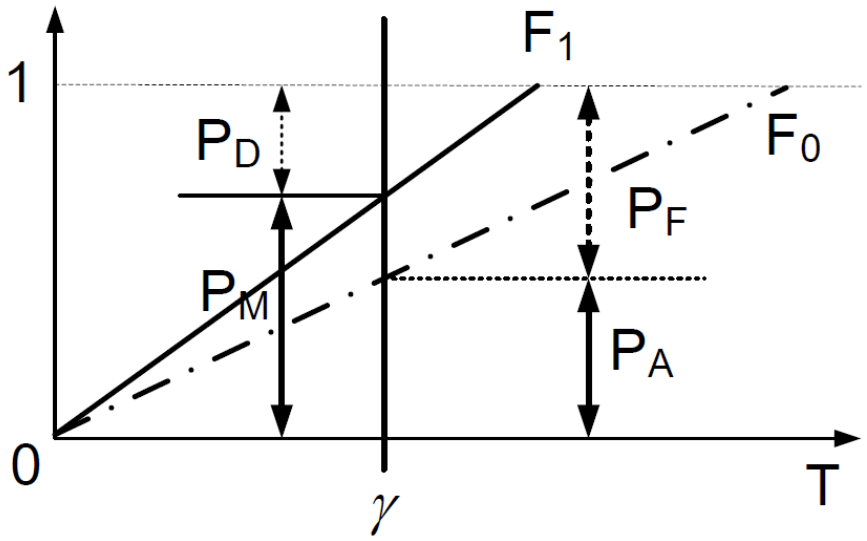

Figure 1.8: Binary hypothesis test and PDFs.

According to the hypotheses test, the test statistic of D_{E} follows a central χ^2-distribution with N degrees of freedom under the hypothesis of $\mathcal{H}_0$. When $\mathcal{H}_1$ is valid, it follows a non-central χ^2-distribution with the same degrees of freedom. Based on the Central Limit Theorem (CLT), the test statistic of D_{E} approximately follows a Gaussian distribution when the number of the samples N is large enough [24, 25]. The test statistic can be approximately described as

$$\begin{aligned} \mathcal{H}_0 \quad &: \quad D_{\mathrm{E}} \sim \mathcal{CN}(N\sigma_w^2, 2N\sigma_w^4) \\ \mathcal{H}_1 \quad &: \quad D_{\mathrm{E}} \sim \mathcal{CN}(N(\eta^2\sigma_x^2 + \sigma_w^2), 2N(\eta^2\sigma_x^2 + \sigma_w^2)^2), \end{aligned} \tag{1.5}$$

where σ_w^2 and σ_x^2 are the variances of the AWGN and the victim signal, respectively. σ_x^2 is also defined as

$$\sigma_x^2 = E[|x[n]|^2], \tag{1.6}$$

where $E[\cdot]$ indicates ensemble average. The channel gain η is defined as

$$\eta = \sum_{p=0}^{P-1} |h[p]|^2. \tag{1.7}$$

Figure 1.9 indicates the PDFs ($p(D_{\mathrm{E}}; \mathcal{H}_0)$, $p(D_{\mathrm{E}}; \mathcal{H}_1)$) of the test statistic of D_{E} under two hypotheses. For a threshold γ, P_{D} of Energy Detection is determined

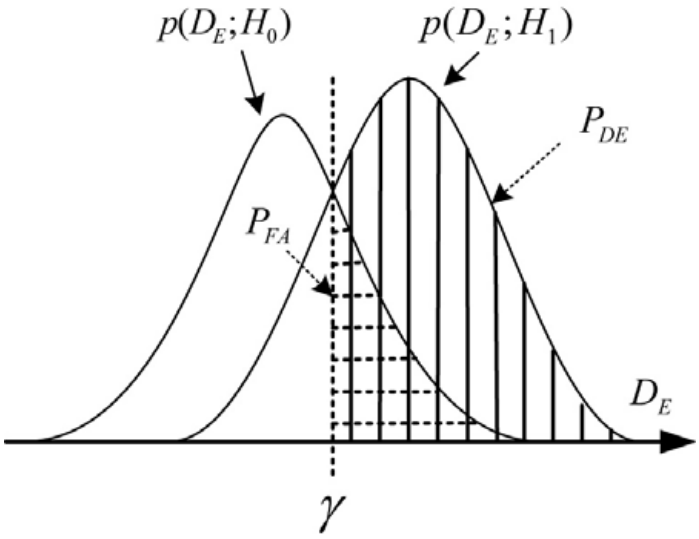

Figure 1.9: Energy detection PDFs.

as

$$P_{\mathrm{D}} = Q\left(\frac{\gamma - N(\eta^2\sigma_x^2 + \sigma_w^2)}{\sqrt{2N(\eta^2\sigma_x^2 + \sigma_w^2)^2}}\right), \tag{1.8}$$

where Q denotes the complementary cumulative distribution function. The probability of false alarm (P_{FA}) is defined as

$$P_{\mathrm{F}} = Q\left(\frac{\gamma - N\sigma_w^2}{\sqrt{2N\sigma_w^4}}\right). \tag{1.9}$$

The ED is simple, but is sensitive to noise uncertainty and is incapable of distinguishing the signal type [26]. On the other hand, it is hard to detect the LTE-Advanced signal or WiMax signal for the energy detector if it occupies only single sub-channel. [17] has indicated that the ED does not reach the required detection performance for the detection of the single sub-channel signal. The cyclostationarity feature detection can overcome those limitations and outperform the energy detection especially in a non-ideal transmission environment, however, it suffers from high computational complexity.

1.2.2.6 Cyclostationarity Feature Detection

The signal cyclostationarity feature is initially discussed and developed by [27–31]. Specially, [28] has illustrated a practical likelihood-ratio detection method with

a BPSK signal based on the regenerated "spectral-line", which is inherently the cyclic-spectrum. [29] developed a statistical χ^2 test for the presence of the cyclo-stationarity feature based on the cyclic-covariances and the cyclic-spectrums. The above references share the same assumption that the cyclic-spectrums are known. However, if the type of PU signal is unclear or the cyclic-spectrums are hard to estimate, the decision of the cyclic-spectrums requires a large number of calculations since the whole occupied spectrums need to be checked. [32] presented so-called "the variability method" for the estimation of cyclo-periods of the cyclostationary signal.

Theorem 1 (Optimum Multicycle Detector (Likelihood-ratio Detector))**.**
Let $D_{\mathrm{S}}[\lambda]$ *denote the optimum spectrum-line regeneration detector, with the cyclic-spectrum* λ*.*

Then

$$D_{\mathrm{S}}[\lambda] \triangleq \sum_{k} \frac{1}{N_w^2} P_s^*[k,\lambda] \cdot P_x[k,\lambda], \tag{1.10}$$

where k *denotes the frequency and* N_w *is the noise power averaged in the frequency domain, which can be omitted due to its unitary, and* * *denotes the complex conjugate.*

$P_s[k,\lambda]$ *is the* ideal *cyclic periodogram of PU signal* $s[m]$*, and the "IDEAL" indicates that the set of the cyclic-spectrums of* $s[m]$ *is assumed to known.* $P_x[k,\lambda]$ *is the cyclic periodogram of received signal* $x[m]$*, which is defined as,*

$$P_x[k,\lambda] \triangleq \frac{1}{M} X_{\mathrm{T}}[k] \cdot X_{\mathrm{T}}^*[k+\lambda], \tag{1.11}$$

where $T = MT_s$ *is the signal segment length and* T_s *is the period.* $X_T[k]$ *is the complex envelope of* $x[m]$ *with the center frequency* k *and bandwidth on the order of* $\frac{1}{T}$*,*

$$X_{\mathrm{T}}[k] \triangleq \sum_{m=0}^{M-1} x[m] e^{-\frac{j2\pi mk}{M}}. \tag{1.12}$$

Hence, the optimum multicycle detector D_M *can be built on the optimum spectrum-line regeneration detector* (1.10)*,*

$$D_{\mathrm{M}} \triangleq \sum_{\lambda} D_{\mathrm{S}}[\lambda]. \tag{1.13}$$

Proof: [28, Eq.31, Eq.47] provided the definitions of the optimum spectrum-line regeneration detector and the optimum multicycle detector, respectively. The cyclic

periodogram was also given in [28, Eq.27]. Note that, this thesis takes discrete variables instead of continuous ones and omits the time notation t for simplicity.

In Theorem 1, there is a assumption that the *ideal* cyclic periodogram $P_s[k, \lambda]$ of PU signal is known or it is easily estimated. However, if the particular PU signal type is not known sufficiently well to decide the *ideal* cyclic periodogram $P_s[k, \lambda]$ utilized in Eq.(1.10) as a weighing function, $P_s[k, \lambda]$ can be replaced with a simple rectangular window [28].

1.2.3 Cooperative Signal Detection Schemes

1.2.3.1 Cooperative Signal Detection Schemes

The overall detection performance of the non-cooperative detection schemes are affected by noise uncertainty, low SNR and nonideal channel effects such as shadowing and fading. In order to overcome such limitations and improve detection performance, the cooperative detection schemes have currently been paid more attention in plenty of papers [33–36] and standards [37].

There are plenty of challenges on cooperative detection technology such as the selection of optimal distributed detectors [38], the combination of the gathered detection information [35] and the decision the detection result [39], and so on.

The conventional non-cooperative detection schemes such as energy detection, cyclostationarity feature detection are usually utilized by the distributed detectors. Among the above mentioned non-cooperative detections, the energy detection is a basic choice since its advantages such as simplicity, no requirement of the target signal information.

The choice of cooperative detection scheme depends on the following factors,

- The practical condition whether there is a fusion center can be used,
- There are multiple detectors can be used,
- The system requires high detection performance.

The detection results from distributed detectors are gathered and combined in the fusion center by varied ways, such as soft combination [40] or hard combination [35]. The total detection result is then decided in the fusion center.

However, the distributed detector using energy detection way still suffers from the noise uncertainty, and nonideal channel effects such as fading and shadowing.

In order to overcome such limitations, [36,41–43] utilize the random matrix theory to build the cooperative detection system. The asymptotic eigenvalues and standard condition number of Wishart random matrices summarized in Appendix A has been utilized. Simulation results on detecting digital TV signals has shown that these methods based on statistical random matrix theories are more robust to noise uncertainty while requiring no a priori information of the signal, the channel, and noise power [41].

Based on such researches, The author firstly construct cooperative detection schemes using exact and finite random matrix theories. The author uses the standard condition numbers and the extreme eigenvalues of Wishart matrix to build the cooperative detection system. Simulation results in Chapter 4 indicate that the superior detection performance can be achieved under a finite number of samples, comparing the asymptotic cases.

1.2.3.2 Cooperative Signal Detection Model

Consider the standard AWGN model for an i-th sample of the baseband received signal

$$h_i = \sqrt{\beta} \cdot s_i + n_i \tag{1.14}$$

where β is the SNR, s_i is the PU signal including the effect of the channel, n_i are i.i.d. variates such that $n_i \sim \mathcal{N}_{\mathbb{C}}(0,1)$ in which $\mathcal{N}_{\mathbb{C}}(0,1)$ denotes the circularly symmetric complex standard normal distribution and the symbol $\sim$ indicates that the variates on the lefthand-side follow the distribution on the righthand-side.

Figure 1.10 indicate the cooperative detection model, in which N detectors gathering K samples of the primary signal cooperatively detect the presence of the "white" spectrum.

Next, consider the Wishart matrix $\mathbf{W} \triangleq \mathbf{H} \cdot \mathbf{H}^{\dagger}$, where † denotes transpose-conjugate (Hermitian).

In the following subsections, the author summarizes several models for the eigenspectrum and Standard Condtion Number (SCN) of $\mathbf{W}$ with $\mathbf{H}$.

Finally, without loss of generality[2], all discussions hereafter are for the case $K \leqslant N$ such that $\mathbf{W}$ is full-rank.

[2]This avoids the unnecessary notational care to handle null eigenvalues.

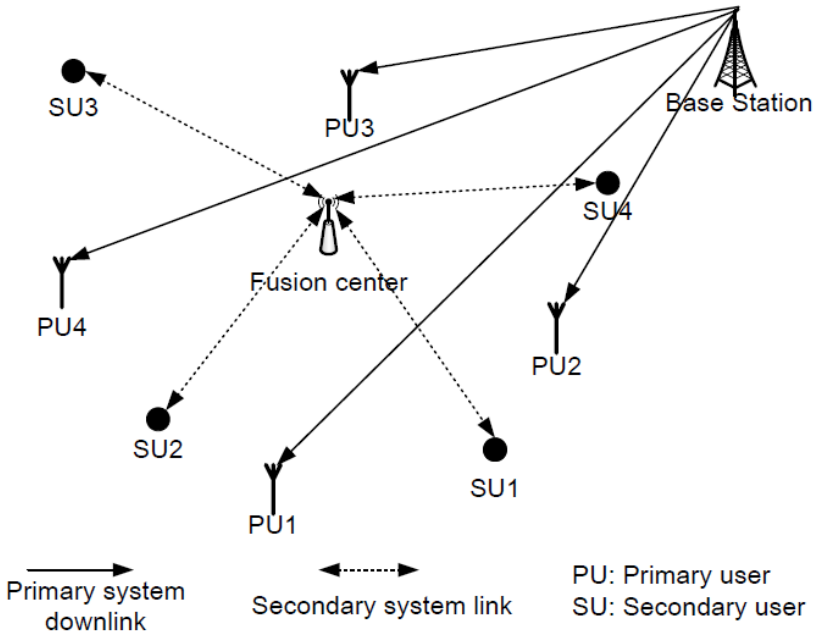

Figure 1.10: Cooperative signal detection model with N detectors.

1.2.3.3 Hypothesis Test in Cooperative Signal Detection

The binary hypothesis test including $\mathcal{H}_0$ and $\mathcal{H}_1$ cases is still utilized in the cooperative detection models. The detection process is shown as follows.

For the $\mathcal{H}_0$ case, the finite-RMT spectrum sensing algorithm can be concisely described as follows. Given a prescribed α and $2 \times N$ samples h_{kn}:

1–Construct $\mathbf{H} \triangleq [h_{kn}]_{k=\{1,2\}\times n=\{1,\cdots N\}}$;

2–Compute the eigenvalues (λ_1, λ_2) of $\mathbf{W} \triangleq \mathbf{H} \cdot \mathbf{H}^{\dagger}$;

3–Evaluate the ratio $\xi_2 \triangleq \lambda_2/\lambda_1$;

4–Accept $\mathcal{H}_0$ if and only if $\xi_2 \leqslant P_{\mathrm{M}}^{(0)^{-1}}(1-\alpha)$.

Likewise, for the $\mathcal{H}_1$ case, given a prescribed δ and $2 \times N$ samples h_{kn} the $\mathcal{H}_1$ test can be summarized as

1–Construct $\mathbf{H} \triangleq [h_{kn}]_{k=\{1,2\}\times n=\{1,\cdots N\}}$;

2–Compute the eigenvalues (λ_1, λ_2) of $\mathbf{W} \triangleq \mathbf{H} \cdot \mathbf{H}^{\dagger}$;

3–Evaluate the ratio $\xi_2 \triangleq \lambda_2/\lambda_1$;

4−Accept $\mathcal{H}_1$ if and only if $\xi_2 \geqslant P_{\mathrm{M}}^{(x)^{-1}}(\delta)$, where $x = s$ if the PU signal is random, or $x = e$ if the PU signal is constant[3].

1.3 Motivation and Relations of This Research

1.3.1 Research Motivation

The signal detection issues are the key points of cognitive radio. This dissertation discusses the signal detection problem from two aspects, non-cooperative signal detection and cooperative detection.

In non-cooperative detection schemes, energy detection and cyclostationarity feature detection are two main detection schemes, each of which possesses limitations and advantages. Energy detection scheme is simple and does not require prior information of the target signal, however, it suffers from noise uncertainty and can not distinguish signal type [17] . Cyclostationarity feature detection is robust to noise uncertainty and able to distinguish the signal type. However, the operation of deciding the cyclic frequency makes cyclostationarity feature detection to be very computational complexity [27, 32].

In order to conquer the main limitations of energy detection and cyclostationarity feature detection, The author proposed a low-complexity cyclostationarity feature detection scheme [44]. This scheme can get better detection performance compared with energy detection with low computational complexity.

Based on the proposed low-complexity cyclostationarity feature detection scheme, the author furthermore propose a dual-stage detection scheme, combining the coarse detection stage and the refined detection scheme [45]. The energy detection and the low-complexity cyclostationarity feature detection work as the coarse detection stage and the refined detection stage, respectively.

The author firstly proposed the threshold factor and the probability of indefinite detection to combine such detection stages. The theoretical analysis and the computer simulations indicate that the proposed scheme can make a tradeoff between the computational complexity and the detection performance.

For cooperative detection schemes, the conventional non-cooperative detections schemes such as energy detection, cyclostationarity feature detection are usually

[3]Notice that in the absence of any knowledge on the PU signal, the assumption of a random signal leads to conservative detection.

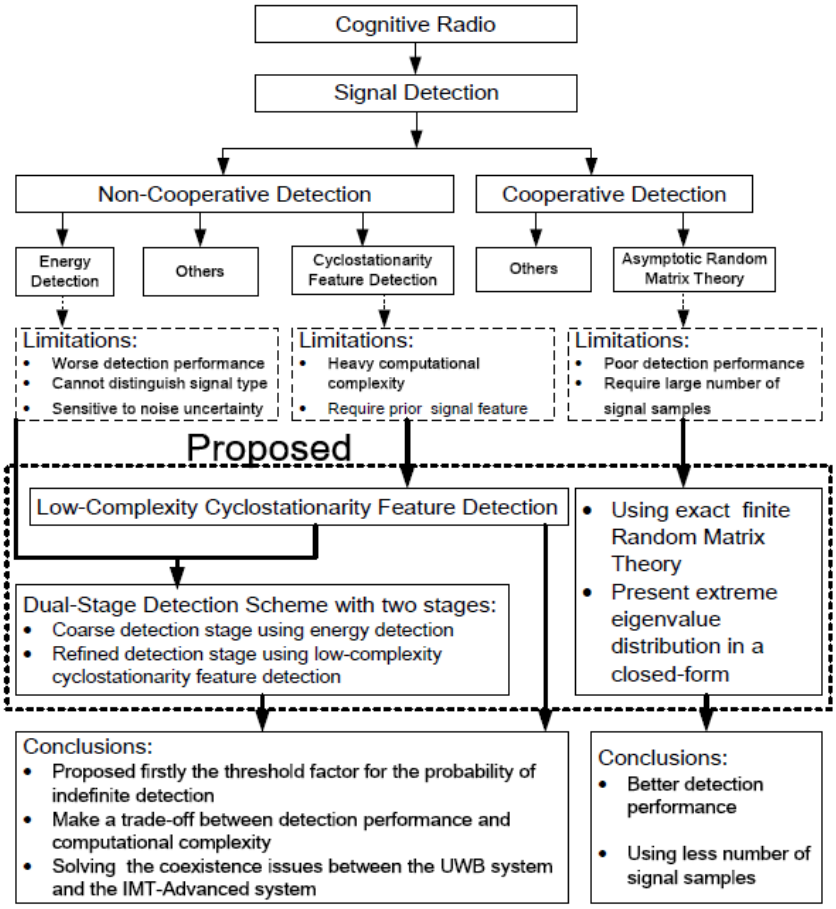

Figure 1.11: Research motivation.

utilized by the distributed detectors. The energy detection is a basic choice since its advantages such as simplicity, no requirements of the target signal information.

The limitation of individual distributed energy detector reduces the whole detection performance of the cooperative system. In order to overcome such limitations, the asymptotic random matrix theories are utilized to build the cooperative detection system [36, 41–43].

Simulation results indicate that the cooperative detection schemes based on asymptotic random matrix theories are more robust to noise uncertainty and can achieve better detection performance [36, 41].

However, the above cooperative detection schemes based on asymptotic random matrix theories require large number of received signal samples (more than 1000 [36]) to achieve the required detection performance.

In order to reduce the required number of samples and improve the detection

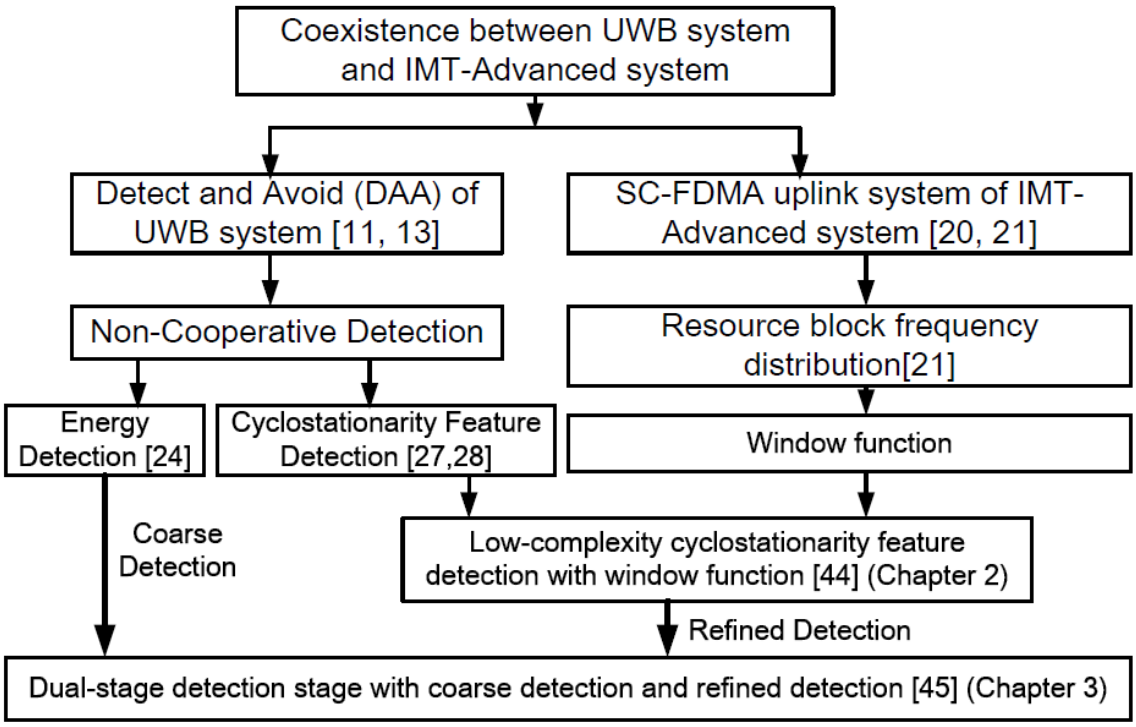

Figure 1.12: Research relation of non-cooperative detection.

performance, the author firstly construct cooperative detection schemes using exact and finite random matrix theories. The author uses the standard condition numbers and the extreme eigenvalues of Wishart matrix to build the cooperative detection system. Simulation results in Chapter 4 indicate that the superior detection performance can be achieved under a finite number of samples (less than 100 samples, Chapter 4), comparing the asymptotic cases.

The achievements of the research and the relations of the research are shown in Fig. 1.11, in which the low-complexity cyclostationarity feature scheme, dual-stage detection scheme and exact finite random theory scheme are given in Chapter 2, Chapter 3 and Chapter 4, respectively.

1.3.2 Research Relations of Non-cooperative Detection Schemes

The research relations of non-cooperative detection schemes are shown in Fig. 1.12, in which the relations between the conventional schemes and the proposed detection schemes are denoted.

The coexistence model between the UWB system and the IMT-Advanced sys-

tem can be regarded as a practical model of cognitive radio, in which the IMT-Advanced system works as the primary user system and the UWB system is the secondary user system. The detect and avoid mechanism operating in the UWB system is the key technique to keep such two systems working smoothly [9, 10].

The energy detection and the cyclostationarity feature detection are two important detection schemes in DAA mechanism. They both hold advantages and limitations.

The energy detection is simple, but is sensitive to noise uncertainty and is incapable of distinguishing the signal type [26]. On the other hand, it is hard to detect the LTE-Advanced signal or WiMax signal for the energy detector if it occupies only single sub-channel. [17] has indicated that the energy detection does not reach the required detection performance for the detection of the single sub-channel signal. The cyclostationarity feature detection can overcome those limitations and outperform the energy detection especially in a non-ideal transmission environment, however, it suffers from high computational complexity.

Detection of the SC-FDMA uplink signal is an easy way to decide the presence of the IMT-Advanced system signal. SC-FDMA uplink system has been described in [20, 22].

The author proposes to reduce the computational complexity of the conventional cyclostationarity feature detection scheme using the window function in the frequency domain, basing on the characteristics of the frequency distributions of SC-FDMA uplink system. The frequency distribution of SC-FDMA is given in [19, 20].

In order to utilize the advantages and avoid the limitations of both detection schemes, the author proposed the dual-stage detection scheme. This detector is robust and can make a tradeoff between the detection performance and the computational complexity by setting different the threshold factor and the probability of indefinite detection, which parameters are firstly proposed by authors (to the best of our knowledge).

1.3.3 Research Relations of Cooperative Detection Schemes

In this dissertation, the author have discussed the cooperative detection schemes using random matrix theory. The research relations are shown in Fig. 1.13.

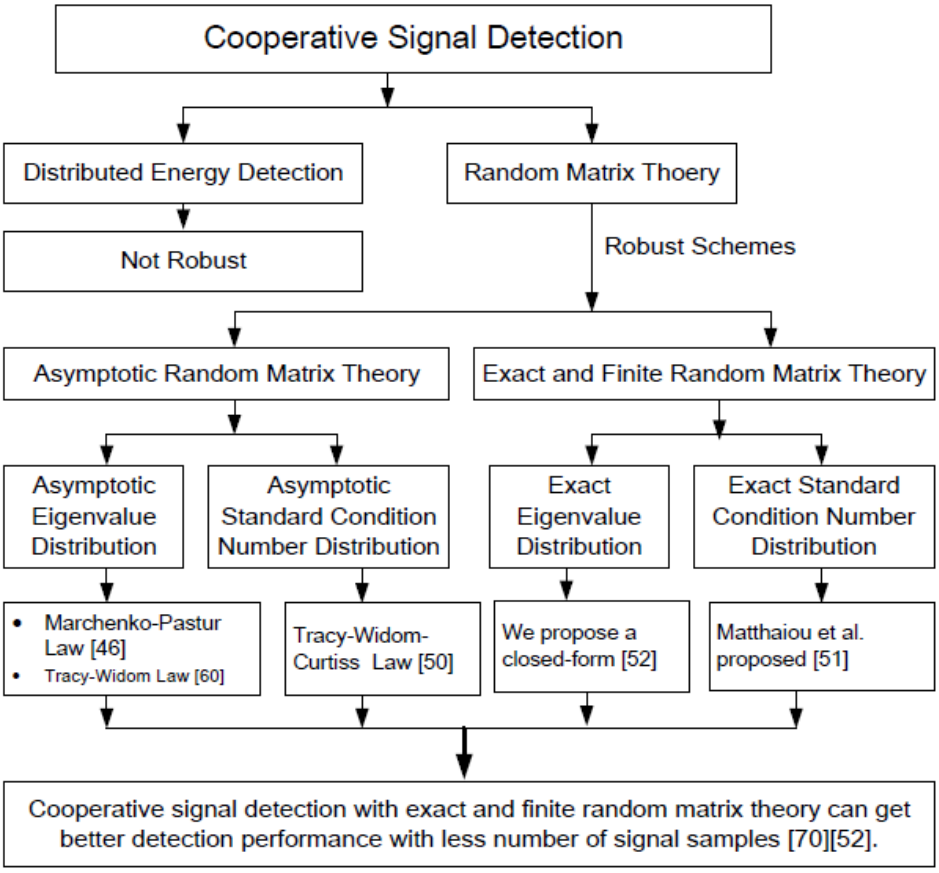

Figure 1.13: Research relation of cooperative detection.

The author firstly include exact finite random matrix theory to solve the signal detection problems, comparing with counterpart asymptotic random matrix theory.

The Marchenko-Pastur law [46,47], the Tracy-Widom law [48,49] and the Tracy-Widom-Curtiss law [48, 50] have been utilized to solve signal detection problems [36, 41, 42]. The exact finite standard condition number distribution has been proposed in [51] and the exact finite extreme eigenvalue distribution has been discussed in [52].

The theoretical analysis and computer simulation results have indicated that the proposed detection schemes can get the better performance and use less number of received signal samples.

1.3.4 Research Relations of Chapters

The research relations in non-cooperative detection schemes and cooperative detection schemes have been presented in Section 1.3.2 and Section 1.3.3, respectively. The proposed schemes including non-cooperative schemes and cooperative schemes will be discussed in the following chapters as indicated respectively in Fig. 1.12 and Fig. 1.13.

The relations between the following chapters will be given here.

In Chapter 2, a low-complexity cyclostationarity feature detection scheme for detect and avoid of the UWB system in order to solve the coexistence issues between UWB system and the LIMT-Advanced system is discussed.

Chapter 3 discusses a dual-stage detection scheme composed of coarse detection stage and refined detection stage for the continuous detection operation of Ultra-Wideband DAA.

Both Chapter 2 and Chapter 3 discuss the non-cooperative detection schemes. The dual-stage detection scheme in Chapter 3 combines the low-complexity cyclostationarity feature detection scheme proposed in Chcpter 2 and the energy detection.

The cooperative detections scheme using Random Matrix Theory is presented in Chapter 4. Specifically, I employ recently-derived closed-form and exact expressions for the distribution of the standard condition number (SCN) of uncorrelated and semi-correlated random dual central Wishart matrices of *finite* sizes in the design Hypothesis-Testing algorithms to detect the presence of PU signals.

In this Chapter, several new results on the distributions of eigenvalues and SCNs of random Wishart Matrices are offered.

The thesis is concluded in Chapter 5.

Chapter 2

Low-complexity Cyclostationarity Feature Detection Scheme

2.1 Introduction

DAA mechanisms are essential for UWB system to coexist with the existing systems operating in the frequencies below 5GHz [9,13]. The frequency band 3.4∼3.6GHz has been identified to IMT-Advanced systems at International Telecommunication Union (ITU) World Radiocommunication Conference 2007 (WRC-07). Within such spectrum, the coexistence issues between UWB systems and Worldwide Interoperability for Microwave Access systems (WiMAX) or Universal Mobile Telecommunication Systems (UMTS) have been discussed in [17, 53], respectively. Different from [53] which has tried to deal with the coexistence issues by analyzing the UWB interference on the victim systems, this chapter focuses on the detection function of the DAA mechanism. The coexistence issues between UWB systems and IMT-Advanced systems should be considered since IMT-Advanced systems will be implemented in the near future. On the other hand, from the view of CR perspective, the IMT-Advanced system and UWB system can also be considered as the PU system and the SU system, respectively.

The SC-FDMA has been adopted as the uplink system by the 3GPP LTE-Advanced systems, which can fully reach or even surpass the requirements on IMT-Advanced systems within the ITU-R time plan [15, 20]. In 3.4∼3.6GHz band, only the TDD mode is recommended for downlink and uplink in the specification of LTE-Advanced [20]. Therefore, the detection of the uplink signal is adequate

since the downlink also utilizes the same band.

The coherent detection, the energy detection and the cyclostationarity feature detection are three typical detection techniques [17]. The energy detection is simple, but is sensitive to noise uncertainty and is incapable of distinguishing the signal type [26]. On the other hand, it is hard to detect the LTE-Advanced signal or WiMax signal for the energy detector if it occupies only single sub-channel. [17] has indicated that the energy detection does not reach the required detection performance for the detection of the single sub-channel signal. The cyclostationarity feature detection can overcome those limitations and outperform the energy detection especially in a non-ideal transmission environment but suffers from high computational complexity.

The signal cyclostationarity feature is initially discussed and developed by [27–31]. Specially, [28] has illustrated a practical likelihood-ratio detection method with a BPSK signal based on the regenerated "spectral-line", which is inherently the cyclic-spectrum. [29] developed a statistical χ^2 test for the presence of the cyclostationarity feature based on the cyclic-covariances and the cyclic-spectrums. The above references share the same assumption that the cyclic-spectrums are known. However, if the type of PU signal is unclear or the cyclic-spectrums are hard to estimate, the decision of the cyclic-spectrums requires a large number of calculations due to the whole occupied spectrums need to be checked. [32] presented so-called "the variability method" for the estimation of cyclo-periods of the cyclostationary signal.

A low-complexity cyclostationarity feature detection scheme for DAA of UWB system in order to solve the coexistence issues between UWB system and LTE-Advanced system which can be considered as a practical model of CR. The localized Single-carrier Frequency Division Multiple Access signal utilized in the uplink of LTE-Advanced system is utilized to be detected.

The remainder of the chapter is organized as follows. Subsection 2.2 firstly presents a coexistence model of UWB systems and IMT-Advanced systems, followed by an introduction of the SC-FDMA uplink system. In Subsection 2.3, the low-complexity cyclostatioarity feature detection scheme is presented. A detection application on the SC-FDMA signal utilizing the proposed scheme is illustrated in Subsection 2.4. The simulation results are shown in Subsection 2.5 and the chapter is concluded in Subsection 2.6.

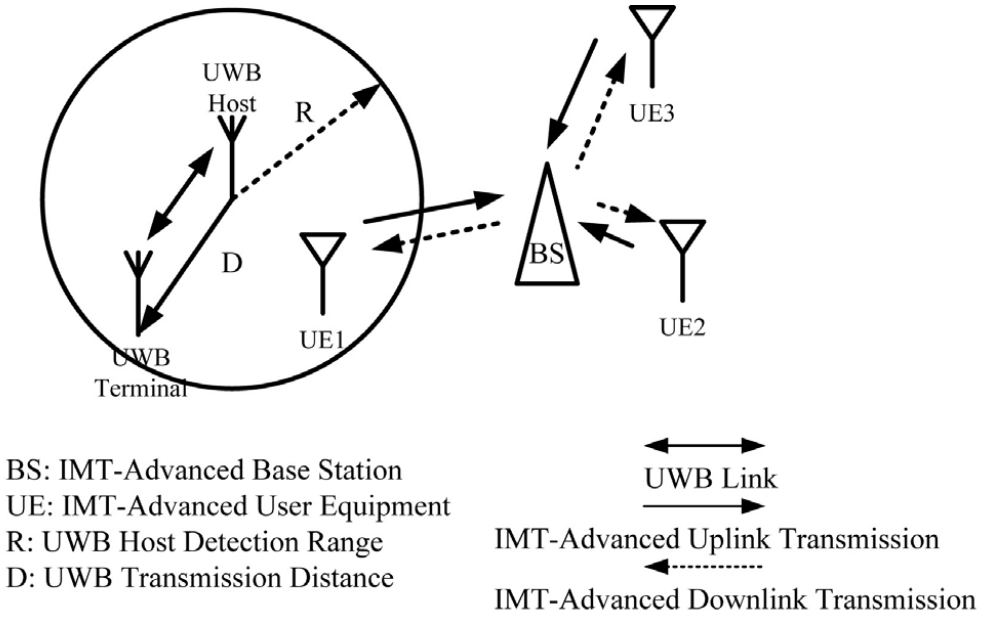

Figure 2.1: Coexistence model.

2.2 Coexistence Model and the SC-FDMA Uplink system

2.2.1 Coexistence Model of UWB Systems and IMT-Advanced System

A coexistence model of UWB system and IMT-Advanced system is indicated in Fig.2.1, in which the IMT-Advanced system works as the victim system. The coexistence model is similar to the Zone Model proposed in [9]. The detection radius R of the detector should be larger than the UWB transmission distance D. Different from the reference model, the detector instead of the victim system is located in the zone center and the victim terminal located in the detection area will be detected.

The DAA mechanism is performed by UWB system to avoid the harmful interference on [9] the victim system. In DAA, the transmission of the LTE-Advanced system including downlink and uplink should be detected and protected by UWB system. For 3.4∼3.6GHz band, LTE-Advanced system takes the TDD mode for the downlink and the uplink [16]. In this case, the detection of the uplink is adequate since the downlink also uses the same band. On the other hand, the detection of the uplink is relatively easier than that of the downlink due to the UWB device is closer to the UE than to the Base Station (BS) [17]. Therefore,

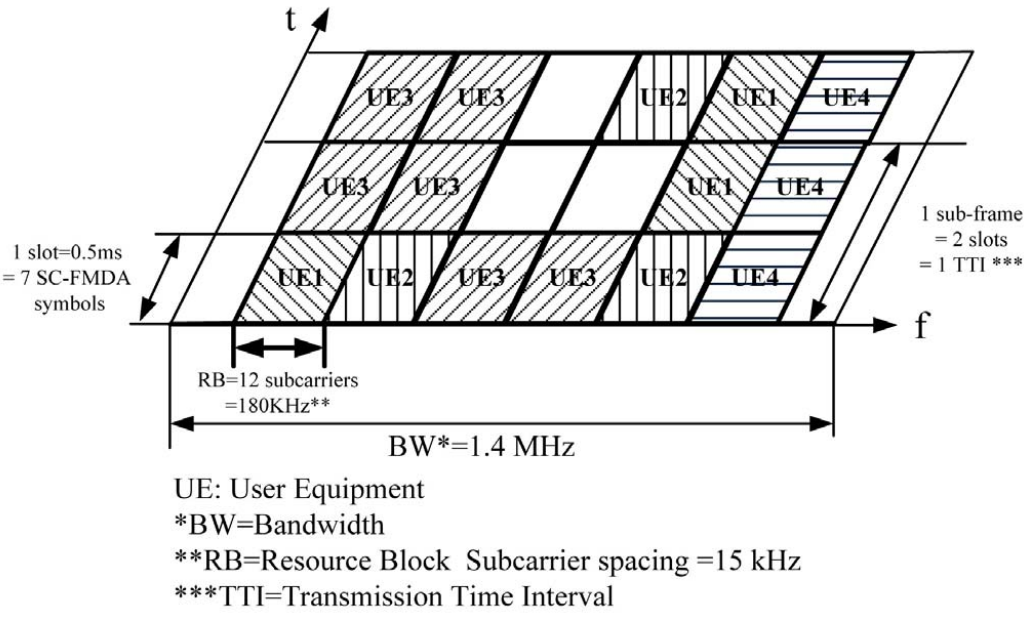

Figure 2.2: SC-FDMA signal distribution.

only SC-FDMA uplink system operating in the TDD mode is considered in this chapter.

2.2.2 A Description of SC-FDMA Uplink System

The theoretical description of the SC-FDMA signal is originally described in [54]. The practical implementation of the SC-FDMA uplink system is presented in [20, 22]. The input symbols $v^{(u)}[n](n = 0, ..., N-1)$ of the UE u are grouped into blocks containing N symbols and transformed into the frequency domain $V^{(u)}[l]$ through

$$V^{(u)}[l] = \sum_{n=0}^{N-1} v^{(u)}[n] e^{-j\frac{2\pi}{N}nl}, l = 0, ..., N-1, \tag{2.1}$$

where $u = 0, ...U-1$ is the UE index and U is the total UE number. Each of DFT output $\mathbf{V}^{(u)}$ is then mapped to one of the M orthogonal subcarriers, where $M \geqslant NU$. There are two main subcarrier mapping ways, distributed mapping (or interleaved mapping) and localized mapping [22]. In order to achieve high terminal throughput and low system complexity, the localized mapping scheme is only supported in 3GPP [20].

Here $\mathbf{S}^{(u)}$ is utilized to indicate the mapped symbol vector in the frequency

domain,

$$S^{(u)}[k] = \begin{cases} V^{(u)}[l], & k = uN + l \\ 0, & k = \text{others} \end{cases} \tag{2.2}$$

where the indices $k = 0, ...M-1$, $u = 0, ...U-1$ and $l = 0, ..., N-1$. [20, 21] provide the details about the mapping and frequency-hopping mechanisms.

The output signal $s^{(u)}[m]$ expressed in the time domain is generated by M-point inverse DFT (IDFT),

$$s^{(u)}[m] = \frac{1}{M} \sum_{k=0}^{\mathrm{M}-1} S^{(u)}[k] e^{j\frac{2\pi}{M}mk}, m = 0, 1, ..., \mathrm{M}-1. \tag{2.3}$$

The receiver does the inverse action compared to the transmitter to receive the transmitted SC-FDMA signal tainted from the non-ideal channel.

Figure 2.2 presents an example of the SC-FDMA signal distribution way. This example is based on a practical SC-FDMA uplink system with 1.4 MHz channel bandwidth (BW) [20]. The duration of the time slot including 7 SC-FDMA symbols and associated cyclic prefixes (CPs) is 0.5ms. Two slots construct one subframe, which is defined as a transmission time interval (TTI). In the frequency domain, SC-FDMA signal occupies 6 resource blocks (RBs) ($N_{\mathrm{RB}} = 6$), each containing 12 continuous subcarriers ($N_{\mathrm{sub}} = 12$). The subcarrier spacing is 15 KHz ($F_{\mathrm{sub}} = 15\mathrm{KHz}$). During a slot, one UE may occupy one or more RBs according to its data rate requirements. The same RB may be taken by the other UEs in different slot.

2.3 Low-complexity Cyclostationarity Feature Detection Scheme

2.3.1 Low-complexity Windowed Multicycle Detector

In order to reduce the system complexity and conquer the limitations of the optimum multicycle detection scheme given in Theorem 1, the windowed multicycle detection scheme is given as follows.

Lemma 1 (Windowed Multicycle Detector)**.**
Let $D_{\mathrm{M}}^{(w)}$ denote the windowed multicycle detector,

$$D_{\mathrm{M}}^{(w)} = \sum_{\lambda} \sum_{k} P_x[k, \lambda] \cdot W[k], \tag{2.4}$$

where $W[k]$ denote a rectangular window with width $\Delta f = VF_s$, in which $F_s = \frac{1}{MT_s}$ is the frequency sampling increment. If the data segment is $T = (M-1)T_s$, the resolution product is $T \cdot \Delta f = \frac{V(M-1)}{M} \cong V$.

Proof: [28, Eq.32] and the related discussions in [28] presented the proof, but using continuous variables.

Note that, Lemma 1 assumes that the cyclic-spectrum is known and Theorem 1 obtains the cyclic-spectrum using the *ideal* cyclic periodogram $P_s[k, \lambda]$. However, if the cyclic-spectrums or $P_s[k, \lambda]$ is not known well enough to be included in the detection processing, the extra estimation of the cyclic-spectrums is required. Usually, the estimation processing requires the large number of calculations since the whole spectrums occupied by PU signal need to be checked. [32] presented the estimation of cyclic period, then the estimation of cyclic-spectrum is straightforward.

In order to avoid the estimation of cyclic-spectrums and reduce the computational complexity, we can utilize all possible cyclic-spectrums located in one window function interval by adjusting the window width V and the central frequency k.

According to such idea, the low-complexity windowed multicycle detector is straightforward by rewriting Eq.(2.4),

$$D_{\text{ML}}^{(w)} = \sum_{\lambda \in \mathbf{\Lambda}} \sum_{k} P_x[k, \lambda] \cdot W[k], \tag{2.5}$$

where $\mathbf{\Lambda}$ denotes all the possible cyclic-spectrums located in the window $W[k]$. This operation inherently alters the estimation interval of cyclic-spectrums from the whole occupied spectrum by PU signal to a window width. Note that, the problem of *cycle leakage* [27] [1] can also be conquered by adjusting the window width. Finally, the tradeoff of the detection performance and the computational complexity can be achieved.

The proposed low-complexity windowed multicycle detection scheme can be directly applied to the detection of SC-FDMA system and the window function is decided by the distribution of SC-FDMA signal in the frequency domain. The coming section will illustrate the application with the practical SC-FDMA uplink system.

[1] Some of the cyclic frequencies are not included in the detection.

The detection rule can be defined as follows,

$$D_{\text{ML}}^{(w)} \underset{\mathcal{H}_0}{\overset{\mathcal{H}_1}{\gtrless}} \gamma, \tag{2.6}$$

where γ denotes the detection threshold.

The detection performance is statistically measured by the probability of detection $P_{\text{D}} = Pr\{D_{\text{ML}}^{(w)} > \gamma|\mathcal{H}_1\}$ and the probability of false alarm $P_{\text{F}} = Pr\{D_{\text{ML}}^{(w)} > \gamma|\mathcal{H}_0\}$ denoted by α. $Pr\{\}$ indicates the probability distribution. Therefore, the threshold can be decided ahead and saved as a lookup table for varied α under the condition $\mathcal{H}_0$ that there is no PU signal, $\gamma = P_{\text{F}}^{-1}(1-\alpha)$.

2.4 Detection Application for the SC-FDMA Uplink Signal Using the Proposed Scheme

The SC-FDMA symbols of a specific UE u occupy one or more RBs. Such distribution is shown in Fig.2.2 and indicated in Eq.(2.2). Based on the distribution of SC-FDMA signal, the window $W[k]$ in Eq.(2.5) can be designed to *cover* each of all distributed RBs and the window width should be same with the length of RB.

For example, for a practical 1.4MHz SC-FDMA uplink system with 12 subcarriers ($N_{\text{sub}} = 12$) per RB and 15 KHz per subcarrier ($F_{\text{sub}} = 15$KHz), the width Δf of window function can be set to $\Phi \times 12 \times 15 = \Phi \times 180$ KHz and the frequency resolution is the same as the sbucarrier spacing 15 KHz. For 1.4MHz SC-FDMA uplink system, Φ can be set to be one of $\{1 \quad 2 \quad ... \quad 6\}$ since the total number of RBs is 6. For the reduction of the computational complexity, Φ is thereafter set to be 1, indicating only one RB is orderly covered.

During a detection interval in the frequency domain decided by the window width, the set of the cyclic-spectrums $\mathbf{\Lambda}$ composed of all possible cyclic-spectrums is $\mathbf{\Lambda} = \{F_{\text{sub}} \quad 2F_{\text{sub}} \quad ... \quad (N_{\text{sub}} - 1)F_{\text{sub}}\}$.

During a detection interval in the frequency domain decided by the window width, the set of the cyclic-spectrums $\mathbf{\Lambda}$ composed of all possible cyclic-spectrums is $\mathbf{\Lambda} = \{F_{\text{sub}} \quad 2F_{\text{sub}} \quad ... \quad (N_{\text{sub}} - 1)F_{\text{sub}}\}$.

During the detection operation in one slot, the detector checks each of total 6 RBs one by one and obtains 6 distributed results. The detection result generated from the n-th RB can be denoted by $D_{\text{ML}}^{(w_n)}$, in which the n-th widow width is

decided by the corresponding RB. Finally, in each slot, the detector chooses the maximum result from the total 6 results as the last detection value. Then, the detection result is generated by comparing with the given threshold γ.

The widowed multicycle detector for the 1.4MHz SC-FDMA signal can be summarized as,

$$D_{\mathrm{ML}}^{(w)} = \max_{n} \left| D_{\mathrm{ML}}^{(w_n)} \right|, \tag{2.7}$$

where the symbol || indicates that the amplitude is taken.

Table 2.1: Complexity Analysis

Channel Bandwidth (MHz)	1.4	3	5	10	15	20
Sampling frequency (MHz)	1.92	3.84	7.68	15.36	23.04	30.72
FFT Size N_{FFT}	128	256	512	1024	1536	2048
Number of RB N_{RB}	6	15	25	50	75	100
Number of Cyclic prefix for symbol 1 N_{CP1}	10	20	40	80	120	160
Number of Cyclic prefix for symbol 2-7 N_{CP2}	9	18	36	72	108	144
Subcarrier spacing (KHz)	15					
Number of Subcarrier per RB N_{sub}	12					
Number of Symbol per Slot N_{symb}	7					
Slot duration (ms)	0.5					
Detection duration N_{slot}	1 Slot					
Number of Multiplication for Energy detection ${N_{\mathrm{E}}}^{1*}$	960	1920	3840	7680	11520	15360
Number of Correlation for Proposed Scheme detection ${N_{\mathrm{S}}}^{2*}$	9044	21266	43806	94780	148621	203896
Number of Correlation for Conventional Scheme ${N_{\mathrm{C}}}^{3*}$	63168	242816	947968	3738112	8366131	14830592
$(1*)N_{\mathrm{E}}$	$((N_{\mathrm{FFT}} + N_{\mathrm{CP1}}) + (N_{\mathrm{FFT}} + N_{\mathrm{CP2}}) \cdot (N_{\mathrm{symb}} - 1)) \cdot N_{\mathrm{slot}}$					
$(2*)N_{\mathrm{S}}$ (Including $N_{\mathrm{FFT}} log2(N_{\mathrm{FFT}})$)	$(C^2_{N_{\mathrm{sub}}} \cdot N_{\mathrm{RB}} + N_{\mathrm{FFT}} log2(N_{\mathrm{FFT}})) \cdot N_{\mathrm{symb}} \cdot N_{\mathrm{slot}}$					
$(3*)N_{\mathrm{C}}$ (Including $N_{\mathrm{FFT}} log2(N_{\mathrm{FFT}})$)	$(C^2_{N_{\mathrm{FFT}}} + N_{\mathrm{FFT}} log2(N_{\mathrm{FFT}})) \cdot N_{\mathrm{symb}} \cdot N_{\mathrm{slot}}$					

The computational complexity analysis of the proposed detection scheme is

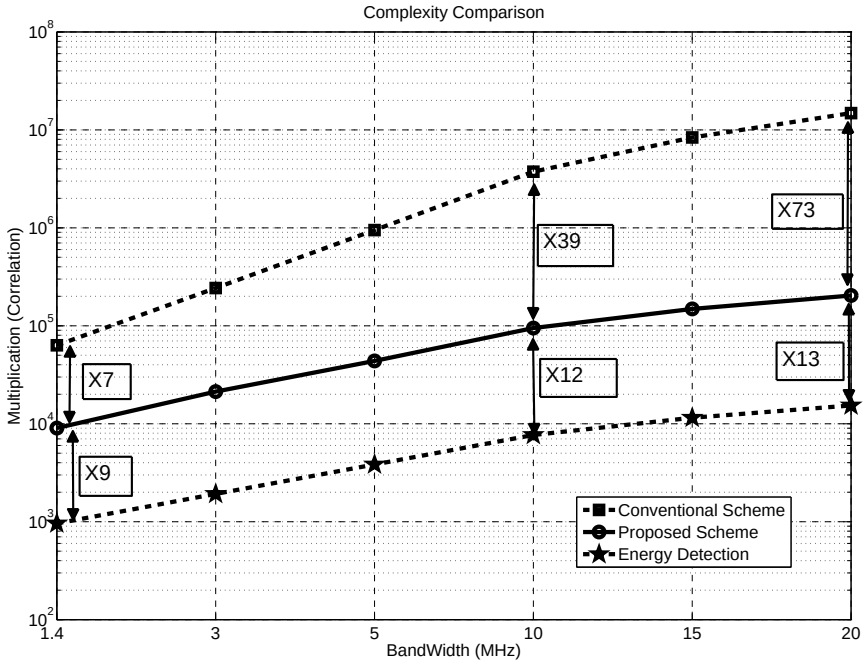

Figure 2.3: Complexity comparison. The number in box indicates the multiples of operation between two schemes.

shown in Table 2.1. The PU signal is the SC-FMDA uplink signal with varied bandwidths from 1.4-20MHz [20]. The complexities of the proposed scheme and that of the conventional scheme are measured by the number of correlation operation in the frequency domain, and that of the energy detection is indicated by the number of the multiplication operation in the time domain. Note that, so-called conventional scheme takes Eq.(2.4) as the detector and all possible cyclic-spectrums are generated from the whole occupied spectrum. The complexities of the correlation operation and that of the multiplication operation are almost the same. Figure 2.3 presents the complexities of three schemes. The complexity of the proposed scheme is almost one seventh of that of the conventional scheme, and almost nine times of that of the energy detection scheme for the 1.4 MHz channel bandwidth system. However, the complexity difference between the proposed scheme and the conventional scheme increases quickly and that difference between the proposed scheme and the energy detection is almost stable. The complexity of the conventional scheme is almost 73 times of that of the proposed scheme when the channel bandwidth is 20MHz. It should be clarified that the computational complexity of

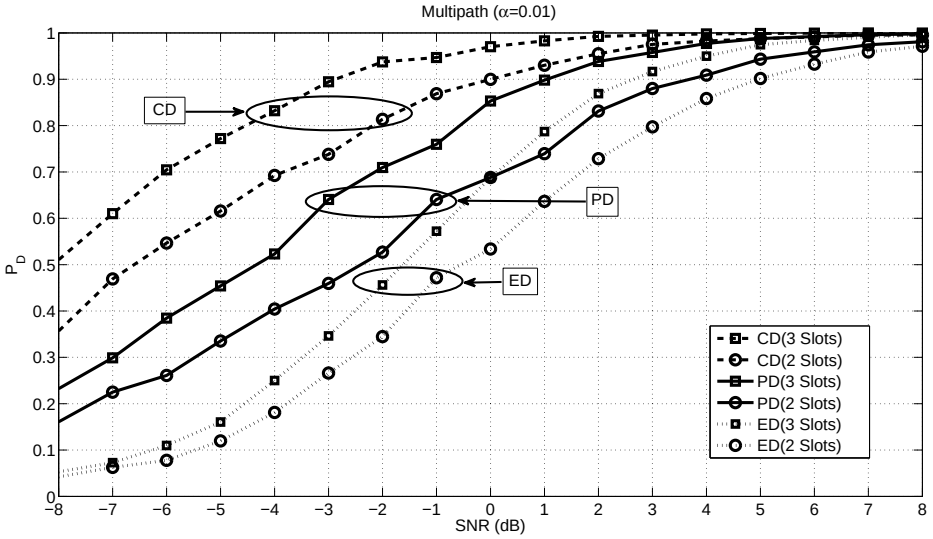

Figure 2.4: P_{D} vs. SNR(dB) on the multipath channel.

the FFT component ($O(N_{FFT}log_2(N_{FFT}))$) is included in the complexity analysis of the proposed scheme and that of the conventional scheme (see Table 2.1). However, the computational complexity of the FFT block is not counted in the number of multiplication of the energy detector that works in the time domain.

2.5 Simulation Results

In this section, the performance of the proposed detection scheme is evaluated through the computer simulations. The 1.4MHz SC-FDMA uplink system is included [20] and the simulation parameters are shown in Table 2.2.

PD is the abbreviation of the proposed detector illustrated by (2.5). CD and ED are the abbreviations of the conventional cyclostationarity feature detector (2.4) and the energy detection, respectively. *Although the authors understand that the energy detector is inherently simple and works worse in a non-ideal transmission environment, it is still included as the benchmark to evaluate the detection performance and the computational complexity of the proposed scheme.*

Figure 2.4 presents the detection performances of the PD, the CD and the ED in the multipath environment with the constraint condition $P_{\mathrm{F}} = \alpha = 0.01$. The JTC 94 Indoor Office B channel model [23] is utilized to simulate the multipath environment. Both the number of the active UEs and the occupied RBs are sup-

Table 2.2: Simulation Parameters

Carrier frequency (GHz)	3.5
Channel Bandwidth (MHz)	1.4
Sampling frequency (MHz)	1.92
Subcarrier spacing F_{sub}(KHz)	15
Number of active UE	1
Number of RB N_{RB}	6
Number of occupied RB N_{O}	1
FFT Size N_{FFT}	128
Number of Subcarrier per RB N_{sub}	12
Slot duration (ms)	0.5
Number of Symbol per Slot N_{symb}	7
N_{CP1} (Table 2.1)	10
N_{CP2} (Table 2.1)	9
Frame Structure Type I	TDD
Subframe duration (ms)	1
Modulation type	QPSK SC-FDMA
SNR (dB)	-8 $\sim$ 8
Detection duration	1 Slot (0.5 ms) 2 Slots (1 ms) 3 Slots (1.5 ms)
Channel model	Rayleigh Indoor Office B [23]
Number of simulation trials	5000

posed to be 1. The window length Φ is also set to be one in all simulations. That is, only one UE which occupies one RB is supposed to be active. The detection durations are 2 slots (1ms) and 3 slots (1.5ms), respectively. It is found that the proposed scheme based on windowed multicycle detector outperforms the energy detector and works worse than the conventional scheme, exhibiting a 2 dB advantage over ED at – the "high" SNR region around 0 dB – and several dB at the low SNR region. It can be seen that the detection performance of ED is not good at the low SNR region.

In order to illustrate the detection performance of the proposed scheme under varied α, the Receiver Operating Characteristic (ROC) performance for an SNR of -5 dB on the multipath channel is also presented. It is obvious that the proposed

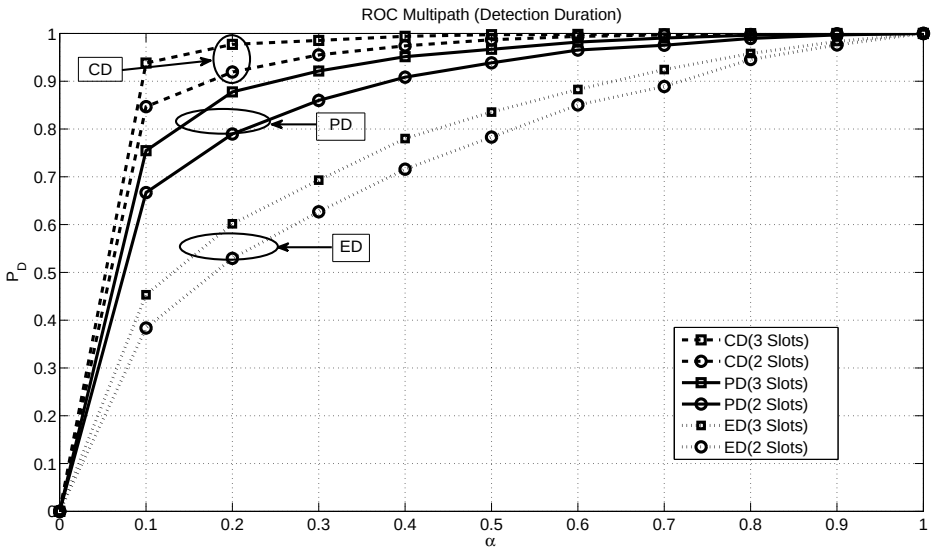

Figure 2.5: The ROC performance on the multipath channel. SNR=-5 dB.

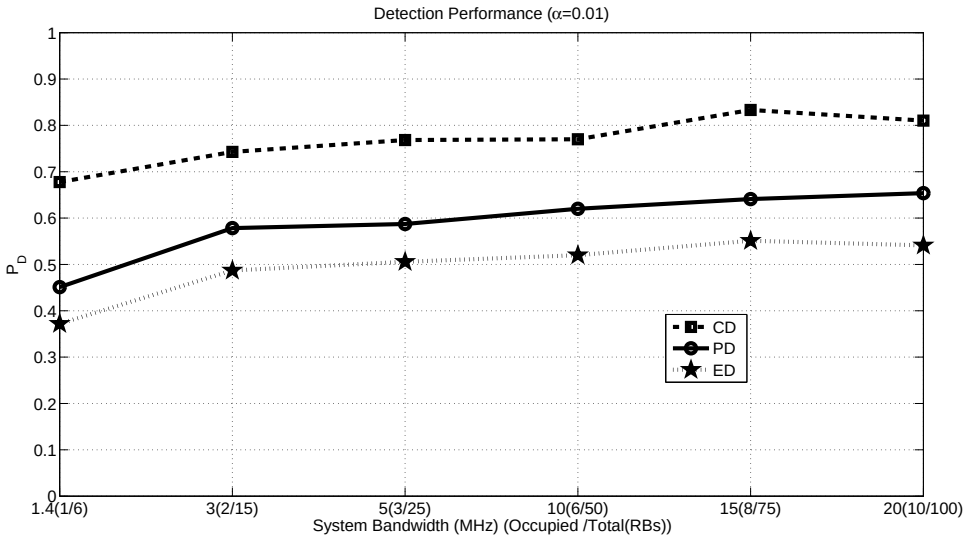

Figure 2.6: Detection performance of varied bandwidth systems on the multipath channel. The detection duration is 1 Slot (0.5 ms) and the SNR is 0 dB. The number of occupied RBs and the total number of RBs are shown.

scheme outperforms ED at all α region.

The detection performances for the SC-FDMA uplink signal with 1.4MHz channel bandwidth have been illustrated in Fig.2.4-2.5. For the SC-FDMA uplink signal with varied bandwidth, the detection performances of the PD, the CD and the ED

are shown in Fig.2.6. The simulation parameters of varied bandwidth systems (1.4MHz, 3MHz, 5MHz, 10MHz, 15MHz, 20MHz) are taken from Table 2.1 and Table 2.2. The number of the active UE is UE=1, and the constraint condition is $\alpha = 0.01$, and the multipath channel (SNR=-5 dB) is still chosen. The number of occupied RBs (UE data rate) for each system is given in the figure. Almost the same ratio between occupied RBs and total RBs is selected for different bandwidth systems. Considering the complexity analysis Table 2.1 and Fig.2.3, the proposed scheme makes a tradeoff between the detection performance and the computational complexity. Compared with the conventional cyclostationarity detection, the proposed scheme can keep almost similar detection performance with low computational complexity especially for the high bandwidth system.

2.6 Conclusions of this chapter

A low-complexity cyclostationarity feature detection scheme has been discussed in this chapter. The inherent frequency distribution of the target signal is utilized to generate the cyclostationarity feature. The detection of the SC-FDMA uplink signal with the proposed method is focused when the coexistence issues of the UWB systems and the IMT-Advanced systems need to be dealt with. The theoretical analysis has been given to indicate that the proposed scheme is low computational complexity, especially when the target bandwidth is large. At the cost of low complexity, the detection performance of the proposed scheme slightly decreases shown in the simulation results. The proposed detection scheme also can be considered as the substitute for the energy detection in DAA mechanism when the transmission environment is not ideal.

Chapter 3

Dual-stage Detection Scheme for Ultra-Wideband Detect and Avoid

3.1 Introduction

DAA is essential for UWB system to coexist with IMT-Advanced system, which will be implemented and occupy 3.4∼3.6GHz band in the near future [9, 13]. The 3rd GPP LTE-Advanced system can fully reach or even surpass the requirements on IMT-Advanced system within the ITU-R time plan [14, 15]. Therefore, the LTE-Advanced system is supposed to be the victim system for UWB system and the coexistence issues between these two systems should be investigated.

The coexistence issues between WiMAX system and UWB system have been discussed in [17]. The detection of the transmitted signal of the victim system is prerequisite for DAA. Comparing with WiMAX signal detection, the minimum bandwidth of LTE-Advanced signal is narrower and more sophisticated detection scheme is required. The SC-FDMA system has been selected as the uplink of LTE-Advanced system. There are two main types of subcarrier mapping ways in frequency domain, distributed mapping (or interleaved mapping) and localized mapping [22]. In order to achieve high throughput and low system complexity, the localized mapping scheme is only supported in 3GPP. The distribution feature of the localized mapping way in frequency domain can be utilized by UWB systems in DAA for the detection for SC-FDMA signal.

The energy detection scheme has been investigated in DAA [9]. ED is simple and efficient, however, it suffers from noise uncertainty and cannot distinguish a signal type [33]. CFD can differentiate the signal type in low signal-to-noise ratio (SNR) [33] and reach better detection performance. However, the large computational complexity is its limitation. Therefore, a dual-stage detection scheme combined with ED and CFD is proposed, which hopefully utilizes the spectrum features of the victim signal and conquers the limitations of ED and CFD. Moreover, a tradeoff between the detection performance and the computational complexity may be achieved.

Coarse detection (CD) and refined detection (RD) are two detection stages of the proposed dual-stage detection scheme. CD is the first detection stage and RD works as the second detection stage. CD initially senses the victim signal of the target frequency band. When CD cannot provide a definite detection result, the same signal samples saved in the detector will be check again by RD and the final detection result will be determined. The advantages and limitations of ED and CFD make them be the natural candidates for CD and RD, respectively. To further reduce the complexity of the whole system and make full use of the characteristics of the victim signal, the low-complexity cyclostationarity feature detection approach (abbreviated to Low-complexity Spectrum Correlation Density, LSCD) [44] is supposed to be utilized.

The two-stage (or two-step) detection schemes have been discussed in [55, 56] and a bi-thresholds method has been proposed in [57]. [55] presents the performance analysis based on detection time and [56] introduces an autoregressive (AR) model in the analysis of two-step sensing scheme. [57] uses a sensing approach with a double-threshold to decrease the transmission burden of sensing information. Different from the above schemes, this chapter focuses on the combination of two detection stages with two different detection schemes by using the threshold factor and the probability of indefinite detection (P_{ID}). The first stage of the detection selects RBs that may be in use and the second stage checks the existence of the LTE-Advanced signal with cyclostationarity detection. A tradeoff between the detection performance and the computational complexity can be achieved by setting P_{ID}.

In this chapter, the author propose a dual-stage detection scheme composed of coarse detection stage and refined detection stage for the continuous detection

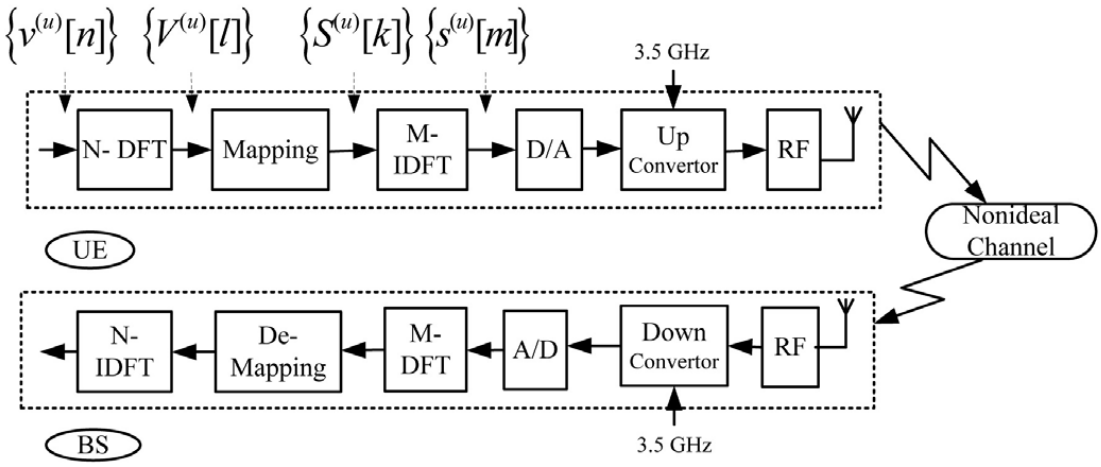

Figure 3.1: SC-FDMA uplink system.

operation of UWB DAA. The threshold factor for the probability of indefinite detection is first proposed and defined to combine the two stages.

The remainder of the chapter is organized as follows. Subsection 3.2 firstly presents a coexistence model of UWB systems and LTE-Advanced systems, followed by a simple introduction of the DAA mechanism. The SC-FDMA uplink system is also introduced. The dual-stage detection scheme with CD and RD is presented in Subsection 3.3. The definitions of the threshold factor and the probability of indefinite detection are also given in the same section. Subsection 3.4 shows the simulation results and the chapter is concluded in Subsection 3.5.

3.2 Coexistence Model and the SC-FDMA Uplink System

3.2.1 Coexistence Model of UWB system and LTE-Advanced system

In the coexistence model, the LTE-Advanced system is the victim system to the UWB system. The transmission included downlink and uplink should be detected and protected by UWB system with the DAA mechanism. In 3.4∼3.6GHz band, LTE-Advanced system takes the TDD mode for the downlink and the uplink [16]. In this case, detecting the uplink is adequate since the downlink also uses the same band. On the other hand, detecting the uplink is relatively easier than detecting the downlink because the UWB device is closer to the UE than to the Base Station (BS) [17]. Therefore, only SC-FDMA uplink system operating in the TDD mode

is considered in this chapter.

In DAA, there are two types of detection operations, initial detection and continuous detection [9] [10]. The initial detection is used to sense the victim signal of the target frequency band initially, and the continuous detection is utilized to monitor regularly the target band. In the continuous detection operation, the signal level of the victim system is sensed continuously [9]. The proposed dual-stage detection scheme can be utilized in the continuous detection operation in order to reduce the computational complexity and improve the detection performance.

3.3 Proposed Dual-stage Detection Scheme with Threshold Factor and Probability of indefinite detection

3.3.1 Dual-stage Detection Scheme for SC-FDMA Uplink Signal

In detection operation, ED working as CD tests the victim signal. When CD cannot provide a definite result, RD is required to check the existence of the cyclostationarity feature from the same victim signal samples. RD takes the LSCD scheme and presents the last detection result.

Both ED and LSCD follow a binary hypothesis test. The test can be described as,

$$\begin{aligned} \mathcal{H}_0 &: y[n] = w[n], \\ \mathcal{H}_1 &: y[n] = \sum_{p=0}^{P-1} h[p]x[p-n] + w[n], \end{aligned} \tag{3.1}$$

where $y[n]$, $x[n]$ and $w[n]$ are the n-th samples of the received signal, the transmitted SC-FDMA signal and the additive white Gaussian noise (AWGN), respectively. The channel type (AWGN or Multipath) is indicated by the factor h and the number of multipaths P. For the AWGN channel, the parameter P is set to be 1 and only $h[0]$ is calculated. For a multipath fading channel, $h[p]$ is a complex random variable denoting the channel fading on the p-th path. Two Rayleigh fading models (JTC Indoor Office A and JTC Indoor Office B) are included in simulations [23]. Suppose that $x[n]$, $w[n]$ and $h[p]$ are independent of one another. $\mathcal{H}_1$ indicates the SC-FDMA uplink signal is present and the target frequency band is occupied while $\mathcal{H}_0$ denotes that the target frequency band is empty.

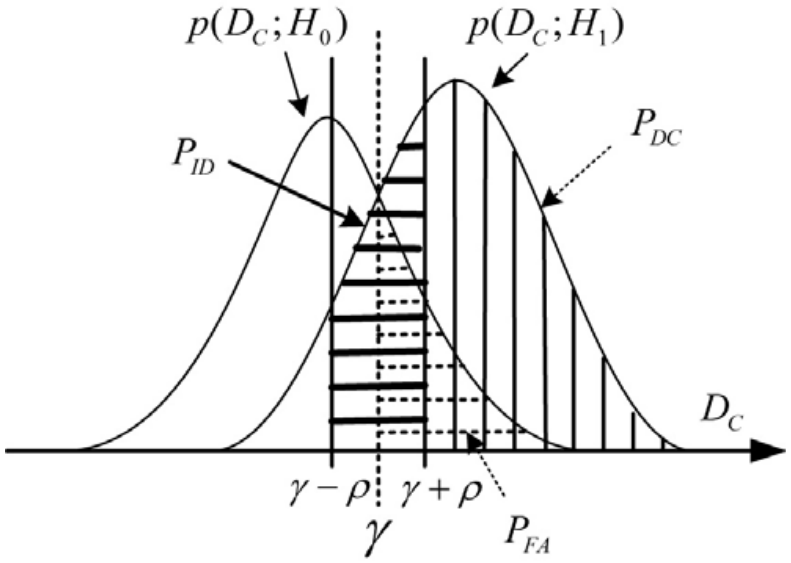

Figure 3.2: Test statistic of CD, the threshold factor ρ and the probability of indefinite detection P_{ID}.

3.3.2 Coarse Detection Stage with Energy Detection Scheme

The energy detection presented in Section 1.2.2.5 can be used as the coarse detection.

In order to integrate the two detection stages, the threshold factor ρ and the probability of indefinite detection P_{ID} are proposed. Figure 3.2 denotes their definitions. ρ is defined to be a small bidirectional shift, which can be calibrated with the ratio of the given specific threshold γ. ρ changes the single threshold to an interval $\gamma \rightarrow [\gamma-\rho, \gamma+\rho]$. $\gamma+\rho$ is the high threshold γ_{CH} and $\gamma-\rho$ is the low threshold γ_{CL}.

$$\gamma_{CH} = \gamma + \rho, \tag{3.2}$$

and

$$\gamma_{\mathrm{CL}} = \gamma - \rho. \tag{3.3}$$

Note that both ρ beside the threshold γ are set to be equivalent for simplicity. There should be other schemes such as choosing the same "area" at each side of γ under $p\left(D_c; H_1\right)$ to decide the threshold factor ρ.

When the detector of CD is greater than the high threshold $D_{\mathrm{C}} \geqslant \gamma_{\mathrm{CH}}$, it means that SC-FDMA uplink signal from the target frequency fragment is detected. If

$D_{\mathrm{C}} < \gamma_{\mathrm{CL}}$, it means that the target fragment is available. Otherwise, when $\gamma_{\mathrm{CH}} > D_{\mathrm{C}} \geqslant \gamma_{\mathrm{CL}}$, it means that CD cannot present a definite result and RD will be required.

The probability of indefinite detection is defined as

$$P_{\mathrm{ID}} = Q\left(\frac{\gamma - \rho - N(\eta^2\sigma_x^2 + \sigma_w^2)}{\sqrt{2N(\eta^2\sigma_x^2 + \sigma_w^2)^2}}\right) - Q\left(\frac{\gamma + \rho - N(\eta^2\sigma_x^2 + \sigma_w^2)}{\sqrt{2N(\eta^2\sigma_x^2 + \sigma_w^2)^2}}\right). \tag{3.4}$$

P_{ID} indicates the probability that CD locates in the threshold interval $[\gamma_{\mathrm{CL}}, \gamma_{\mathrm{CH}}]$, on the other hand, it also indicates the probability that the target frequency band needs to be checked by RD.

Substituting Eq. (1.9) into Eq. (3.4) gives the expression of P_{ID},

$$P_{\mathrm{ID}} = Q\left(\frac{Q^{-1}(P_{\mathrm{FA}}) - \rho/(\varepsilon\sqrt{2N}) - \varepsilon\sqrt{N/2}}{\varepsilon + 1}\right) - Q\left(\frac{Q^{-1}(P_{\mathrm{FA}}) + \rho/(\varepsilon\sqrt{2N}) - \varepsilon\sqrt{N/2}}{\varepsilon + 1}\right), \tag{3.5}$$

where Q^{-1} denotes the inverse complementary cumulative distribution function. In Eq. (3.5), ε is defined as the signal-to-noise ratio (SNR),

$$\varepsilon = \frac{\eta^2\sigma_x^2}{\sigma_w^2}. \tag{3.6}$$

For the constant false alarm probability (CFAR) test, P_{ID} is mainly determined by ρ under the conditions of the fixed number of samples N and the specific SNR environment. Under such assumption, P_{ID} and ρ can determine mutually. For a practical detection system, P_{ID} (or ρ) can be determined ahead according to the signal level or the signal type of the victim signal. Those information can be available in the continuous operation stage of DAA [9].

The probability of the coarse detection can be calculated by

$$\begin{aligned} P_{\mathrm{DC}} &= Q\left(\frac{\gamma + \rho - N(\eta^2\sigma_x^2 + \sigma_w^2)}{\sqrt{2N(\eta^2\sigma_x^2 + \sigma_w^2)^2}}\right) \\ &= Q\left(\frac{Q^{-1}(P_{\mathrm{FA}}) - \rho/(\varepsilon\sqrt{2N}) - \varepsilon\sqrt{N/2}}{\varepsilon + 1}\right). \end{aligned} \tag{3.7}$$

Table 3.1: System Parameters

Carrier frequency	3.5 GHz
Channel Bandwidth	10 MHz
Sampling frequency	15.36 MHz
DFT size (N_{DFT})	1024
Number of RB (N_{RB})	50
Subcarrier spacing	15 kHz
Number of subcarrier per RB (N_{Sub})	12
Number of symbol per Slot (N_{Symb})	7
Slot duration	0.5 ms
Detection duration for LSCD and ED (N_{Slot})	2 Slots
Detection duration for CD and RD (N_{Slot})	1 Slot
Modulation type	QPSK SC-FDMA
Number of Cyclic prefix for symbol 1 N_{CP1}	80
Number of Cyclic prefix for symbol 2-7 N_{CP2}	72
probability of indefinite detection P_{ID}	Eq. (3.5)

Note that, P_{FA} is still for the whole detection process. P_{DC} is obviously less than P_{DE} for the shift of the threshold. However, the refined detector will check the 'suspicious' sub-band and compensate the reduction.

3.3.3 Refined Detection Stage with Low-complexity Cyclostationarity Feature Detection Scheme

The low-complexity cyclostationarity feature detection method (LSCD) proposed in [44] works as RD. The cyclostationarity feature detector is denoted by the accumulative sum of spectral correlation density (SCD) function [44] [27]. The detector for the received SC-FDMA uplink signal in frequency domain can be described as

$$D = \sum_{k=0}^{N-1} \sum_{\lambda=-(N-1)}^{N-1} Y[k] \cdot Y^*[k+\lambda], \tag{3.8}$$

where k and λ are the discrete frequency index and the discrete cyclic frequency index, and N is the total number of subcarriers. $Y[k]$ and $Y^*[k+\lambda]$ are the

Table 3.2: Complexity Analysis

Probability of false alarm P_{FA}	0.01
Signal-to-noise ratio SNR	-5 dB
	0 dB
	5 dB
Number of multiplication for CD N_{CD} ^{1*}	7168
Number of correlation for RD N_{RD} ^{2*}	23100
Number of multiplication for ED N_{ED} ^{3*}	14336
Number of correlation for LSCD N_{LSCD} ^{4*}	46200
$^{1*}N_{\mathrm{CD}} = N_{\mathrm{DFT}} \cdot N_{\mathrm{Symb}} \cdot N_{\mathrm{Slot}}$	
$^{2*}N_{\mathrm{RD}} = C^2_{N_{\mathrm{Sub}}} \cdot N_{\mathrm{RB}} \cdot N_{\mathrm{Symb}} \cdot N_{\mathrm{Slot}}$	
$^{3*}N_{\mathrm{ED}} = N_{\mathrm{DFT}} \cdot N_{\mathrm{Symb}} \cdot 2N_{\mathrm{Slot}}$	
$^{4*}N_{\mathrm{LSCD}} = C^2_{N_{\mathrm{Sub}}} \cdot N_{\mathrm{RB}} \cdot N_{\mathrm{Symb}} \cdot 2N_{\mathrm{Slot}}$	
Complexity of proposed scheme $N_{\mathrm{DD}} = N_{\mathrm{CD}} + P_{\mathrm{ID}} \cdot N_{\mathrm{RD}}$	

received SC-FDMA signal in frequency domain, and the symbol $*$ denotes complex conjugate.

The LSCD can be defined as

$$D_{\mathrm{R}}^{\mathrm{RB}_r} = \sum_{k=0}^{N_{\mathrm{RB}}-1} \sum_{\lambda=-(N_{\mathrm{Sub}}-1)}^{(N_{\mathrm{Sub}}-1)} Y[k + N_{\mathrm{Sub}} \cdot r] \cdot Y^*[k + \lambda + N_{\mathrm{Sub}} \cdot r] \cdot \Psi_r[k, \lambda], \tag{3.9}$$

where $\Psi_r[k, \lambda]$ is a block window function for the r-th RB. The block window function $\Psi_r[k, \lambda]$ is determined by the spectrum feature of the victim signal and can be defined as

$$\Psi_r[k, \lambda] = \begin{cases} 1, (E[|X[k + N_{\mathrm{Sub}} \cdot r] \cdot \\ X^*[k + \lambda + N_{\mathrm{Sub}} \cdot r]|] > 0) \\ 0.(others) \end{cases} \tag{3.10}$$

The index of RB is r, $r = 0, ..., N_{\mathrm{RB}} - 1$. Here for all RBs, the following block window function is employed

$$\Psi[k, \lambda] = \begin{cases} 1, & (k \in [0, ..., 11], (k + \lambda) \in [0, ..., 11]) \\ 0, & (others). \end{cases} \tag{3.11}$$

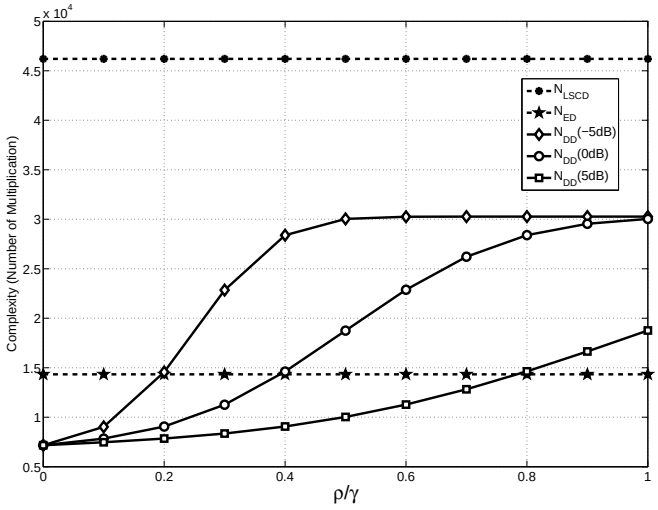

Figure 3.3: Complexity versus the ratio of the threshold factor to the threshold ρ/γ, with P_{FA}=0.01 and SNR=-5 dB, 0dB and 5 dB.

In a detection slot, the detector checks each of all N_{RB} RBs and the maximum of them will be the last result. Therefore, the result of RD is

$$D_{\mathrm{R}} = \max_{0 \leqslant r \leqslant N_{\mathrm{RB}}} \left| D_{\mathrm{R}}^{\mathrm{RB}_r} \right|, \tag{3.12}$$

where the symbol $||$ means that the amplitude of the detection and $D_{\mathrm{R}}^{RB_r}$ indicates the detection result generated from the r-th RB.

The detection rule for RD is straightforward,

$$D_{\mathrm{R}} \underset{\mathrm{H_0}}{\overset{\mathrm{H_1}}{\gtrless}} \gamma_{\mathrm{R}}, \tag{3.13}$$

where γ_{R} denotes the detection threshold of RD.

The detection result of the whole detection scheme is defined as

$$P_{\mathrm{D}} = P_{\mathrm{DC}} + P_{\mathrm{DR}}, \tag{3.14}$$

where P_{DR} is the probability of detection of RD. The proposed dual-stage detection scheme can fulfill the varied detection requirements by setting different threshold factor ρ.

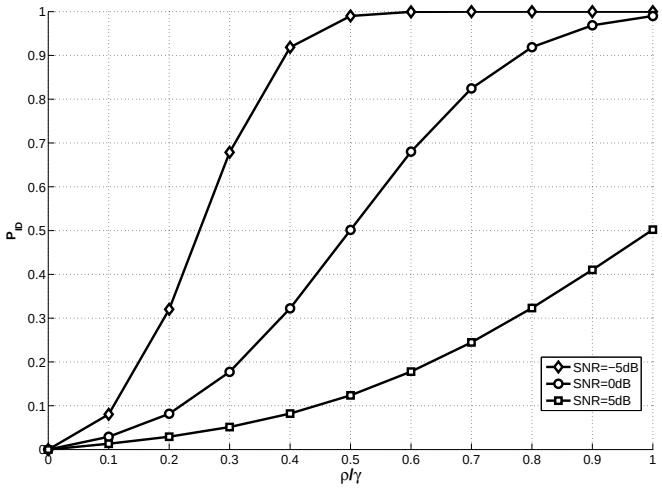

Figure 3.4: Relation between the probability of indefinite detection P_{ID} and the ratio of threshold factor to threshold ρ/γ, for P_{FA}=0.01 and SNR=-5 dB, 0 dB and 5 dB.

The computational complexity analyses of the proposed detection scheme and the coming computer simulations both consider a practical 10MHz SC-FDMA uplink system, with parameters given in Table 3.1 [20] [19] [18]. LSCD, DD and ED are the abbreviations of the low-complexity cyclostationarity detection, the proposed dual-stage detection and the energy detection, respectively.

Table 3.2 shows the computational complexities of the proposed scheme, comparing with those of ED and LSCD. The complexity is measured by the number of multiplication operations. For CD (N_{CD}) and ED (N_{ED}), the operations of multiplication are in time domain shown in Eq. (1.4). The multiplication operations of RD (N_{RD}) and LSCD (N_{LSCD}) are in frequency domain shown in Eq. (3.8). The computational complexities of such two operations can be regarded as the same for each multiplication operation. The complexity of the proposed dual-stage scheme (N_{DD}) is calculated from N_{CD}, N_{RD} and the probability of indefinite detection P_{ID}. The complexity of the proposed scheme is inherently determined by the threshold factor ρ.

Figure 3.3 presents the complexities of the proposed dual-stage scheme, ED and LSCD. The complexity of the proposed scheme is lower than that of LSCD. The maximum complexity of DD with SNR=-5 dB almost is 70% of that of LSCD. The complexity of DD decreases when SNR is large. It indicates that the complexity

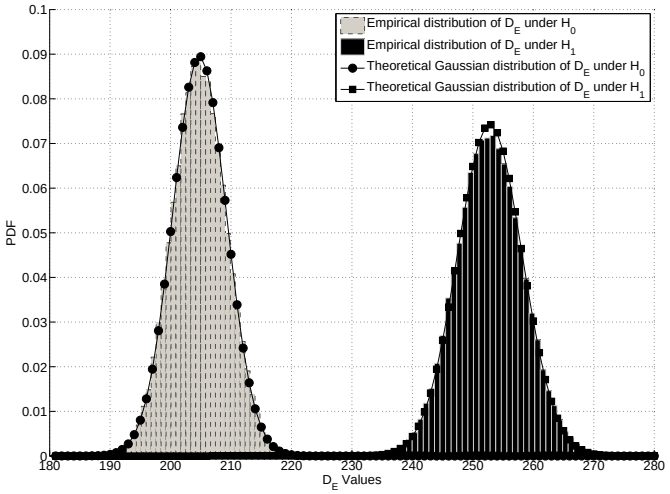

Figure 3.5: PDFs of D_E under two hypotheses $\mathcal{H}_0$ and $\mathcal{H}_1$.

Table 3.3: Simulation Parameters

Number of active UE	1
Number of occupied RBs	3
SNR	$0 \sim 20$ dB
Number of simulation trials	5000
Channel Model 1	
Rayleigh Multipath	Indoor Office A
RMS Delay Spread	35 ns
Number of Tap	3
Channel Model 2	
Rayleigh Multipath	Indoor Office B
RMS Delay Spread	100 ns
Number of Tap	6

of the proposed scheme can be reduced when the detection environment is good.

Figure 3.4 presents the relation between the threshold factor ρ and the probability of indefinite detection P_{ID}. ρ is calibrated with the ratio to the threshold γ and the probability of false alarm (P_{FA}) is set to be 0.01. This figure indicates that P_{ID} is mainly determined by ρ, which has been also given in Eq. (3.5). It is obvious that P_{ID} is more sensitive to ρ in a low SNR environment. P_{ID} can achieve 1 when ρ is the half of γ under the condition SNR of -5 dB. However, P_{ID} is 0.5 when SNR is almost equal to γ under the condition SNR of 5 dB. This figure also

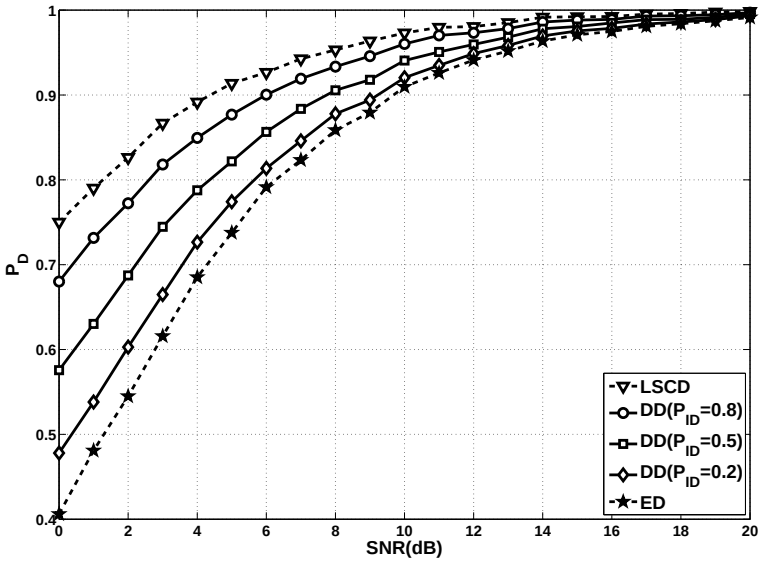

Figure 3.6: Probability of Detection (P_{D}) vs. SNR (dB) (Indoor Office A channel, for $P_{\mathrm{FA}} = 0.01$ and P_{ID}= 0.2, 0.5, and 0.8, No. of occupied RBs is 3).

indicates that the threshold factor ρ and the probability of indefinite detection P_{ID} can determine each other.

Figure 3.5 shows the empirical PDF distributions of D_{E} under two hypotheses hypotheses $\mathcal{H}_0$ and $\mathcal{H}_1$, respectively, comparing with the theoretical Gaussian distributions using the same means and variances. SC-FDMA signal with parameters shown in Table 3.1 is included in this simulation. SNR is 10 dB and 2 time slots with $2 \times N_{\mathrm{DFT}} = 2048$ samples in the time domain are utilized. The channel mode is AWGN and the number of occupied RB is set to be 1 (12 subcarriers). This figure verifies that energy detection approximately follows Gaussian distribution very well.

3.4 Simulation Results

In computer simulation, the 10MHz SC-FDMA uplink system with parameters shown in Table 3.1 is also included. Extra parameters (e.g., channel models) for simulations are given in Table 3.3.

To evaluate the proposed scheme with fair comparisons, the detection periods of LSCD and ED are set to be 2 time slots and those of CD and RD are set to be 1

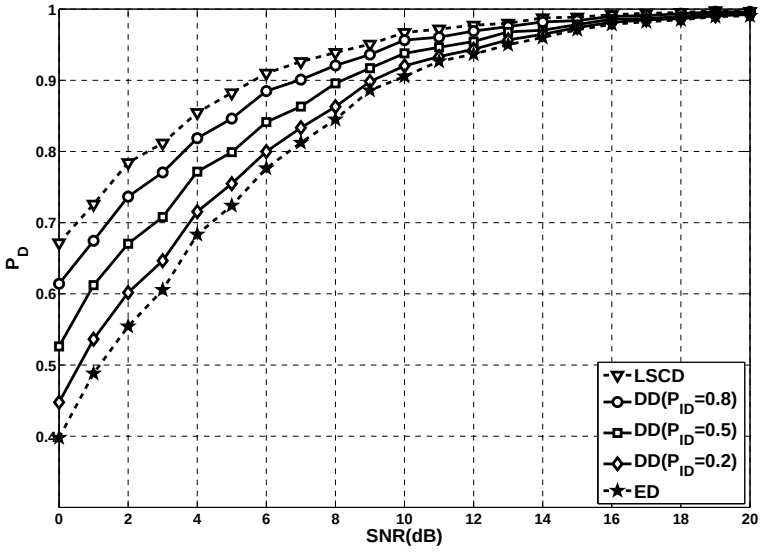

Figure 3.7: Probability of Detection (P_{D}) vs. SNR (dB) (Indoor Office B channel, for $P_{\mathrm{FA}} = 0.01$ and P_{ID}= 0.2, 0.5, and 0.8, No. of occupied RBs is 3).

time slot. The multipath Rayleigh channel models are Indoor Office A and Indoor Office B [23]. Table 3.3 gives also main parameters of the JTC Indoor Office A model and the JTC Indoor Office B model. The probability of indefinite detection P_{ID} is utilized to indicate the threshold factor ρ. On the other hand, P_{ID} also indicates the probability that the second detection stage is required.

Figures 3.6 and 3.7 denote the detection performances of LSCD, DD and ED under two multipath indoor circumstances. P_{ID} is set to be 0.2, 0.5 and 0.8, respectively. The probability of false alarm (P_{FA}) is 0.01. The detection performance of the proposed scheme achieves gradually that of LSCD with increasing P_{ID}. These two figures indicate that the detection performance of the proposed detection scheme can become controllable by setting varied P_{ID}. The detection performances in Fig. 3.6 are better than those in Fig. 3.7, which indicates the effect of different channel models.

The receiver operating characteristic (ROC) performances under two multipath indoor circumstances are presented in Fig. 3.8 and Fig. 3.9 with 0 dB SNR. ROC performances indicate the detection performance of the proposed scheme under different P_{FA}. The detection performance of dual-stage detection scheme with $P_{\mathrm{ID}} = 0.8$ can achieve 90% when $P_{\mathrm{FA}} = 0.1$ with 0 dB SNR shown in Fig. 3.8.

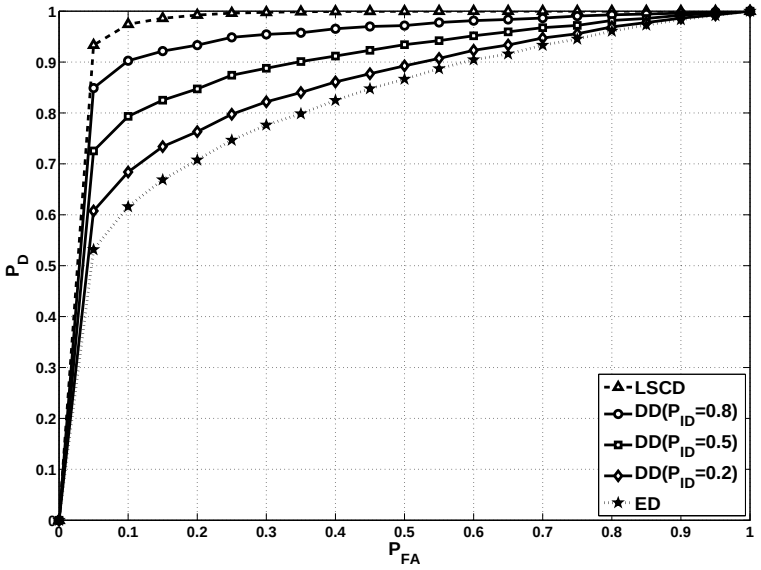

Figure 3.8: ROC performance (P_{D} vs. P_{FA}) in Indoor Office A channel and P_{ID}= 0.2, 0.5, and 0.8. The number of occupied RBs is 3 and SNR=0 dB.

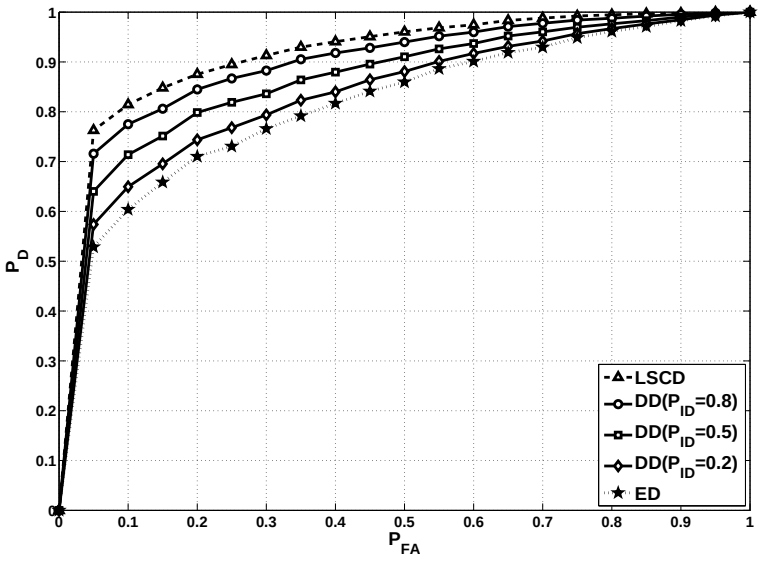

Figure 3.9: ROC performance (P_{D} vs. P_{FA}) in Indoor Office B channel and P_{ID}= 0.2, 0.5, and 0.8. The number of occupied RBs is 3 and SNR=0 dB.

In order to evaluate the detection performance in low P_{FA} situations, Fig. 3.10 presents ROC performance of the proposed scheme in JTC Indoor Office A channel

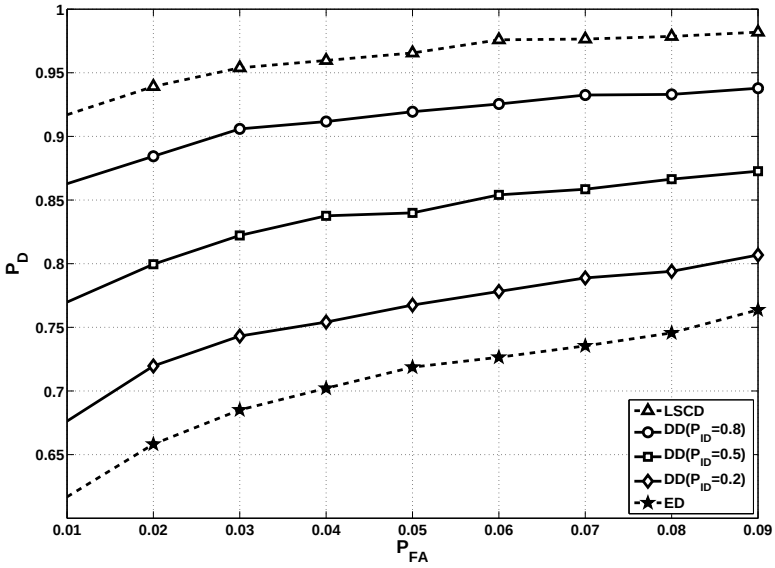

Figure 3.10: ROC performance (P_{D} vs. P_{FA}) for low P_{FA} in Indoor Office A channel and P_{ID}= 0.2, 0.5, and 0.8. The number of occupied RBs is 3 and SNR=3 dB.

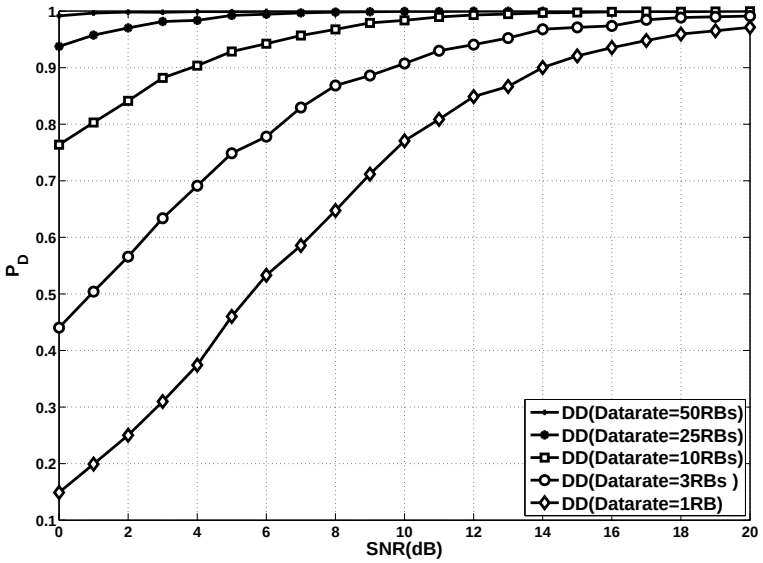

Figure 3.11: Effect of data rate on probability of Detection (Indoor Office B channel, for P_{FA} = 0.01 and P_{ID}= 0.1.)

model. The probability of false alarm is set to from 0.01 to 0.09.

The detection performance is also affected by the data rate of SC-FDMA uplink

signal, which is denoted by the number of the occupied Resource Blocks (RBs). Note that the number of occupied RBs in both of the detection stages in the proposed scheme is the same due to the refined detection will check the same signal samples when the coarse detection cannot provide a definite detection result. The maximum number of occupied RBs in a 10MHz SC-FDMA uplink system is 50. Figure 3.11 shows the effects of different number of occupied RBs on the detection performance. The numbers of occupied RBs are set to be 1, 3, 10, 25, and 50 of total 50 RBs. This figure indicates that the detection performance of the proposed scheme can increase fast when the number of occupied RBs changes from 1 to 10.

3.5 Conclusions of this chapter

The energy detection method and low-complexity cyclostationarity feature detection method are selected to be coarse detection and refined detection, respectively. 10MHz SC-FDMA uplink signal is utilized to evaluate the proposed scheme. The dual-stage detection scheme with the threshold factor and the probability of indefinite detection has been discussed in this chapter. The tradeoff between the detection performance and the computational complexity can be achieved by setting the parameter of the probability of indefinite detection.

Chapter 4

Spectrum Sensing Algorithms via Finite Random Matrices

4.1 Introduction

The ability to reliably detect the presence/absence of an unknown (and possibly weak) signal emitted by a PU amidst AWGN is fundamental to allow future radio systems to efficiently utilize bandwidth resources by temporarily occupying idle frequency bands. This so-called *spectrum sensing problem* is therefore of major importance in the field of wireless communications and at the core[1] of the recent cognitive radio paradigm [2, 4, 58].

It has been recently shown that by relying on limiting distributions of the eigenvalues of Wishart random matrices, spectrum sensing algorithms exhibiting superior performance and robustness over conventional energy detection techniques can be designed [36, 41–43].

In [41], for instance, a couple methods utilizing properties of the eigenvalues of $K \times N$ Wishart random matrices constructed from noisy input samples was proposed. Specifically, the authors rely on the property that for $K \to \infty$ and $N \to \infty$ with a constant aspect ratio $\rho \triangleq N/K$, the eingenvalues of such (asymptotically large) matrices are known to follow the Marchenko-Pastur law [46], which distinctively establishes that the largest (λ_K) and smallest (λ_1) eigenvalues of large matrices converge – under very mild assumptions on the statistics of the matrices'

[1] Recently a decision by the FCC deemed optional the use of spectrum sensing for unlicensed operation in the TV Broadcast Bands (TV White Space). However, the feature remains under investigation as mandatory in other parts of the world including Europe, Japan and China.

entries themselves – to constants (λ_{U} and λ_{L}), determined by the signal and noise powers, as well as the aspect ratio ρ.

Exploiting the relationship with the Marchenko-Pastur law, the authors in [41] designed two Hypothesis Testing (HT) spectrum sensing methods, one based on comparing λ_K against λ_{U}, and the other based on comparing the standard condition number (SCN) λ_K/λ_1 to the ratio $\lambda_{\mathrm{U}}/\lambda_{\mathrm{L}}$. For convenience, we shall hereafter refer to those techniques as Marchenko-Pastur (or MP, for short) methods.

An interesting characteristic of the latter random matrix theoretical (RMT) method based on SCN's is that no estimate of noise and/or signal power is required. This blind feature is of interest since in situations where multiple wireless devices share a crowded spectrum, background interference aggregate into AWGN [59] with power dependent on the number of active users. A major limitation of the MP approaches, however, is that the converge-rate [47] of the Marchenko-Pastur law – which is of order $\mathcal{O}(K^{-\frac{1}{2}})$ – is not fast enough to allow for accurate spectrum sensing with a limited number of samples.

Rather than relying entirely on the Marchenko-Pastur *deterministic* SCN model, in the RMT-based spectrum sensing method proposed in [36] the Tracy-Widom distribution [48] was used as a *statistical* model for the largest eigenvalue [60]. Using both the Tracy-Widom (random nominator) and Marchenko-Pastur (constant denominator) models, an approximate distribution of random SCN's was built and used to derive a relationship between a prescribed probability of false alarm α and a test-threshold γ, which was then used for decision making.

The intuition is that the Tracy-Widom (TW) method in [36] is superior to that in [41] under a smaller number of samples, since the random nature of SCN's of *finite* matrices is accounted for and the rate of convergence of the Tracy-Widom law [61] – which is of order $\mathcal{O}(K^{-\frac{2}{3}})$ – is faster than that of the MP-law. A direct comparison of the MP and TW approaches was not provided in [36], but is given in Fig. 4.1, which reveals (surprisingly) that the TW method outperforms the MP alternative **only** at relatively large SNR's.

This is due to the fact that the SCN is truly a ratio of *two* random variates, such that the approximation implicit in the normalization of λ_K by λ_{L}, as done in [36], is not sufficiently accurate unless λ_K is sufficiently large (which occurs at larger SNR's).

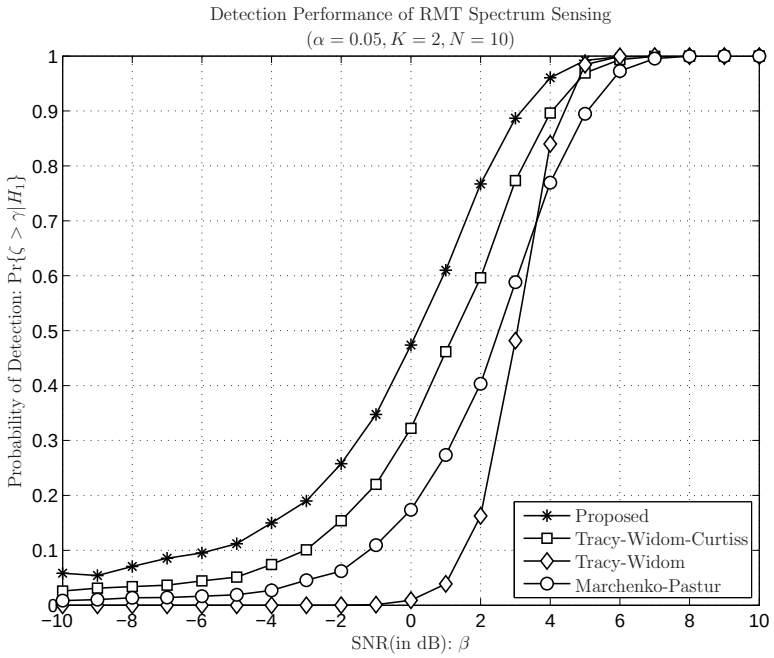

Figure 4.1: PD Versus SNR. Probability of detection of spectrum sensing algorithms based on finite random matrix (proposed) and asymptotic random matrix, as a function of the SNR and the tolerated probability of false-alarm.

This issue was improved upon in [42, 43], where Curtiss formula on the distribution of the ratio of random variates due to [50] was combined with a recent result on the distribution of the smallest [62] and largest [63, 64] eigenvalues of Wishart random matrices, leading to a more accurate model for their SCN's for the case when PU signal is present [65].

It can be seen from Fig. 4.1 that this method – which we dub Trace-Widom-Curtiss (TWC) – indeed outperforms the latter two across a wide SNR range. Unfortunately, the Tracy-Widom distribution [48, 49] and the Curtiss' ratio-of-variates formula [50] are highly involved functions which are hard to evaluate numerically and intractable in mathematical analysis. Adding to (and in spite of) this complexity challenge is the fact that all the aforementioned statistical models are *asymptotic* and thus, not suitable (or ideal) for application to matrices of finite and small sizes.

The preceding rationale aims to highlight the need for a new approach that allows a substantial reduction in the number of samples required by RMT-based spectrum sensing methods. In light of that, this chapter addresses the spectrum

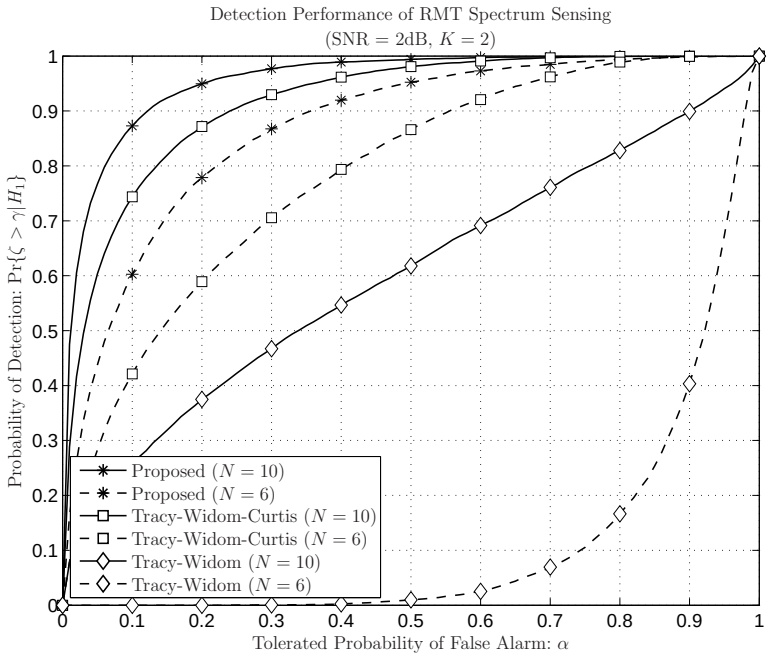

Figure 4.2: PD Versus PF. Probability of detection of spectrum sensing algorithms based on finite random matrix (proposed) and asymptotic random matrix, as a function of the SNR and the tolerated probability of false-alarm.

sensing problem from a *finite* RMT perspective. In particular, the author invokes recent results on the *exact* distribution of standard condition numbers of dual Wishart random matrices in order to design algorithms that require only a few samples to function, and outperform all the RMT techniques currently known under the constraint that the number of samples is finite.

The remainder of the chapter is as follows. In section 4.4, a summary of relevant asymptotic models for the eigen-properties (eigenvalues, extreme eigenvalues and standard condition number) of random Wishart matrices is given. The following original results are also given: the Marchenko-Pastur CDF is derived in closed form (Lemma 2); the asymptotic distribution of the eigenvalues of Wishart matrices constructed from noisy samples of a random (Corollaries 1 and 2) and constant (Lemma 3 and Corollary 3) PU signal, are given; and slightly simplified asymptotic expressions for the PDFs and/or CDFs of SNC's of Wishart matrices based on the Tracy-Widom-Curtiss formulas are given (Corollaries 7 and 5, Lemma 5 and Corollary 6). Finally, comparisons amongst the spectrum sensing algorithms utilizing such models are also provided. In section 4.3, the recently discovered

finite model for the SCN of Wishart matrices is introduced and the corresponding spectrum sensing algorithms with basis on the $\mathcal{H}_0$ and $\mathcal{H}_1$ hypothesis are briefly described. These algorithms are compared to those of asymptotic-RMT methods and shown to outperform the latter.

A simple expression of the relationship between the false alarm and miss-detection probabilities is also offered, based on which it is finally shown that blind spectrum sensing with basis on the $\mathcal{H}_0$ test is superior to the $\mathcal{H}_1$ test at low SNR's and only marginally worse than the latter in the high SNR regime, which indicates that $\mathcal{H}_0$ test is the best overall approach. Finally, concluding remarks are offered in section 4.5

The distributions of the eigenvalues of complex Wishart matrix often arise in the analysis and design of important communication techniques such as multiple-input multiple-output (MIMO) systems [66–69] and cognitive radio systems [36, 42, 70].

Substantial literature exists on the CDF and PDF of the largest eigenvalue of Wishart matrices. Asymptotic models for the extreme (largest and/or smallest) eigenvalues of large matrices with a given aspect ratio can be found for instance in [60, 62–64, 71]. Exact distributions of the eigenvalues of uncorrelated central Wishart matrices of finite size have been presented in [72–74]. A counter-part for the non-central case can also be found in [75].

In light of the result in [76], however, which establishes an accurate mapping between Wishart non-central uncorrelated statistics and a central semi-correlated equivalent, it is in most case sufficient to consider the simplest case of central uncorrelated matrices.

To the best of our knowledge, the framework leading to the simplest expressions for the extreme eigenvalues of Wishart matrices was introduced by James in [77] and further developped by Edelman [78]. In a recent article [69], Dighe *et al.* employed the James-Edelman framework to obtain closed-form algebraic PDFs of the largest eigenvalue of central uncorrelated Wishart matrices of any finite size, which are, for instance, far simpler than those in [66].

In this chapter, the PU detection problem from a finite RMT perspective is discussed. Specifically, the recently-derived closed-form and exact expressions for the distribution of the SCN of uncorrelated and semi-correlated random dual central Wishart matrices of finite sizes in the design Hypothesis-Testing algorithms to detect the presence of PU signals.

I follow similar steps to obtain the corresponding CDF and PDF of the smallest eigenvalues of central uncorrelated Wishart matrices of any size, which are more convenient and general than existing alternatives, *e.g.*, [68].

In comparison to alternative techniques based on asymptotic Random Matrix Theory [36,41,42], the proposed method has the advantage that only a few samples are sufficient to enable detection. As natural consequence of the fact that the distributions of the extreme eigenvalues are *closed-form* and *exact*, for any given matrix size, the proposed scheme outperforms all asymptotic approaches whenever the number of samples is finite.

During the design of the cooperative detection scheme using RMT, main contributions have been done as follows,

- the CDF of Marcheko-Pastur Law;
- the CDF of Tracy-Widom-Curtiss Law;
- exact PDF and CDF of extreme eigenvalues of finite central Wishart matrix.

4.2 Asymptotic Random Matrices Eigenspectrum and SCN Models

4.2.1 Receive Samples Model

Consider the standard AWGN model for an i-th sample of baseband received signal

$$h_i = \sqrt{\beta} \cdot s_i + n_i \tag{4.1}$$

where β is the SNR, s_i is the PU signal[2] including the effect of the channel, n_i are i.i.d. variates such that $n_i \sim \mathcal{N}_{\mathbb{C}}(0,1)$ in which $\mathcal{N}_{\mathbb{C}}(0,1)$ denotes the circularly symmetric complex standard normal distribution and the symbol $\sim$ indicates that the variates on the lefthand-side follow the distribution on the righthand-side.

Hereafter, s_i may be *either* an unknown arbitrary complex constant with $|s| = 1$, which models the case when a single symbol of the PU over an AWGN channel is observed, *or* i.i.d. variates $s_i \sim \mathcal{N}_{\mathbb{C}}(0,1)$, which models the case when the PU signal is sampled subject to uncorrelated (fast) Rayleigh fading, and/or is modulated within the received block of samples.

[2]For simplicity, we follow current literature (*e.g.* [36, 41, 58]) and focus on a single-PU analysis. However, the technique to be described is general under $\mathcal{H}_0$ and can be extended to multi-channel scenarios under $\mathcal{H}_1$.

It will prove convenient to define now the three hypothesis:

- $\mathcal{H}_0 : s = 0$, (no Primary User signal present);
- $\mathcal{H}_1^{\mathrm{c}} : s \neq 0$, (constant Primary User signal present);
- $\mathcal{H}_1^{\mathrm{r}} : s \neq 0$, (random Primary User signal present).

Following the model described by equation (4.1), if a number $M = K \times N$ of samples is available, the receiver may build either of the following $K \times N$ random matrices

$$\mathbf{H} = \frac{1}{\sqrt{K}} \begin{cases} \mathbf{H}_n \text{ if } \mathcal{H}_0 \text{ is true} & \text{(4.2a)} \\ \sqrt{\beta} \cdot \mathbf{H}_s + \mathbf{H}_n \text{ if } \mathcal{H}_1 \text{ is true,} & \text{(4.2b)} \end{cases}$$

where $\mathbf{H}_n$ and $\mathbf{H}_s$ denote the received matrix with noise and signal, respectively.

Next, consider the Wishart matrix $\mathbf{W} \triangleq \mathbf{H} \cdot \mathbf{H}^{\dagger}$, where † denotes transpose-conjugate (Hermitian). In the following subsections, we summarize several models for the eigenspectrum and SCN's of $\mathbf{W}$ with $\mathbf{H}$ given either as (4.2a) or (4.2b). For clarity we shall denote the corresponding probability density functions (PDF's) and cumulative distribution functions (CDF's) by p and P under $\mathcal{H}_0$, $\mathcal{H}_1^{\mathrm{c}}$ and $\mathcal{H}_1^{\mathrm{r}}$, respectively.

Finally, without loss of generality[3], all discussions hereafter are for the case $K \leqslant N$ such that $\mathbf{W}$ is full-rank.

4.2.2 Asymptotic Models for the Eigenspectrum Distribution

4.2.2.1 Under $\mathcal{H}_0$ - The Marchenko-Pastur Model

The Marchenko-Pastur law [46], which models the asymptotic eigenspectrum of $\mathbf{W}$ under $\mathcal{H}_0$, can be concisely stated as follows.

Lemma 2 (Marchenko-Pastur CDF)**.**

$$P_{\mathrm{MP}}(r;\rho) \triangleq \int_{\lambda_{\mathrm{L}}}^{r} p_{\mathrm{MP}}(x;\rho)\mathrm{d}x = \tfrac{1}{2} + p_{\mathrm{MP}}(r;\rho) + \tfrac{(1-\rho)}{2\pi}\mathrm{asin}\left(\tfrac{1+\rho}{2\sqrt{\rho}} - \tfrac{(1-\rho)^2}{2r\sqrt{\rho}}\right) + \tfrac{(1+\rho)}{2\pi}\mathrm{asin}\left(\tfrac{1+\rho}{2\sqrt{\rho}} - \tfrac{r}{2\sqrt{\rho}}\right). \tag{4.3}$$

[3]This avoids the unnecessary notational care to handle null eigenvalues.

Proof: Let $R \triangleq -r^2 + 2(1+\rho)r - (1-\rho)^2$. Then, it is clear from (A-1) that the integral in equation (4.3) relates to [79, Eq. 2.267.1]

$$F(r) \triangleq \int \frac{\sqrt{R}}{r}\mathrm{d}r = \sqrt{R} + a\int \frac{\mathrm{d}r}{r\sqrt{R}} + \frac{b}{2}\int \frac{\mathrm{d}r}{\sqrt{R}}, \tag{4.4}$$

where $a = -(1-\rho)^2 < 0$ and $b = 2(1+\rho) > 0$.

The integrals on the righthand-side of equation (4.4) have closed-form solutions found in [79, Eq. 2.266 and Eq. 2.261], respectively, which yield

$$I_1(r;\rho) \triangleq a\int \frac{\mathrm{d}r}{r\sqrt{R}} = (1-\rho)\cdot\mathrm{asin}\left(\tfrac{(1+\rho)r-(1-\rho)^2}{2r\sqrt{\rho}}\right), \tag{4.5}$$

$$I_2(r;\rho) \triangleq \frac{b}{2}\int \frac{\mathrm{d}r}{\sqrt{R}} = -(1+\rho)\cdot\mathrm{asin}\left(\tfrac{2(1+\rho)-2r}{4\sqrt{\rho}}\right). \tag{4.6}$$

Thus, from equations (A-1), (4.4), (4.5) and (4.6) we obtain

$$F(r) = p_{\text{MP}}(r;\rho) + (1-\rho)\cdot\mathrm{asin}\left(\tfrac{(1+\rho)r-(1-\rho)^2}{2r\sqrt{\rho}}\right) - (1+\rho)\cdot\mathrm{asin}\left(\tfrac{2(1+\rho)-2r}{4\sqrt{\rho}}\right), \tag{4.7}$$

It follows that the Marchenko-Pastur CDF is given by

$$P_{\text{MP}}(r;\rho) = \tfrac{1}{2\pi}F(r) - \tfrac{1}{2\pi}F(\lambda_{\text{L}}). \tag{4.8}$$

Finally, notice that $p_{\text{MP}}(\lambda_{\text{L}};\rho) = 0$, $I_1(\lambda_{\text{L}};\rho) = -\pi/2$ and $I_2(\lambda_{\text{L}};\rho) = \pi/2$, such that equation (4.8) reduces to equation (4.3) after some algebra.

4.2.2.2 Under $\mathcal{H}_1$ - The Scaled and Extended Marchenko-Pastur Models

The eigenspectrum distributions of $\mathbf{W}$ under $\mathcal{H}_1$ differs depending on whether the PU signal is random or constant. In the first case, the following result applies.

Corollary 1 (Scaled Marchenko-Pastur PDF)**.**

Let $\lambda|_{\mathcal{H}_1^{\text{r}}}$ *denote any eigenvalue of* $\mathbf{W}$*, with* $\mathbf{H}$ *as in equation* (4.2b) *and* $\mathbf{H}_s \sim \mathcal{N}_{\mathbb{C}^{K\times N}}(0,1)$*. Then,*

$$\lim_{\substack{(K,N)\to\infty \\ N/K=\rho>1}} \lambda|_{\mathcal{H}_1^{\text{r}}} \sim p_{\text{MP}}^{(s)}(r;\rho,\beta) \triangleq \frac{1}{1+\beta}\cdot p_{\text{MP}}(r/(1+\beta);\rho). \tag{4.9}$$

Proof: Since $\mathbf{H}_n \sim \mathcal{N}_{\mathbb{C}^{K\times N}}(0,1)$, if $\mathbf{H}_s \sim \mathcal{N}_{\mathbb{C}^{K\times N}}(0,1)$ then $\mathbf{H} \sim \mathcal{N}_{\mathbb{C}^{K\times N}}(0,1+\beta)$. Consequently $\lambda|_{\mathcal{H}_1^{\text{r}}}$ behaves as $(1+\beta)\cdot\lambda|_{\mathcal{H}_0}$. In other words, $\lambda|_{\mathcal{H}_1^{\text{r}}}$ is equivalent to a *scaled* MP-variate, with scaling coefficient $(1+\beta)$, which immediately yields equation (4.9).

The distribution $p_{\text{MP}}^{(s)}(r;\rho,\beta)$, which is clearly suitable to Rayleigh fading case, will be henceforth referred to as the *type*-0 model for $\lambda|_{\mathcal{H}_1^{\text{r}}}$.

Corollary 2 (Scaled Marchenko-Pastur CDF)**.**

$$P_{\text{MP}}^{(s)}(r;\rho,\beta) \triangleq \int_0^r p_{\text{MP}}^{(s)}(x;\rho,\beta)\mathrm{d}x = \tfrac{1}{2\pi}F\left(\tfrac{r}{1+\beta}\right) + \tfrac{1}{2}. \tag{4.10}$$

Proof: The result follows immediately from Lemmas 2 and Corollary 1.

The distribution of $\lambda|_{\mathcal{H}_1^{\text{r}}}$ with a constant PU signal is governed by the following result.

Lemma 3 (Extended Marchenko-Pastur PDF)**.**

Let $\lambda|_{\mathcal{H}_1^{\text{c}}}$ *denote any eigenvalue of* $\mathbf{W}$*, with* $\mathbf{H}$ *as in equation* (4.2b) *and* $\mathbf{H}_s = s\cdot\mathbf{1}_{K\times N}$*, where* $\mathbf{1}_{K\times N}$ *is a matrix whose elements are all* 1*'s, while* s *is an unknown complex constant with* $|s| = 1$*. Then,*

$$\lim_{\substack{(K,N)\to\infty\\ N/K=\rho>1}} \lambda|_{\mathcal{H}_1^{\text{c}}} \sim p_{\text{MP}}^{(e)}(r;\rho,\beta) \triangleq \lim_{\substack{(K,N)\to\infty\\ N/K=\rho>1}} \frac{K-1}{K}p_{\text{MP}}(r;\rho) + \frac{\delta(r-N\cdot\beta)}{K}, \tag{4.11}$$

where $\delta(r)$ *is the Dirac delta function and* $\beta > 0$*.*

Proof: Start with the Law of Large numbers [80] which yields, under a constant $\mathbf{H}_s$ and a zero-mean $\mathbf{H}_n$, $\mathbf{W} = \frac{1}{K}(\sqrt{\beta}\cdot\mathbf{H}_s + \mathbf{H}_n)\cdot(\sqrt{\beta}\cdot\mathbf{H}_s + \mathbf{H}_n)^\dagger = \frac{1}{K}(\beta\cdot\mathbf{H}_s\cdot\mathbf{H}_s^\dagger + \mathbf{H}_n\cdot\mathbf{H}_n^\dagger)$.

Obviously the matrix $\frac{\beta}{K}\cdot\mathbf{H}_s\cdot\mathbf{H}_s^\dagger$ has a single non-zero eigenvalue given by $N\cdot\beta$, while the eigenvalues of the matrix $\mathbf{W}_n \triangleq \frac{1}{K}\cdot\mathbf{H}_n\cdot\mathbf{H}_n^\dagger$ are MP-variates.

For convenience, let us denote the k-th largest eigenvalues of $\mathbf{W}$ and $\mathbf{W}_n$ respectively by $\lambda_k(\mathbf{W})$ and $\lambda_k(\mathbf{W}_n)$, such that $0 < \lambda_1(\mathbf{W}) \leqslant \lambda_1(\mathbf{W}) \leqslant \cdots \leqslant \lambda_K(\mathbf{W})$ and likewise $0 < \lambda_1(\mathbf{W}_n) \leqslant \lambda_1(\mathbf{W}_n) \leqslant \cdots \leqslant \lambda_K(\mathbf{W}_n)$.

Next, invoke the refined Wenyl bounds recently derived in [81, Eq. (2.3)], which yield

$$\lambda_k(\mathbf{W}_n) \leqslant \lambda_k(\mathbf{W}) \leqslant \lambda_{k+1}(\mathbf{W}_n), \quad \forall\, 1 \leqslant k \leqslant K-1. \tag{4.12}$$

The latter bound indicates that the k-th eigenvalue of $\mathbf{W}$ is "trapped" between the k-th and $k+1$-th eigenvalues of $\mathbf{W}_n$, with probability 1 as $K\to\infty$. But it has also been recently shown [82] that the mean gap between consecutive eigenvalues of large $K\times K$ random Hermitian matrices is given by $1/\sqrt{K}$, and consequently the implication of inequality (4.12) is that the distribution of the set of eigenvalues $\{\lambda_1(\mathbf{W}),\cdots,\lambda_{K-1}(\mathbf{W})\}$ converges in probability to the distribution of the set $\{\lambda_1(\mathbf{W}_n),\cdots,\lambda_K(\mathbf{W}_n)\}$, which is $p_\lambda(r;\rho)$, as *per* Theorem 4.

It is left to show that the asymptotic distribution of $\lambda_K(\mathbf{W})$ converges in probability to $\delta(r - N \cdot \beta)$. To this end, invoke the recent result on the distribution of spiked eigenvalues [83], from which the expected value of λ_K is given by

$$\mathrm{E}[\lambda_K(\mathbf{W})] = \tfrac{1}{N \cdot \beta}(N \cdot \beta + 1)^2 \underset{N \gg 1/\beta}{\longrightarrow} N \cdot \beta. \tag{4.13}$$

Consequently,

$$\lim_{K \to \infty} \lambda_K(\mathbf{W}) \to N \cdot \beta, \tag{4.14}$$

which means that the distribution of $\lambda_K(\mathbf{W})$ is $\delta(r - N \cdot \beta)$, concluding the proof.

Interpreting Lemma 3 requires care. First, as clarified in the Lemma's statement, the result requires that SNR is strictly non-zero. Otherwise we are obviously in the case discussed in subsection 4.2.2.1. And secondly, the Lemma establishes that for *any* $\beta > 0$, the largest eigenvalue of $\mathbf{W}$ converges, with probability 1, to $\lambda_K = N \cdot \beta \to \infty$ as the dimension K of $\mathbf{W}$ grows unboundedly.

What matters, however, is that in that the distributions of $\lambda|_{\mathcal{H}_1}$ differ substantially depending on whether the PU signal is random or constant. In particular, in the latter case, Lemma 3 implies that there exists a pair critical values of β below which the "constant" eigenvalue located at $n \cdot \beta$ falls inside the range $(\lambda_{\mathrm{L}}, \lambda_{\mathrm{U}})$. Consequently, it can be expected that the presence of a constant PU signal with SNR in the range

$$\frac{(1 - \sqrt{\rho})^2}{N} \leqslant \beta \leqslant \frac{(1 + \sqrt{\rho})^2}{N}, \tag{4.15}$$

cannot be identified with basis on the eigenvalues of $\mathbf{W}$.

For completeness, let us conclude this subsection with the following corollary.

Corollary 3 (Extended Marchenko-Pastur CDF)**.**

$$P_{\mathrm{MP}}^{(e)}(r; \rho, \beta) \triangleq \int_0^r p_{\mathrm{MP}}^{(e)}(x; \rho, \beta)\mathrm{d}x = \lim_{\substack{(K,N) \to \infty \\ N/K = \rho > 1}} \frac{K-1}{K} P_{\mathrm{MP}}(r; \rho) + \frac{u(r - N \cdot \beta)}{K}, \tag{4.16}$$

where $u(r)$ is the unitary step function.

Proof: The result is an immediate consequence of Lemma 3.

4.2.3 Asymptotic Extreme-value Models for the Eigenspectrum Distribution

4.2.3.1 Under $\mathcal{H}_1$ - The Scaled and Extended Tracy-Widom Models

In this subsection we shall follow similar steps to those of the preceding subsection and give a summary of the asymptotic extreme value models for $\mathbf{W}$ originated from sample matrices $\mathbf{H}$ constructed in the presence of PU signal, as defined in equation (4.2b).

Corollary 4 (Scaled Tracy-Widom PDF and CDF)**.**
Consider the centralized and normalized extreme eigenvalues of $\mathbf{W} \triangleq \mathbf{H}\cdot\mathbf{H}^{\dagger}$ *defined below, with* $\mathbf{H}$ *as in equation* (4.2b) *and* $\mathbf{H}_s \sim \mathcal{N}_{\mathbb{C}^{K\times N}}(0,1)$,

$$\bar{\lambda}_K|_{\mathcal{H}_1^{\mathrm{r}}} \triangleq \frac{\lambda_K - (1+\beta)\lambda_{\mathrm{U}}}{(1+\beta)\nu}, \tag{4.17}$$

$$\bar{\lambda}_1|_{\mathcal{H}_1^{\mathrm{r}}} \triangleq \frac{\lambda_1 - (1+\beta)\lambda_{\mathrm{L}}}{(1+\beta)\mu}, \tag{4.18}$$

where μ *and* ν *are as given in Theorem 5.*

Then

$$\lim_{\substack{(K,N)\to\infty \\ N/K=\rho>1}} \bar{\lambda}|_{\mathcal{H}_1^{\mathrm{r}}} \sim p_{\mathrm{TW}}(r) \triangleq \frac{\mathrm{d}P_{\mathrm{TW}}(r)}{\mathrm{d}r}. \tag{4.19}$$

Proof: The result is an immediate consequence of Corollary 1 and Theorem 5.

Lemma 4 (Extended Tracy-Widom PDF and CDF)**.**
Let $\lambda_K|_{\mathcal{H}_1^{\mathrm{c}}}$ *denote the largest eigenvalue of* $\mathbf{W} \triangleq \mathbf{H}\cdot\mathbf{H}^{\dagger}$*, with* $\mathbf{H}$ *as in equation* (4.2b) *and a constant* $\mathbf{H}_s = s\cdot\mathbf{1}_{K\times N}$*, where* $\mathbf{1}_{K\times N}$ *is a matrix whose elements are all* 1*'s, while* s *is an unknown complex constant with* $|s| = 1$*. Consider also the centralized and normalized smallest eigenvalue of* $\mathbf{W}$ *defined by*

$$\bar{\lambda}_1|_{\mathcal{H}_1^{\mathrm{c}}} \triangleq \frac{\lambda_1 - \lambda_{\mathrm{L}}}{\mu}, \tag{4.20}$$

where μ *is as given in Theorem 5.*

Then

$$\lim_{\substack{(K,N)\to\infty \\ N/K=\rho>1}} \lambda_K|_{\mathcal{H}_1^{\mathrm{c}}} \sim \delta(r - N\cdot\beta), \tag{4.21}$$

$$\lim_{\substack{(K,N)\to\infty \\ N/K=\rho>1}} \bar{\lambda}_1|_{\mathcal{H}_1^{\mathrm{c}}} \sim p_{\mathrm{TW}}(r) \triangleq \frac{\mathrm{d}P_{\mathrm{TW}}(r)}{\mathrm{d}r}. \tag{4.22}$$

Proof: The result is an immediate consequence of Lemma 3 and Theorem 5.

4.2.4 Asymptotic Models for the Distribution of Standard Condition Numbers

It has been recently noted [42] that an asymptotic model for the SCN's of complex Wishart matrices can be constructed with basis on the results of Theorem 5 and a

general result on the distribution of the ratio of random variates due to Curtiss [50].

In this subsection we shall revise the results of [42] in light of the distinct extreme-value distributions yielded under $\mathcal{H}_1^{\mathrm{r}}$ and $\mathcal{H}_1^{\mathrm{c}}$.

Before we proceed, let us point out that while the parameters K and N are, rigorously speaking ∞ since the results to follow are all asymptotic, the expressions to be given are typically evaluated for *finite* (large) matrices. Consequently, for the sake of clarity and coherence we shall commit a slight abuse of notation by maintaining K and N, when application, in the formulas.

4.2.4.1 Under $\mathcal{H}_1$ - The Scaled and Extended Tracy-Widom-Curtiss Models

The scaled and extended TWC distributions are given as follows.

Corollary 5 (Scaled Tracy-Widom-Curtiss PDF and CDF)**.**
Let $\xi_K|_{\mathcal{H}_1^{\mathrm{r}}}$ denote the SCN of $\mathbf{W} \triangleq \mathbf{H} \cdot \mathbf{H}^{\dagger}$, with $\mathbf{H}$ constructed in the presence of random *PU signals as shown in equation* (4.2b) *with $\mathbf{H}_s \sim \mathcal{N}_{\mathbb{C}^{K\times N}}(0,1)$. Denote the largest and smallest eigenvalues of $\mathbf{W}$ in this case by $\lambda_K|_{\mathcal{H}_1^{\mathrm{r}}}$ and $\lambda_1|_{\mathcal{H}_1^{\mathrm{r}}}$ respectively, such tha $\xi_K|_{\mathcal{H}_1^{\mathrm{r}}} \triangleq \frac{\lambda_K|_{\mathcal{H}_1^{\mathrm{r}}}}{\lambda_1|_{\mathcal{H}_1^{\mathrm{r}}}}$. Then*

$$\xi_K|_{\mathcal{H}_1^{\mathrm{r}}} \sim p_{\mathrm{TWC}}(r;\mu,\nu,\lambda_L,\lambda_U), \tag{4.23}$$

and its CDF is the same as in equation (A-9)*.*

Proof: First notice that under the same arguments of those in Corollary 1

$$\lambda_K|_{\mathcal{H}_1^{\mathrm{r}}} \triangleq (1+\beta)\lambda_{\mathrm{U}}, \tag{4.24}$$

$$\lambda_1|_{\mathcal{H}_1^{\mathrm{r}}} \triangleq (1+\beta)\lambda_{\mathrm{L}}. \tag{4.25}$$

Then, since the scaling coefficients $(1+\beta)$ cancel out, the results follow immediately from Theorem 6 and Corollary 7.

Lemma 5 (Extended Tracy-Widom-Curtiss PDF (high SNR))**.**
Let $\xi_K|_{\mathcal{H}_1^{\mathrm{c}}} \triangleq \frac{\lambda_K|_{\mathcal{H}_1^{\mathrm{c}}}}{\lambda_1|_{\mathcal{H}_1^{\mathrm{c}}}}$ denote the SCN of $\mathbf{W} \triangleq \mathbf{H} \cdot \mathbf{H}^{\dagger}$ constructed in the presence of a constant *PU signal, that is, with $\mathbf{H}$ as in equation* (4.2b) *and a $\mathbf{H}_s = s \cdot \mathbf{1}_{K\times N}$, where $\mathbf{1}_{K\times N}$ is a matrix whose elements are all 1's, while s is an unknown complex constant with $|s| = 1$. Furthermore, let the SNR ρ be sufficiently high such that*[4]

[4]In [43, Eq.(61) and (62)] distributions of $(rx-\kappa)\sqrt{N}/\tau$ for the cases when $\lambda_K \leqslant 1+\sqrt{\rho^{-1}}$ are also given,

$\lambda_K|_{\mathcal{H}_1^c} > 1+\sqrt{\rho^{-1}}$. *Then,*

$$\xi_K|_{\mathcal{H}_1^c} \sim p^{(e)}_{\text{TWC}}(r;\tilde{\mu},\tilde{\nu},\kappa,\tau) \triangleq \frac{N^{7/6}}{\tau\tilde{\nu}} \int_0^{\infty} x p_{\text{Gauss}}\left(\frac{(r\cdot x-\kappa)\sqrt{N}}{\tau}\right)\cdot p_{\text{TW}}\left(\frac{(\tilde{\mu}-x)N^{2/3}}{\tilde{\nu}}\right) \mathrm{d}x, \tag{4.26}$$

where $p_{\text{Gauss}}(r)$ *is standard Normal distribution and*[5]

$$\tilde{\mu} \triangleq \frac{\left(\sqrt{N}-\sqrt{K-1}\right)^2}{K}, \tag{4.27}$$

$$\tilde{\nu} \triangleq \frac{\left(\sqrt{N}-\sqrt{K-1}\right)^{4/3}}{\sqrt{N}\cdot\sqrt[6]{K-1}}, \tag{4.28}$$

$$\kappa \triangleq \frac{\beta+1}{\beta}\left(\beta+\rho^{-1/2}\right), \tag{4.29}$$

$$\tau \triangleq \frac{\beta+1}{\beta}\sqrt{\beta^2-\rho^{-\frac{1}{2}}}. \tag{4.30}$$

Proof: The standard normality of the scaled and normalized largest eigenvalue of Wishart matrices constructed as indicated in the statement of the Lemma was established in [64, 71]. Specifically, it was shown thereby, with basis on the spiked population model of [83], that under the condition $\lambda_K|_{\mathcal{H}_1^c} > 1+\sqrt{\rho^{-1}}$,

$$\lim_{\substack{(K,N)\to\infty \\ N/K=\rho>1}} \frac{1}{\tau}\cdot(\lambda_K|_{\mathcal{H}_1^c}-\kappa)N^{1/2} \sim \mathcal{N}(0,1). \tag{4.31}$$

Likewise, it has been shown in [48, 62] that

$$\lim_{\substack{(K,N)\to\infty \\ N/K=\rho>1}} \frac{1}{\tilde{\nu}}\cdot(\tilde{\mu}-\lambda_1|_{\mathcal{H}_1^c})N^{2/3} \sim p_{\text{TW}}(r). \tag{4.32}$$

The result in equation (4.26) then follows by applying Curtiss formula [50, Eq. (3.2)].

Corollary 6 (Extended Tracy-Widom-Curtiss CDF)**.**

$$P^{(e)}_{\text{TWC}}(r;\kappa,\tau,\tilde{\mu},\tilde{\nu}) = \int_{\frac{-N^{2/3}\cdot\tilde{\mu}}{\tilde{\nu}}}^{\infty} p_{\text{TW}}(-x)\cdot Q\left(\frac{1}{\tau}\cdot\left(r\cdot(\tilde{\mu}+\tfrac{\tilde{\nu}}{N^{2/3}}x)-\kappa\right)\sqrt{N}\right)\mathrm{d}x, \tag{4.33}$$

where Q *is the Gaussian Q-function.*

which if replaced for $p_{\text{Gauss}}(r)$ would immediately lead to corresponding alternative distributions of $\xi_K|_{\mathcal{H}_1^c}$ in the same form of equation (4.26). In the context of our chapter, however, these are unnecessary since it will be ultimately shown that the finite random matrices models introduced in Section 4.3 are superior to the asymptotic ones discussed here.

[5] In general, $\tilde{\mu}$ and $\tilde{\nu}$ can be defined as $\tilde{\mu} \triangleq \frac{\left(\sqrt{N}-\sqrt{K-U}\right)^2}{K}$ and $\tilde{\nu} \triangleq \frac{\left(\sqrt{N}-\sqrt{K-U}\right)^{4/3}}{\sqrt{N}\cdot\sqrt[6]{K-U}}$, where U denotes the number of PU's, such that the result can be extended to multiple PU's.

Table 4.1: Asymptotic Random Matrix Models for Spectrum Sensing

Variable	**Signal Absent:** $\mathcal{H}_0$		**Signal Random:** $\mathcal{H}_1^r$		**Signal Constant:** $\mathcal{H}_1^c$	
	PDF	CDF	PDF	CDF	PDF	CDF
All Eigenvalues: λ	Theorem 4	Lemma 2 [a]	Corollary 1	Corollary 2 [a]	Lemma 3 [a]	Corollary 3 [a]
Ext. Eigenvalues:	Theorem 5		Corollary 4		Lemma 4	
SCN: ξ_K	Theorem 6	Corollary 7 [a]	Corollary 5		Lemma 5 [a]	Corollary 6 [a,b]

[a] New result.

[b] For high SNR.

Proof: The result follows directly by integration of equation (4.26) from Lemma 5, with steps similar to those of the proof of Corollary 7.

4.2.5 Summary and Comments on Asymptotic-RMT Spectrum Sensing Algorithms

In this subsection we summarize relevant results on asymptotic random matrices and briefly discuss their application to spectrum sensing. For convenience, the results of subsections 4.2.2 and 4.2.3 are gathered in Table 4.1.

The table also allows a quick identification of the new contributions made thereby. Specifically, the closed-form expression of the Marchenko-Pastur CDF given in Lemma 2; and the corresponding scaled variation given in Corollary 2 are new. So are the density and distribution of the eigenvalues of the sum of a constant and a random Wishart matrix (*i.e.*, the *extended* MP PDF and CDF) given in Lemma 3 and Corollary 3. Likewise, the simplified expression of the CDF of the SCN of Wishart matrices based on the Tracy-Widom extreme-value distributions and the Curtiss formulas given in Corollary 7 as well as the *extended* TWC PDF and CDF that model the case when a constant PU signal is present, given respectively in Lemma 5 and Corollary 6, are minor, but novel contributions.

The key functions, such as CDF's and parameters such as Test Statistic ζ and Threshold γ, required to design Hypothesis Tests for spectrum sensing with basis on the models described above given a prescribed probability of false-alarm α or probability of miss-detection δ are summarized in Table 4.4.

Table 4.2: Spectrum Sensing Algorithms from Random Matrix Theory

	Method	Test Statistic ζ	Threshold γ	CDF $P(r)$ [a]
$\mathcal{H}_0$ Test	Marchenko Pastur	$\lambda_K\vert_{\mathcal{H}_0}$	$\frac{(1+\sqrt{\rho})^2}{(1-\sqrt{\rho})^2}$	$P_{\mathrm{MP}}(r)=\frac{1}{2}+p_{\mathrm{MP}}(r;\rho)+\frac{(1-\rho)}{2\pi}\operatorname{asin}\left(\frac{1+\rho}{2\sqrt{\rho}}-\frac{(1-\rho)^2}{2r\sqrt{\rho}}\right)+\frac{(1+\rho)}{2\pi}\operatorname{asin}\left(\frac{1+\rho}{2\sqrt{\rho}}-\frac{r}{2\sqrt{\rho}}\right)$
	Tracy Widom	$\bar{\lambda}_K\vert_{\mathcal{H}_0}$	$\frac{N+K+2\sqrt{NK}}{N+K-2\sqrt{NK}}\cdot\left[1+\frac{P_{\mathrm{TW}}^{-1}(1-\alpha)}{\sqrt[3]{(\sqrt{N}+\sqrt{K})^2\sqrt{NK}}}\right]$	$P_{\mathrm{TW}}(r)=\exp\left(-\int_r^\infty(x-r)q^2(x)\mathrm{d}x\right)$
	Tracy Widom Curtiss	$\xi_K\vert_{\mathcal{H}_0}$	$P_{\mathrm{TWC}}^{-1}(1-\alpha)$	$P_{\mathrm{TWC}}(r)=\int_{\frac{\lambda_L}{\mu}}^{\infty}p_{\mathrm{TW}}(-z)\cdot P_{\mathrm{TW}}\left(\frac{r\cdot(\lambda_L-\mu\cdot z)-\lambda_U}{\nu}\right)\mathrm{d}z$
	Finite RMT (Proposed)	$\xi_2\vert_{\mathcal{H}_0}$	$P_{\mathrm{M}}^{-1}(1-\alpha)$	$P_{\mathrm{M}}(r)=\frac{S_2(r;N)-S_2(1;N)}{2(N-1)!(N-2)!}$ [b]
$\mathcal{H}_1$ Test	Extended Tracy Widom Curtiss	$\xi_K\vert_{\mathcal{H}_1^c}$	$P_{\mathrm{TWC}}^{(e)-1}(\delta)$	$P_{\mathrm{TWC}}^{(e)}(r)=\int_{\frac{-\tilde{\mu}}{\tilde{\nu}}N^{2/3}}^{\infty}p_{\mathrm{TW}}(-x)\cdot Q\left(\frac{\left(r\cdot(\tilde{\mu}+\frac{\tilde{\nu}}{N^{2/3}}x)-\kappa\right)\sqrt{N}}{\tau}\right)\mathrm{d}x$
	Finite RMT (Proposed)	$\xi_2\vert_{\mathcal{H}_1^c}$	$P_{\mathrm{M}}^{(e)-1}(\delta)$	$P_{\mathrm{M}}^{(e)}(r)=\Phi(N,\theta_1,\theta_2)(S_4(r;N,\theta_1,\theta_2)-S_4(1;N,\theta_1,\theta_2))$ [c]

[b] For conciseness, a slight abuse of notation is committed by omitting the parameters of each distribution

[b] See equations (4.36) through (4.37)

[c] See equations (4.41) and (4.42) through (4.44)

The corresponding functions and parameters required to design equivalent spectrum sensing algorithms with basis on the Finite Random Matrix models to be discussed in Section 4.3 are also included for conciseness and future reference.

The performances of these algorithms are compared in Fig. 4.4 and Fig. 4.8.

All comparisons were evaluated via Monte-Carlo simulations assuming a constant complex signal[6] and random circular complex AWGN according to the model shown in (4.2). Leaving aside the proposed method for the time being, it can be seen that amongst the techniques relying on asymptotic random matrix models, the TWC-based algorithms (*e.g.* [42, 43]) are generally superior to TW-based algorithms (*e.g.* [36]), which in turn outperform MP-based algorithms (*e.g.* [41]).

The underperformance of the MP-based algorithm results from the inaccuracy of the model with small sample sizes. To illustrate, the Marchenko-Pastur limiting distribution is compared in Fig. 4.5 against exact equivalents introduced later in

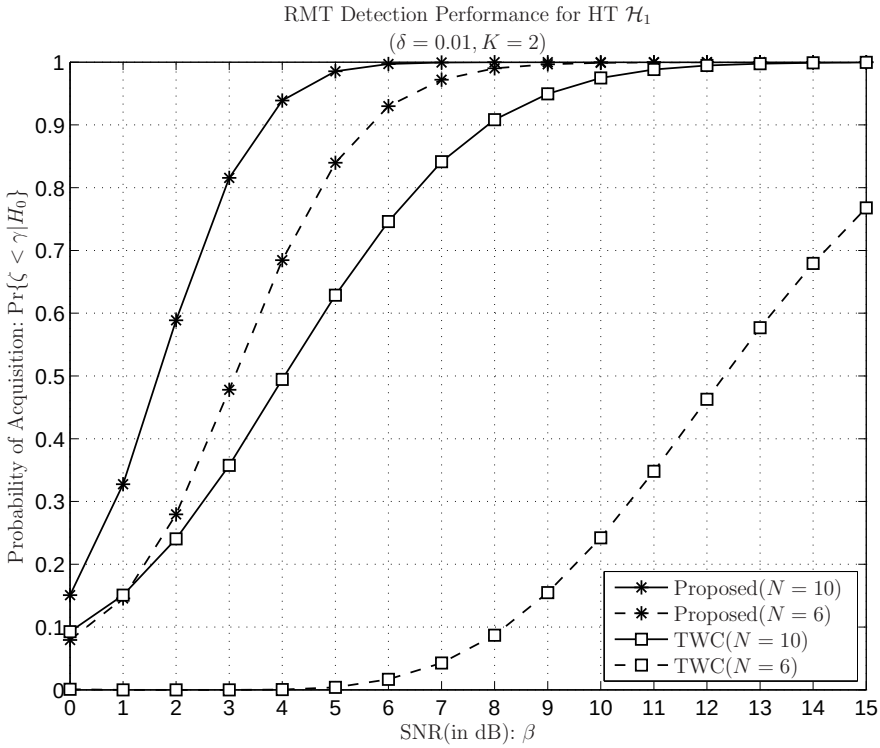

Figure 4.3: PD Versus SNR. Probability of Acquisition of spectrum sensing algorithms based on finite random matrix (proposed), as a function of the SNR and the tolerated probability of false-alarm.

Lemma 8.

The figure shows that the Marchenko-Pastur model is sufficiently accurate only of the number of samples ($K \times N$) is in the order of thousands.

It must be noticed, however, that the densities and distribution functions given in Theorem 6, Lemma 5 and Corollaries 7 and 6 are hard to evaluate, which is in stark contrast with the simplicity of the classic Marchenko-Pastur models of subsection 4.2.2. In other words, the improvement achieved by moving from MP-based to TW-based to TWC-based methods comes at the expense of an increase in complexity and a loss of mathematical tractability.

Nevertheless, an interesting connection between the MP-based technique proposed in [41, Sec. III-B] and the TWC-based technique using SCN's as proposed in [42, 43], is that **neither** require the knowledge of noise power, although the MP-based method has a fundamental limitation compared to the alternatives as it does not admit a tolerated probability of false alarm to be accommodated in the

[6]Results for the case of random U signals are similar.

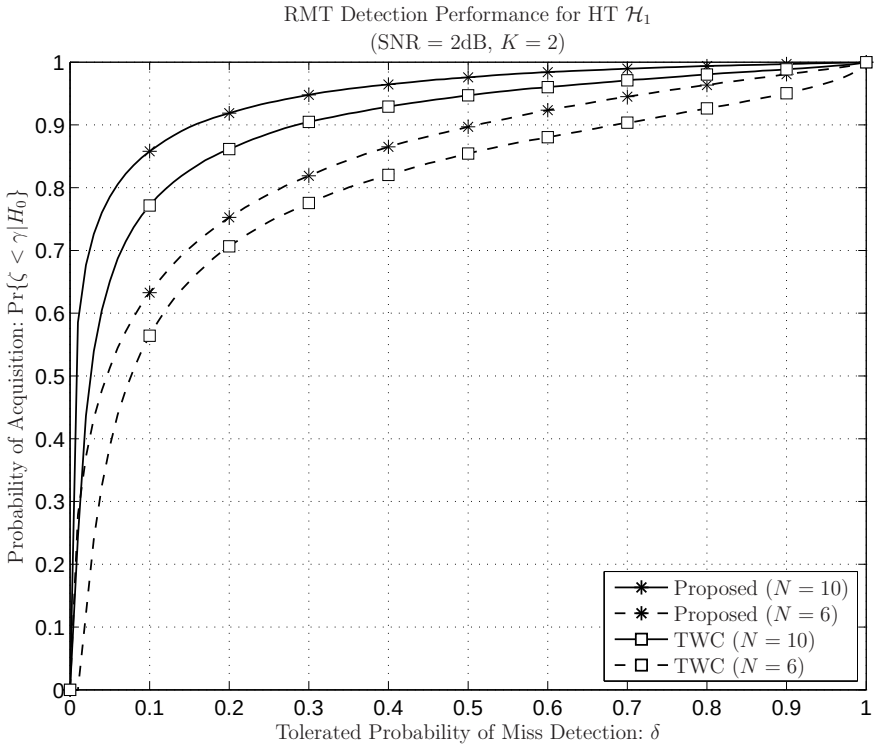

Figure 4.4: PD Versus PF. Probability of Acquisition of spectrum sensing algorithms based on finite random matrix (proposed), as a function of the SNR and the tolerated probability of false-alarm.

hypothesis test.

This blind feature is highly desirable since in situations where multiple wireless devices share a crowded spectrum, background noise levels vary with the number of users accessing the channel.

Unfortunately, this potential advantage is undermined by the fact that all the aforementioned methods require a large number of samples (large matrices), which in turn implies (contradictorily) that an accurate estimate of the average noise power can be obtained directly from the samples, with accuracy proportional to their number!

In conclusion, it is reasonable to say that in order to truly exploit the potential of random-matrix-theoretical approaches to blind spectrum sensing, novel techniques requiring a *limited* number of samples is required. This is the subject of the subsequent section.

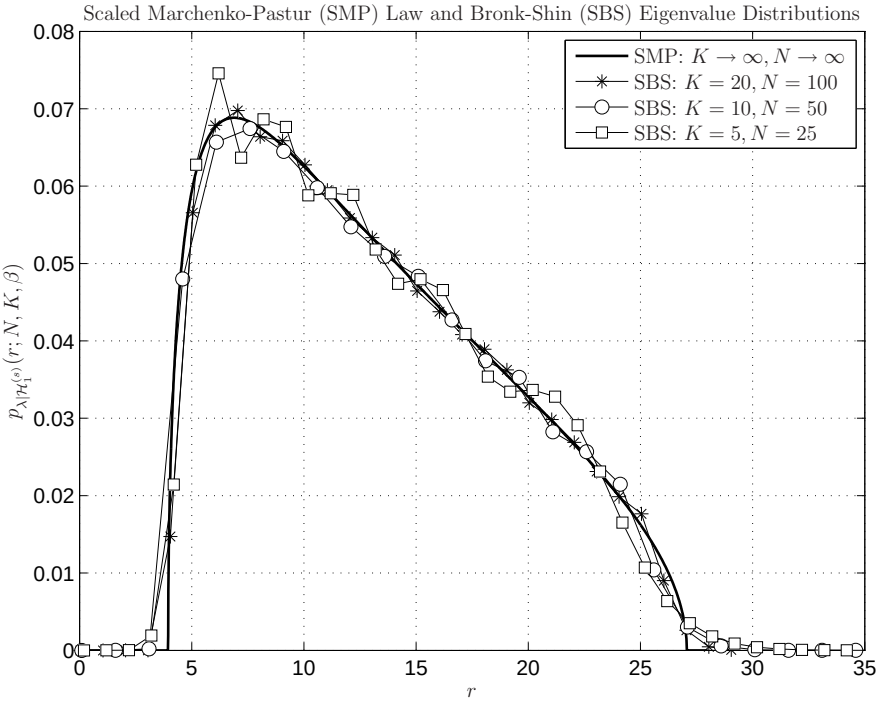

Figure 4.5: The Marchenko-Pastur asymptotic model for the eigenvalues of random Wishart matrices under $\mathcal{H}_1$ with a random PU signal, compared against corresponding exact distributions given in Lemma 8 for a few finite random Wishart matrices.

4.3 Finite Random Matrices EigenSpectrum and SCN Models

4.3.1 Finite Models for SCN Distribution

4.3.1.1 Under $\mathcal{H}_0$ - Distribution of SCN of Finite Uncorrelated Central Wishart Matrices

New results on the distribution of the SCN of finite complex random Wishart matrices have been recently reported in [51]. Amongst others, the following closed-form expressions for the distribution of the SCN of dual Wishart matrices are of particular relevance here.

Theorem 2 (PDF and CDF for Uncorrelated Central Wishart Matrix ($K = 2$))**.** *Let* $\xi_2|_{\mathcal{H}_0} \triangleq \lambda_2|_{\mathcal{H}_0}/\lambda_1|_{\mathcal{H}_0} \geqslant 1$ *denote the SCN of* dual *uncorrelated central Wishart matrices* $\mathbf{W}$*, with* $\mathbf{H}$ *as in equation* (4.2a)*.*

Then

$$\xi_2|_{\mathcal{H}_0} \sim p_{\text{M}}(r;N) \triangleq \frac{S_1(r;N)}{2(N-1)!(N-2)!}, \tag{4.34}$$

$$P_{\text{M}}(r;N) = \frac{S_2(r;N) - S_2(1;N)}{2(N-1)!(N-2)!}, \tag{4.35}$$

where

$$S_i(r;N) \triangleq \Delta_i(r;N,N-1) - 2\Delta_i(r;N-1,N) + \Delta_i(r;N-2,N+1), \tag{4.36}$$

with $i = \{1,2\}$ *and*

$$\Delta_1(r;M,N) \triangleq \frac{(N-1)!}{(r+1)^2}\left[\sum_{n=0}^{N-1}\frac{(M+1-\frac{n}{r})r^n}{(r+1)^n}\prod_{m=1}^{M}\frac{n+m}{r+1}\right].$$

$$\Delta_2(r;M,N) \triangleq (N-1)!\left[M! - \frac{1}{r+1}\sum_{n=0}^{N-1}\frac{r^n}{(r+1)^n}\prod_{m=1}^{M}\frac{n+m}{r+1}\right].$$

Proof: Provided in [51].

4.3.1.2 Under $\mathcal{H}_1$ - Scaled and Extended SCN Distributions

The scaled and extended SCN distributions are given as follows.

Lemma 6 (Scaled SCN Model)**.**

Let $\xi_2|_{\mathcal{H}_1^r} \triangleq \lambda_2|_{\mathcal{H}_1^r}/\lambda_1|_{\mathcal{H}_1^r} \geqslant 1$ *denote the SCN of* dual *uncorrelated central wishart matrices* $\mathbf{W}$*, with* $\mathbf{H}$ *as in equation* (4.2b) *and* $\mathbf{H}_s \sim \mathcal{N}_{\mathbb{C}^{K\times N}}(0,\beta)$*. Then,*

$$\xi_2|_{\mathcal{H}_1^r} \sim p_{\text{M}}(r;N), \tag{4.37}$$

$$\Pr\{\xi_2|_{\mathcal{H}_1^r} \leqslant r\} = P_{\text{M}}(r;N). \tag{4.38}$$

Proof: Clearly $\lambda_k|_{\mathcal{H}_1^r}$ follows the same distribution of $\lambda_k|_{\mathcal{H}_0}$ – which incidentally can be found in [66, 72, 84] scaled by $(1+\beta)$. Consequently, $\lambda_2|_{\mathcal{H}_1^r}/\lambda_1|_{\mathcal{H}_1^r}$ follows the same distribution of $\lambda_2|_{\mathcal{H}_0}/\lambda_1|_{\mathcal{H}_0}$, concluding the proof.

Lemma 7 (Non-central and Semi-correlated Wishart Matrices)**.**
Let $\tilde{\mathbf{W}} = \tilde{\mathbf{S}}\cdot\tilde{\mathbf{S}}^\dagger$ *be a* non-central *Wishart matrix with* $\tilde{\mathbf{S}} \in \mathbb{C}^{K\times N}$*,* $\text{E}[\tilde{\mathbf{W}}] = \mathbf{I}_K/(\beta+1)$

and $\mathrm{E}[\tilde{\mathbf{W}} \cdot \tilde{\mathbf{W}}] = \mathbf{\Omega}$. *Consider the* central *semi-correlated complex Wishart matrix* $\mathbf{W} = \mathbf{S} \cdot \mathbf{S}^{\dagger}$ *with* $\mathbf{S} \in \mathbb{C}^{K \times N}$ *and effective covariance*

$$\mathbf{\Sigma}_K = \frac{\mathbf{I}_K}{\beta + 1} + \frac{\beta \cdot \mathbf{\Omega}}{(\beta + 1)N}. \tag{4.39}$$

Then, the first- and second-order moments of $\mathbf{W}$ *differ from those of* $\tilde{\mathbf{W}}$ *only by* $\mathbf{\Omega}/N$.

Proof: Provided in [76]

Lemma 7 presents a way to approximate the complex non-central Wishart matrix with the complex semi-correlated central Wishart matrix. In light of this result, the $\mathcal{H}_1$ test can be designed based on the properties of semi-correlated central Wishart matrices.

Theorem 3 (PDF and CDF for Semi-Correlated Central Wishart Matrix ($K = 2$))**.**

Let $\xi_2|_{\mathcal{H}_1^c} \triangleq \lambda_2|_{\mathcal{H}_1^c}/\lambda_1|_{\mathcal{H}_1^c} \geqslant 1$ *denote the SCN of* dual *semi-correlated central Wishart matrices* $\mathbf{W} \triangleq (\mathbf{\Sigma}_2^{1/2}\mathbf{H}) \cdot (\mathbf{\Sigma}_2^{1/2}\mathbf{H})^{\dagger}$ *with* $\mathbf{H}$ *as in equation* (4.2a)*, where* $\mathbf{\Sigma}_2$*, given in* (4.39)*, is the associated correlation matrix and* $\theta 1 > \theta 2$ *are its corresponding ordered eigenvalues. Then*

$$\xi_2|_{\mathcal{H}_1^c} \sim p_{\mathrm{M}}^{(e)}(r; N, \theta_1, \theta_2) \triangleq \frac{S_3(r; N, \theta_1, \theta_2)}{\Phi(N, \theta_1, \theta_2)}, \tag{4.40}$$

$$P_{\mathrm{M}}^{(e)}(r; N, \theta_1, \theta_2) = \frac{S_4(r; N, \theta_1, \theta_2) - S_4(1; N, \theta_1, \theta_2)}{\Phi(N, \theta_1, \theta_2)}, \tag{4.41}$$

where

$$\Phi(N, \theta_1, \theta_2) \triangleq \frac{(\theta_2 - \theta_1) \cdot (N-1)!(N-2)!}{(\theta_1 \cdot \theta_2)^{1-N}}, \tag{4.42}$$

and

$$S_i(r; N, \theta_1, \theta_2) \triangleq \Delta_i\left(r; N-1, N-1, \tfrac{1}{\theta_1}, \tfrac{1}{\theta_2}\right) - \Delta_i\left(r; N-2, N, \tfrac{1}{\theta_1}, \tfrac{1}{\theta_2}\right) - \Delta_i\left(r; N-1, N-1, \tfrac{1}{\theta_2}, \tfrac{1}{\theta_1}\right) + \Delta_i\left(r; N-2, N, \tfrac{1}{\theta_2}, \tfrac{1}{\theta_1}\right), \tag{4.43}$$

with $i = \{3, 4\}$ *and*

$$\Delta_3(r; M, N, \theta_1, \theta_2) \frac{(N-1)!}{(r + \theta_2)^{m+2}} \left[\sum_{n=0}^{N-1} \frac{(M + 1 - \frac{n}{r}) \cdot (\theta_1 \cdot r)^n}{(\theta_1 \cdot r + \theta_2)^n} \prod_{m=1}^{M} (n+m) \right],$$

$$\Delta_4(r; M, N, \theta_1, \theta_2) \triangleq \frac{(N-1)!}{\theta_1^N} \left[\frac{M!}{\theta_2^{M+1}} - \frac{1}{(\theta_1 \cdot r + \theta_2)^{M+1}} \sum_{n=0}^{N-1} \frac{(\theta_1 \cdot r)^n}{(\theta_1 \cdot r + \theta_2)^n} \prod_{m=1}^{M} (n+m) \right].$$

Proof: Provided in [51].

4.3.2 Summary and Comments on Finite-RMT Spectrum Sensing Algorithms

The random matrix models discussed in section 4.3.1 are summarized in Table 4.3. Unlike the asymptotic models given in sections 4.2.2, 4.2.3 and 4.2.4, the above eigenspectrum and SCN distributions are *exact*.

First, notice that the close-form CDF expressions of Lemma 8, Lemma 8 and Lemma 10, besides being hard to evaluate, if used to design spectrum-sensing algorithms would inevitably lead to techniques that would fail at medium to low SNRs. This is because in that range the eigenvalue associated with an eventual PU signal is no longer the largest and therefore is "trapped" in between noise-related eigenvalues, by force of the Wenyl inequality results [81, 82, Eq. (2.3)] invoked in the proof of Lemma 3.

Finite random matrix theoretical spectrum sensing algorithms could likewise be designed with basis on the extreme eigenvalue models lised in Table 4.3.

Table 4.3: Finite Random Matrix Models for Spectrum Sensing

Variable	**PU Absent:** $\mathcal{H}_0$		**PU Random:** $\mathcal{H}_1^r$		**PU Constant:** $\mathcal{H}_1^c$	
	PDF	CDF	PDF	CDF	PDF	CDF
All Eigenvalues: λ	Lemma 8 [a]		Lemma 8 [a]		Lemma 10 [a]	
Largest Eigenvalue: λ_K	[66, Eq.17] [84, Eq.38]	[72, Eq.6] [66, Eq.9]	[66, Eq.17] [b] [84, Eq.38]	[72, Eq.6] [b] [66, Eq.9]	[66, Eq.12] [84, Eq.43]	[66, Eq.2]
Smallest Eigenvalue: λ_1	[84, Eq.38]	[84, Eq.47]	[84, Eq.38] [b]	[84, Eq.47] [b]	[84, Eq.44]	[84, Eq.97]
SCN: ξ_K	Theorem 2		Theorem 2 [b]		Theorem 3	

[a] CDF obtained by numerical integration from the PDF

[b] Obtained by scaling from the $\mathcal{H}_0$ distribution

Unfortunately, since these expressions are also very hard to evaluate, and by force of the Wenyl inequalities [81,82, Eq. (2.3)], such approaches would be likewise plagued by the same issues of computational complexity and poor performance at medium to low SNRS observed in the asymptotic RMT-based approaches discussed previously.

Furthermore, both eigenspectrum- and extreme eigenvalue-based techniques do not have the blindness advantage of SCN-based alternatives.

Consequently, the most interesting approach is to rely on SCN models. Obvi-

ously one could in principle employ the Curtiss formula [50] in combination with the extreme-eigenvalue models offered in [66, 72, 84] (see Table 4.3) to obtain such SCN models, but such an approach would clearly lead to cumbersome expressions.

Fortunately, Theorems 2 and 3 present exact and relatively simple PDF and CDF expressions for finite random Wishart matrices that can be readily employed in the design of spectrum-sensing algorithms. The required parameters for a Hypothesis Test method equivalent to those discussed in subsection 4.2.5 are summarized in Table 4.4.

For the $\mathcal{H}_0$ case, the finite-RMT spectrum sensing algorithm can be concisely described as follows. Given a prescribed α and $2 \times N$ samples h_{kn}:

1–Construct $\mathbf{H} \triangleq [h_{kn}]_{k=\{1,2\}\times n=\{1,\cdots N\}}$;

2–Compute the eigenvalues (λ_1, λ_2) of $\mathbf{W} \triangleq \mathbf{H} \cdot \mathbf{H}^\dagger$;

3–Evaluate the ratio $\xi_2 \triangleq \lambda_2/\lambda_1$;

4–Accept $\mathcal{H}_0$ if and only if $\xi_2 \leqslant P_{\mathrm{M}}^{(0)^{-1}}(1-\alpha)$.

Likewise, for the $\mathcal{H}_1$ case, given a prescribed δ and $2 \times N$ samples h_{kn} the $\mathcal{H}_1$ test can be summarized as

1–Construct $\mathbf{H} \triangleq [h_{kn}]_{k=\{1,2\}\times n=\{1,\cdots N\}}$;

2–Compute the eigenvalues (λ_1, λ_2) of $\mathbf{W} \triangleq \mathbf{H} \cdot \mathbf{H}^\dagger$;

3–Evaluate the ratio $\xi_2 \triangleq \lambda_2/\lambda_1$;

4–Accept $\mathcal{H}_1$ if and only if $\xi_2 \geqslant P_{\mathrm{M}}^{(x)^{-1}}(\delta)$, where $x = s$ if the PU signal is random, or $x = e$ if the PU signal is constant[7].

The performances of these algorithms are compared against those of the asymptotic-RMT alternatives in Fig. 4.4.

First, in Fig. 4.1, the probability of detection of the RMT-based methods over 20 samples are plotted against the signal-to-noise-ratio. It is found that the proposed scheme based on Matthatiou *et al.*'s SCN CDF for finite random Wishart matrices outperforms all the alternatives, exhibiting a 2 dB advantage over the asymptotic Tracy-Widom-based method proposed in [36] – at the "high"

[7]Notice that in the absence of any knowledge on the PU signal, the assumption of a random signal leads to conservative detection.

SNR region around 0 dB – and several dB over the Marchenko-Pastur method at the low SNR region.

Notice that the detection probability of all these methods improve(degrade) if either the number of samples or the tolerated probability of false alarm increases(decreases). In order to illustrate this effect, the algorithms are compared in terms of their probability of detection as a function of the tolerated (prescribed) probability of false alarm in Fig. 4.1.

The experiments were conducted for an SNR of 2 dB. Notice that results for the Marchenko-Pastur method are not shown since this method does not allow for any *a priori* estimate of the probability of false alarm.

It is found not only that the proposed finite RMT-based technique is consistently superior to the alternatives, but also very consistent on its own, in so far as a gradual degradation(improvement) is observed as the tolerated α or the number of samples available for decision decrease(increase), while techniques relying on asymptotic RMT results suffer from catastrophic degradation.

Results for the $\mathcal{H}_1$ test in terms of the probability of acquisition as a function of the SNR are illustrated in Fig. 4.3. It can be seen, for instance, that with an SNR of 4 dB a probability of acquisition of 96% under the constraint that the probability of miss-detection is $\delta = 0.05$ is achieved with only 20 samples. Only the SNR information of PU signal is needed in the detection, which means the proposed scheme is semi-blind.

The superiority of the finite-RMT methods are a direct consequence of the accuracy of the models described by equations (4.34) and (4.40), as illustrated in Fig. 4.6.

An additional advantage of the finite-RMT framework is that, since both accurate and simple models for the SCN of finite Wishart matrices exist, it is easy to draw a relationship between the probability of false-alarm α and probability of miss-detection δ, namely

$$\delta = P_{\mathrm{M}}^{(x)}(P_{\mathrm{M}}{}^{-1}(1-\alpha)), \tag{4.44}$$

$$\alpha = 1 - P_{\mathrm{M}}(P_{\mathrm{M}}^{(x)}{}^{-1}(\delta)), \tag{4.45}$$

where $x = s$ if the PU signal is random, or $x = e$ if the PU signal is constant.

These relations can be used to design $\mathcal{H}_0$ tests starting from a prescribed probability of miss-detection, as desired in cognitive-radio applications.

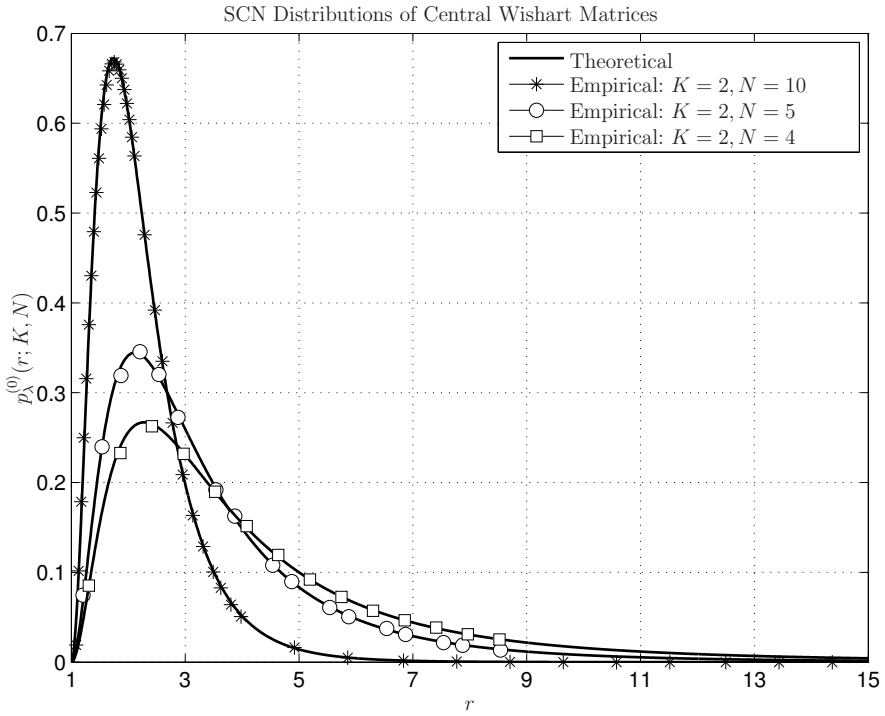

Figure 4.6: PDF under $\mathcal{H}_0$. Probability density function of the SCN of uncorrelated and semi-correlated ($\theta_1 = 1, \theta_2 = 0.6$) central dual Wishart random matrices and corresponding empirical distributions of central and non-central dual Wishart random matrices.

Plots of α as a function of δ are shown in Fig. 4.8. For comparison purposes, the relationship evaluated numerically using the asymptotic model is also shown. It can be seen that great discrepancy is observed between the exact (finite-RMT) and the approximate (asymptotic-RMT) approaches, further strengthening the point made in this chapter.

Given these two alternative designs, a question could be asked as to which approach is most effective. To be specific, staring from a prescribed probability of miss-detection, and under a given SNR, should one employ an $\mathcal{H}_1$ test directly, or convert δ to α and employ an $\mathcal{H}_0$ instead?

In order to answer (partly) this question, we perform the following experiment. Let both α and δ take the same value – say, 3% or 10%.

Then, compare the two approaches in terms of the number of samples required to achieve the complementary probabilities of detection P_{D} and acquisition P_{A} – that is, 97% or 90%, respectively – as a function of the SNR. The detection performances under the $\mathcal{H}_0$ and the $\mathcal{H}_1$ tests under such conditions are compared

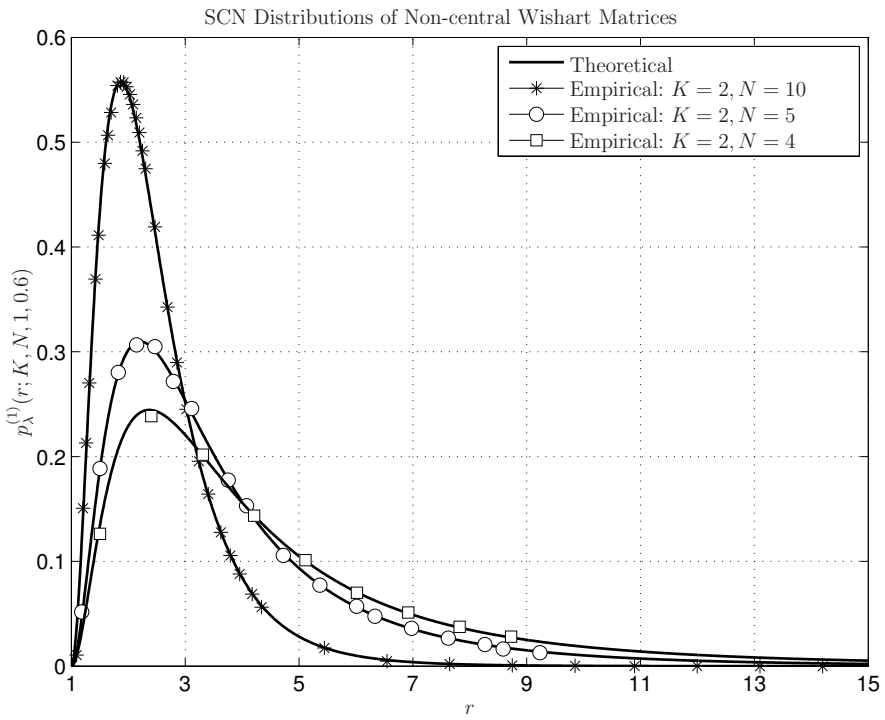

Figure 4.7: PDF under $\mathcal{H}_1$. Probability density function of the SCN of uncorrelated and semi-correlated ($\theta_1 = 1, \theta_2 = 0.6$) central dual Wishart random matrices and corresponding empirical distributions of central and non-central dual Wishart random matrices.

in Fig. 4.9.

It can be seen that, in general, at the low SNR regime the $\mathcal{H}_0$ test far is superior than the $\mathcal{H}_1$ test. On the other hand, at high SNR's, the $\mathcal{H}_0$ test is only marginally inferior to the $\mathcal{H}_1$ test. In other words, this results supports the approach of always (regardless of SNR) converting the tolerated probability of mis-detection δ into an equivalent probability of false alarm α and employing $\mathcal{H}_0$, rather than employ the $\mathcal{H}_1$ test over δ directly. This, in turn, further strengthens the relevance of the blind approach advocated in this chapter.

4.4 CDF and PDF of Extreme Eigenvalues

Throughout the chapter upper and lower case boldface will be used to denote matrices and vectors, respectively. The transpose conjugate and the determinant operators are denoted by $^{\mathrm{H}}$ and $|\cdot|$, respectively, and the (i, j)-th entry of a matrix

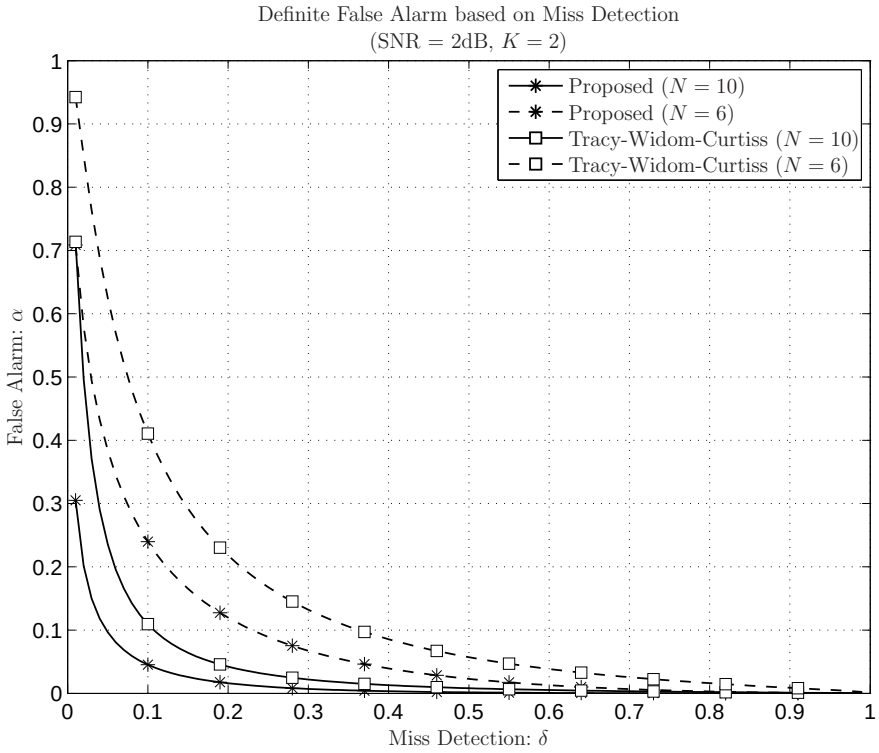

Figure 4.8: Relationship between the probability of false alarm α and the probability of miss-detection δ under hypothesis tests based on the SCN's of a finite (dual) random Wishart matrices evaluated from exact and asymptotic (Tracy-Widom-Curtiss) models.

$\mathbf{Y}$ is denoted by $y_{i,j}$.

Let $\mathbf{Y}$ denote a $K \times N$ random matrix with independent identical distributed (i.i.d.) circularly symmetric complex Gaussian entries of zero mean and unit variance. The corresponding Wishart matrix $\mathbf{W}$ can then be defined as

$$\mathbf{W} \triangleq \begin{cases} \mathbf{Y}\mathbf{Y}^H, & K \leqslant N \\ \mathbf{Y}^H\mathbf{Y}, & K > N. \end{cases} \tag{4.46}$$

Without loss of generality, we shall hereafter consider only the case of $K \leqslant N$, and index the eigenvalues of $\mathbf{W}$ such that $\lambda_1 \geqslant \cdots \geqslant \lambda_K > 0$.

4.4.1 Distributions of Largest Eigenvalues

Here we briefly revise the James-Edelman framework, with the recent improvement offered in [69], as employed to drive the CDF and PDF of λ_1.

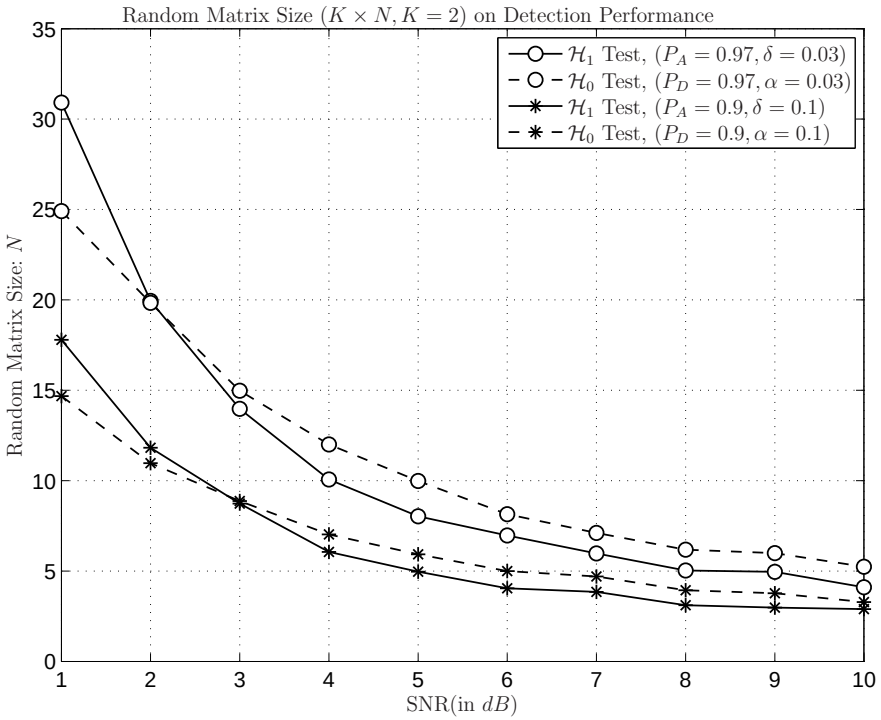

Figure 4.9: Sample size $K \times N$ required by $\mathcal{H}_1$ test and $\mathcal{H}_0$ tests, to achieve the same performances as a function of the SNR.

The joint PDF of the K ordered eigenvalues of $\mathbf{W}$ is given by [69, 77]

$$f_{\mathbf{\Lambda}}(\lambda_1, ..., \lambda_K) = \frac{1}{K!} \prod_{i=1}^{K} \frac{\lambda_i^{N-K} \exp(-\lambda_i)}{(K-i)!(N-i)!} \prod_{1 \leqslant i < j \leqslant K} (\lambda_i - \lambda_j)^2, \tag{4.47}$$

where $\mathbf{\Lambda} \triangleq \{\lambda_1, ..., \lambda_K\}$.

The CDF of the largest eigenvalue λ_1 can be obtained by integration of the joint PDF in (4.47), *i.e.*

$$F_{\lambda_1}(\lambda) = \int_0^{\lambda} \cdots \int_0^{\lambda} \prod_{i=1}^{K} \frac{\lambda_i^{N-K} \exp(-\lambda_i)}{K!(K-i)!(N-i)!} \cdot |\mathbf{\Omega}| \, \mathrm{d}\lambda_1 \cdots \mathrm{d}\lambda_K, \tag{4.48}$$

where $\mathbf{\Omega}$ is the square Vandermonde matrix of

$\{\lambda_1, ..., \lambda_K\}$, such that

$$|\mathbf{\Omega}| \triangleq \left| \begin{bmatrix} 1 & \cdots & 1 \\ \lambda_1 & \cdots & \lambda_K \\ \vdots & \ddots & \vdots \\ \lambda_1^{K-1} & \cdots & \lambda_K^{K-1} \end{bmatrix} \cdot \begin{bmatrix} 1 & \lambda_1 & \cdots & \lambda_1^{K-1} \\ \vdots & \vdots & \ddots & \vdots \\ 1 & \lambda_K & \cdots & \lambda_K^{K-1} \end{bmatrix} \right| = \tag{4.49}$$

$$\begin{vmatrix} K & \cdots & \sum_{i=1}^{K} \lambda_i^{K-1} \\ \sum_{i=1}^{K} \lambda_i & \cdots & \sum_{i=1}^{K} \lambda_i^{K} \\ \vdots & \ddots & \vdots \\ \sum_{i=1}^{K} \lambda_i^{K-1} & \cdots & \sum_{i=1}^{K} \lambda_i^{2(K-1)} \end{vmatrix} = K! \begin{vmatrix} \lambda_1^0 & \lambda_1 & \cdots & \lambda_1^{K-1} \\ \lambda_2 & \lambda_2^2 & \cdots & \lambda_2^{K} \\ \vdots & \vdots & & \vdots \\ \lambda_K^{K-1} & \lambda_K^{K} & \cdots & \lambda_K^{2(K-1)} \end{vmatrix}$$

where the last equality is due to the transformation given in [69, Appendix A].

Thanks to Dighe *et al.*'s result, the i-th row of the determinant depends only on λ_i, such that equation (4.48) can be rewritten as

$$F_{\lambda_1}(\lambda) = \int_0^{\lambda} \cdots \int_0^{\lambda} |\mathbf{\Omega}^*| \, \mathrm{d}\lambda_1 \cdots \mathrm{d}\lambda_K, \tag{4.50}$$

where the (i,j)-th entry of $\mathbf{\Omega}^*$ is

$\omega_{i,j}^* \triangleq \dfrac{\lambda_i^{N+K+i+j-2} \exp(-\lambda_i)}{\sqrt[K]{\Delta}}$

and $\Delta \triangleq \prod_{i=1}^{K} (K-i)!(N-i)!$.

Recognizing the numerator of $\omega_{i,j}^*$ as the integrand of the lower incomplete Gamma function $\gamma(N+K+i+j-1, \lambda)$, where $\gamma(n+1, \lambda) \triangleq \int_0^{\lambda} x^n \exp(-x) \, \mathrm{d}x$, and due to the independence of λ_i's one obtains

$$F_{\lambda_1}(\lambda) = |\mathbf{L}(\lambda)|, \tag{4.51}$$

where $\mathbf{L}(\lambda)$ is a Hankel matrix whose (i,j)-th entry element

is given by $l_{i,j}(\lambda) \triangleq \frac{\gamma(N-K+i+j-1,\lambda)}{\sqrt[K]{\Delta}}$.

For an integer n and $\lambda > 0$, the lower incomplete gamma function can be rewritten as

$$\gamma(n+1, \lambda) = n! \left(1 - \exp(-\lambda) \sum_{k=0}^{n} \frac{\lambda^k}{k!} \right). \tag{4.52}$$

Till now, each entry of $\mathbf{L}$ in (4.51) can be expressed as a finite polynomial of the product of exponent and power series decided by the specific matrix size K

and N. It is not difficult to calculate the determinant of (4.51) and express the result in a closed-form polynomial.

We can consequently rewrite (4.51) in closed-form as

$$F_{\lambda_1}(\lambda) = \sum_{i=0}^{K} \exp(-i\lambda) \sum_{m=1}^{(N+K)i-2i^2+1} [\mathbf{C}(K,N)]_{i+1,m} \lambda^{m-1}, \tag{4.53}$$

where $[\mathbf{C}(K,N)]_{(i+1),m}$ is the $(i+1,m)$-th entry of the coefficient matrix $\mathbf{C}(K,N)$ obtained from equation (4.51).

The interesting thing about the CDF of λ_1 in the form given by equation (4.53) is that the coefficients of the polynomial, generated from the determinant of $\mathbf{L}(\lambda)$ and stored in the coefficient matrix $\mathbf{C}(K,N)$, can all be evaluated *a priori* and *tabulated*.

Furthermore, we remark that equation (4.53) can be put in the following convenient form

$$F_{\lambda_1}(\lambda) = \begin{bmatrix} 1 \, e^{-\lambda} \cdots e^{-K\lambda} \end{bmatrix} \cdot \mathbf{C}(K,N) \cdot \begin{bmatrix} 1 \\ \lambda \\ \vdots \\ \lambda^{\max\limits_{1 \leqslant i \leqslant K} (N+K)i-2i^2} \end{bmatrix}. \tag{4.54}$$

The corresponding PDF is obtained by derivation, yielding

$$f_{\lambda_1}(\lambda) = \frac{F_{\lambda_1}(\lambda)}{\mathrm{d}\lambda} = \sum_{i=1}^{K} \exp(-i\lambda) \sum_{m=N-K}^{(N+K)i-2i^2} [\mathbf{P}(K,N)]_{i,m-(N-K-1)} \lambda^m, \tag{4.55}$$

where $[\mathbf{P}(K,N)]_{i,m-(N-K-1)}$ is the $(i, m-(N-K-1))$-th entry of the coefficient matrix $\mathbf{P}(K,N)$ associated with $\mathbf{C}(K,N)$.

Again, equation (4.55) can be put in the form

$$f_{\lambda_1}(\lambda) = \begin{bmatrix} e^{-\lambda} & \cdots & e^{-K\lambda} \end{bmatrix} \cdot \mathbf{P}(K,N) \cdot \begin{bmatrix} \lambda^{N-K} \\ \lambda^{N-K+1} \\ \vdots \\ \lambda^{\max\limits_{1 \leqslant i \leqslant K} (N+K)i-2i^2} \end{bmatrix}. \tag{4.56}$$

4.4.2 Distributions of Smallest Eigenvalues

In order to obtain as simple expressions for the *smallest* eigenvalues using the James-Edelman framework, start from the equivalent of equations (4.48) and (4.51)

for λ_K, namely

$$F_{\lambda_K}(\lambda) = 1 - \int_{\lambda}^{\infty} \cdots \int_{\lambda}^{\infty} \prod_{i=1}^{K} \frac{\lambda_i^{N-K} \exp(-\lambda_i)}{K!(K-i)!(N-i)!} \times |\mathbf{\Omega}| \mathrm{d}\lambda_1 \cdots \mathrm{d}\lambda_K$$
$$= 1 - |\mathbf{S}(\lambda)|, \tag{4.57}$$

where $\mathbf{S}$ is a $K \times K$ Hankel matrix whose (i,j)-th entry of is given by $s_{i,j} = \frac{\Gamma(N-K+i+j-1,\lambda)}{\sqrt[K]{\Delta}}$ where $\Gamma(n+1,\lambda)$ is the upper incomplete gamma function $\Gamma(n+1,\lambda) \triangleq \int_{\lambda}^{\infty} x^n \exp(-x)\,\mathrm{d}x$.

For an integer n and $\lambda > 0$ we may also write

$$\Gamma(n+1,\lambda) = n! \exp(-\lambda) \sum_{k=1}^{n} \frac{\lambda^k}{k!}, \tag{4.58}$$

From which it follows that the CDF of λ_K finally becomes

$$F_{\lambda_K}(\lambda) = 1 - \exp(-K\lambda) \sum_{m=1}^{NK-K^2+1} [\mathbf{c}(K,N)]_m \lambda^{m-1}, \tag{4.59}$$

where $[\mathbf{c}(K,N)]_m$ is the m-th entry of the coefficient vector obtained from equation (4.57). Different from the coefficient matrix $\mathbf{C}[K,N]$, $\mathbf{c}[K,N]$ is a vector.

As before, the corresponding PDF obtained by derivation is

$$f_{\lambda_K}(\lambda) = \frac{\mathrm{d}F_{\lambda_K}(\lambda)}{\mathrm{d}\lambda} = -\exp(-K\lambda) \sum_{m=N-K}^{NK-K^2} [\mathbf{p}(K,N)]_{m-(N-K-1)} \lambda^m, \tag{4.60}$$

where $[\mathbf{p}(K,N)]_{m-(N-K-1)}$ is the $(m-(N-K-1))$-th entry of the coefficient vector.

Finally, we remark that both equations (4.59) and (4.60) can be written respectively as

$$F_{\lambda_K}(\lambda) = 1 - e^{-K\lambda} \cdot \mathbf{c}(K,N) \cdot \begin{bmatrix} 1 \\ \lambda \\ \vdots \\ \lambda^{NK-K^2} \end{bmatrix}, \tag{4.61}$$

$$f_{\lambda_K}(\lambda) = e^{-K\lambda} \cdot \mathbf{p}(K,N) \cdot \begin{bmatrix} \lambda^{N-K} \\ \lambda^{N-K+1} \\ \vdots \\ \lambda^{NK-K^2} \end{bmatrix}. \tag{4.62}$$

4.4.3 Illustrative Results for Extreme Eigenvalue Distributions

The coefficient matrices and vectors $\mathbf{C}(K,N)$, $\mathbf{P}(K,N)$, $\mathbf{c}(K,N)$ and $\mathbf{p}(K,N)$ required in equations (4.53), (4.55), (4.59) and (4.60) are easy to obtain for any size (K, N) of the matrix $\mathbf{Y}$ composing the Wishart matrices under consideration. Obviously, however, the cases for relatively small K and N are the ones of greater interest, not only because asymptotic results [46] become increasingly satisfactory as $K$and N grow, but also because in the intended application of spectrum sensing, it is desirable to maintain the number of samples required (given by $K \times N$) as small as possible. Some of such coefficient matrices/vectors are given below.

$$\mathbf{C}(2,3) = \begin{bmatrix} 1 & 0 & 0 & 0 \\ -2 & -2 & \frac{1}{2} & -\frac{1}{2} \\ 1 & 2 & \frac{1}{2} & 0 \end{bmatrix}, \tag{4.63a}$$

$$\mathbf{c}\,(2,3) = \begin{bmatrix} -1 & -2 & -\frac{1}{2} \end{bmatrix}, \tag{4.63b}$$

$$\mathbf{P}(2,3) = \begin{bmatrix} 3 & -2 & \frac{1}{2} \\ -3 & -1 & 0 \end{bmatrix}, \tag{4.63c}$$

$$\mathbf{p}(2,3) = \begin{bmatrix} 3 & 1 \end{bmatrix}. \tag{4.63d}$$

$$\mathbf{C}(3,5) = \begin{bmatrix} 1 & 0 & 0 & 0 & 0 & 0 & 0 & 0 & 0 \\ -3 & -3 & -\frac{3}{28} & \frac{7}{6} & -\frac{23}{24} & \frac{5}{24} & -\frac{1}{48} & 0 & 0 \\ 3 & 6 & 6 & \frac{2}{3} & \frac{1}{3} & \frac{1}{3} & \frac{1}{9} & \frac{1}{72} & \frac{1}{288} \\ -1 & -3 & -\frac{9}{2} & -\frac{17}{6} & -\frac{7}{8} & -\frac{1}{8} & -\frac{1}{144} & 0 & 0 \end{bmatrix}, \tag{4.64a}$$

$$\mathbf{c}(3,5) = \begin{bmatrix} -1 & -3 & -\frac{9}{2} & -\frac{17}{6} & -\frac{7}{6} & -\frac{1}{8} & -\frac{1}{144} \end{bmatrix}, \tag{4.64b}$$

$$\mathbf{P}(3,5) = \begin{bmatrix} 5 & -5 & 2 & -\frac{1}{3} & \frac{1}{48} & 0 & 0 \\ -10 & 0 & 1 & 0 & -\frac{1}{8} & 0 & -\frac{1}{144} \\ 5 & 5 & 2 & 1/3 & \frac{1}{48} & 0 & 0 \end{bmatrix}, \tag{4.64c}$$

$$\mathbf{p}(3,5) = \begin{bmatrix} 5 & 5 & 2 & \frac{1}{3} & \frac{1}{48} \end{bmatrix}. \tag{4.64d}$$

$$\mathbf{C}(4,5)=\begin{bmatrix} 1 & 0 & 0 & 0 & 0 & 0 & 0 & 0 & 0 & 0 & 0 \\ -4 & -4 & 3 & -\frac{17}{3} & \frac{71}{24} & -\frac{7}{8} & \frac{17}{144} & -\frac{1}{144} & 0 & 0 & 0 \\ 6 & 12 & -3 & 8 & \frac{17}{8} & -\frac{1}{4} & \frac{2}{9} & -\frac{1}{18} & \frac{1}{32} & -\frac{1}{432} & \frac{1}{1728} \\ -4 & -12 & -3 & -3 & -\frac{33}{8} & -\frac{15}{8} & -\frac{97}{144} & -\frac{7}{48} & -\frac{5}{288} & -\frac{1}{864} & 0 \\ 1 & 4 & 3 & \frac{2}{3} & \frac{1}{24} & 0 & 0 & 0 & 0 & 0 & 0 \end{bmatrix}, \tag{4.65}$$

$$\mathbf{c}\,(4,5)=\begin{bmatrix} -1 & -4 & -3 & -\frac{2}{3} & -\frac{1}{24} \end{bmatrix}, \tag{4.66}$$

$$\mathbf{P}(4,5)=\begin{bmatrix} 10 & -20 & \frac{35}{2} & -\frac{22}{3} & \frac{19}{12} & -\frac{1}{6} & \frac{1}{144} & 0 & 0 & 0 \\ -30 & 30 & -\frac{15}{2} & -\frac{11}{2} & \frac{11}{6} & -\frac{5}{6} & \frac{13}{36} & -\frac{1}{12} & \frac{1}{96} & -\frac{1}{864} \\ 30 & 0 & -\frac{15}{2} & 3 & \frac{19}{12} & 1 & \frac{43}{144} & \frac{1}{24} & \frac{1}{288} & 0 \\ -10 & -10 & -\frac{5}{2} & -\frac{1}{6} & 0 & 0 & 0 & 0 & 0 & 0 \end{bmatrix}, \tag{4.67}$$

$$\mathbf{p}(4,5)=\begin{bmatrix} 10 & 10 & \frac{5}{2} & \frac{1}{6} \end{bmatrix}. \tag{4.68}$$

The CDF's and PDF's obtained through James-Edelman-Dighe framework described in section 4.4.1 are given in Tables 4.5 and 4.6 for $K = \{2,3,4\}$ and $N = \{K, \cdots, 7\}$ (see last page of the chapter). Some of those analytical extreme eigenvalue distributions are compared against corresponding empirical distributions in Fig. 4.10 and Fig. 4.11. The accuracy (exactness) can be appreciated.

Table 4.4: Spectrum Sensing Algorithms from Random Matrix Theory

Method	**Test Statistic** ζ	**Threshold** ζ^*	**CDF** $F(\lambda)$
Tracy-Widom	$\bar{\lambda}_1 = \frac{\lambda_1 - \lambda_U}{\nu}$	$\left(\frac{\sqrt{N}+\sqrt{K}}{\sqrt{N}-\sqrt{K}}\right)^2 \cdot \left(1+\frac{F^{-1}(1-\alpha)}{\sqrt[3]{(\sqrt{N}+\sqrt{K})^2\sqrt{NK}}}\right)$	$F_{\bar{\lambda}_1}(\lambda)$
Tracy-Widom -Curtis	$\bar{\xi}_K = \frac{\bar{\lambda}_1}{\bar{\lambda}_K}$	$F^{-1}(1-\alpha)$	$F_{\bar{\xi}_K}(\xi)$
Proposed	λ_1	$F^{-1}(1-\alpha)$	$F_{\lambda_1}(\lambda)$

[a] Tolerated Probability of False Alarm: α

[b] Aspect Ratio of Random Matrices: $\rho \triangleq N/K$

4.4.4 Application to Spectrum Sensing

In this section the author employs the extreme eigenvalue distributions given above to design Hypothesis-Test-based spectrum sensing algorithms that require a finite number of samples. For comparison purposes, the author shall also consider two asymptotic methods given in [36] and [42], respectively, which are briefly revised

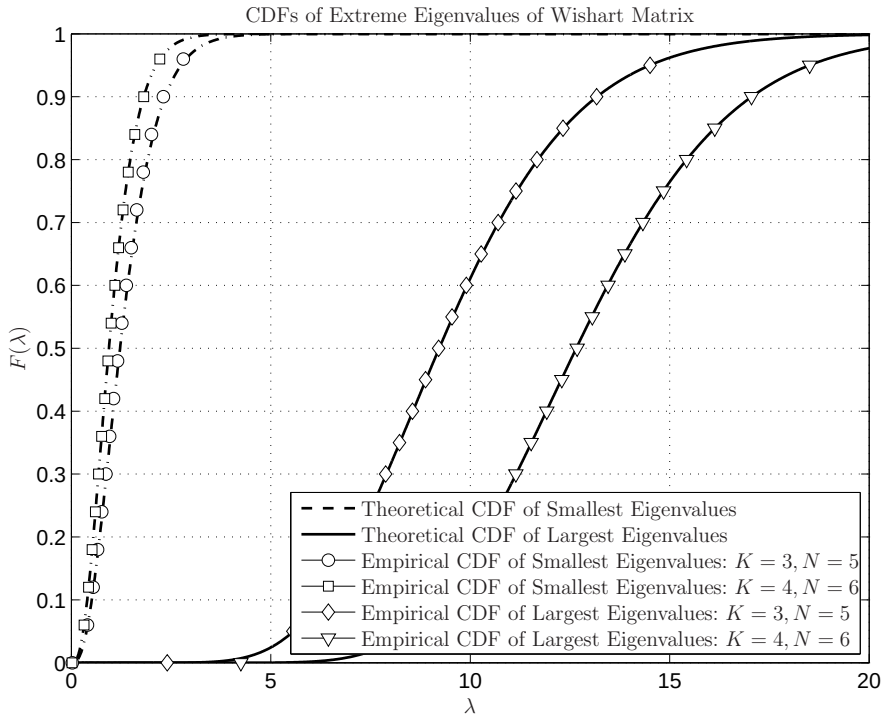

Figure 4.10: CDF. Distributions of extreme eigenvalues of finite Wishart matrices.

hereafter.

For convenience, the three algorithms to be compared are also summarized in Table 4.4.

The methods proposed in [36] is henceforth referred to as the "Tracy-Widom" (TC) method, as it relies on the asymptotic distribution of the normalized extreme eigenvalues

$$\bar{\lambda}_1 \triangleq \frac{\lambda_1 - \lambda_{\mathrm{U}}}{\mu}, \tag{4.69}$$

$$\bar{\lambda}_K \triangleq \frac{\lambda_K - \lambda_{\mathrm{L}}}{\nu}, \tag{4.70}$$

where $\lambda_{\mathrm{L}} \triangleq (1 - \sqrt{N/K})^2$, $\lambda_{\mathrm{U}} \triangleq (1 + \sqrt{N/K})^2$ and

$$\mu \triangleq \frac{(\sqrt{N} + \sqrt{K})^{\frac{4}{3}}}{\sqrt[6]{KN}}, \tag{4.71}$$

$$\nu \triangleq -\frac{(\sqrt{N} - \sqrt{K})^{\frac{4}{3}}}{\sqrt[6]{KN}}. \tag{4.72}$$

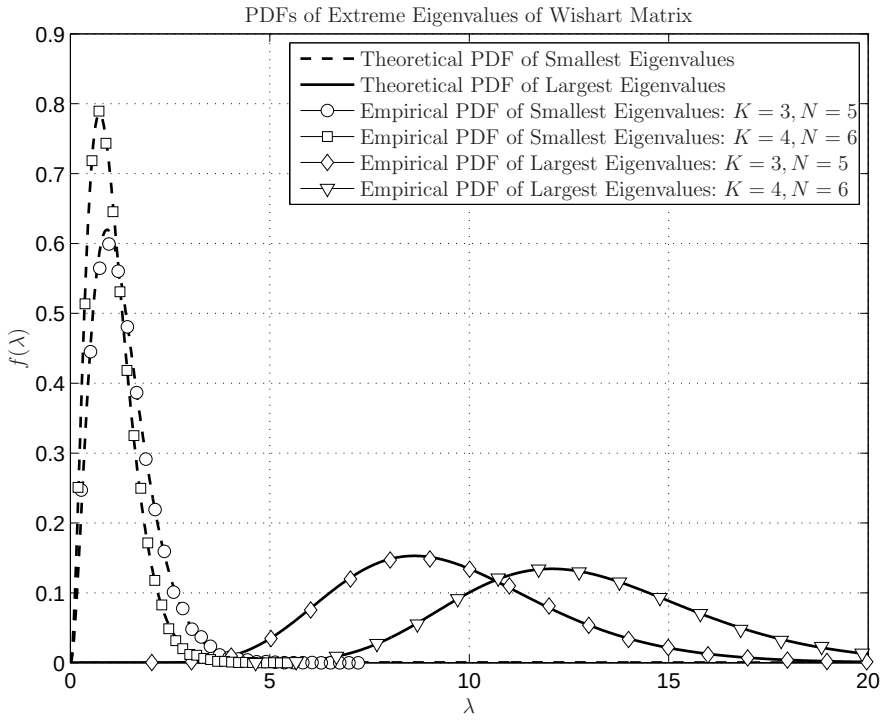

Figure 4.11: PDF. Distributions of extreme eigenvalues of finite Wishart matrices.

Both the quantities $\bar{\lambda}_1$ and $\bar{\lambda}_K$ were shown in [60] and [62], respectively, to follow the Tracy-Widom distribution

$$F_{\bar{\lambda}}(\lambda) \triangleq \exp\left(-\int_{\lambda}^{\infty}(x-r)q^2(x)\mathrm{d}x\right), \tag{4.73}$$

where $q^2(x)$ is the Hastings-McLeod solution of the Painlevé differential equation of type II [48, 49].

The algorithm proposed in [42], on the other hand relies on the normalized standard condition number (SCN) defined as

$$\bar{\xi}_K \triangleq \frac{\bar{\lambda}_1}{\bar{\lambda}_K}. \tag{4.74}$$

The CDF of $\bar{\xi}_1$ can be obtained from the Tracy-Widom distribution by application of the Curtiss formula [50]. Due to this approach, this algorithm is referred here as the "Tracy-Widom-Curtiss" (TWC) method.

In possession of a given distribution, the spectrum sensing algorithms in question can be summarized as follows

1–Collect $K \times N$ base-band (complex) samples of the channel in to the matrix $\mathbf{Y}$;

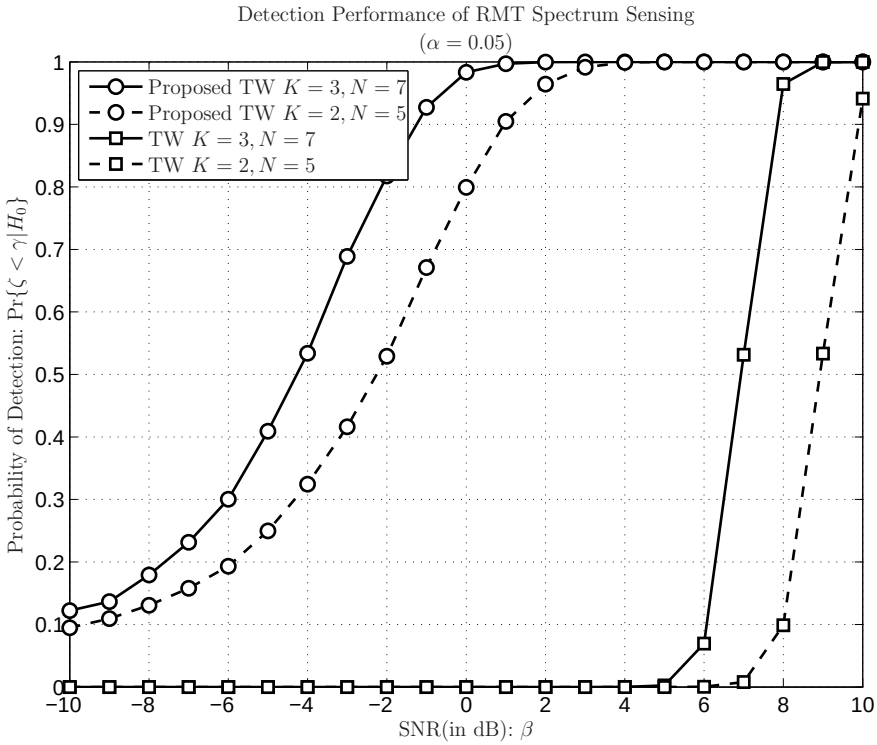

Figure 4.12: PD vs. SNR. Detection performances of spectrum sensing algorithms.

2–Compute the eigenvalues of the corresponding Wishart matrix as in equation (4.46);

3–Obtain the test statistic ζ as follows:

- For TC-method: $\zeta \triangleq \bar{\lambda}_1 = \frac{\lambda_1 - \lambda_{\mathrm{U}}}{\mu}$;
- For TCW-method: $\zeta \triangleq \bar{\xi}_K = \frac{\bar{\lambda}_K}{\lambda_1}$;
- For Proposed method: $\zeta \triangleq \lambda_1$;

4–Compare ζ against the threshold ζ^* (see Table 4.4):

- Hypothesis $\mathcal{H}_0$ is true (channel is free) if $\zeta \leqslant \zeta^*$;
- Hypothesis $\mathcal{H}_0$ is false (channel is busy) otherwise.

The performances of the spectrum sensing algorithms described above are compared against one another in Fig. 4.13. First, in Fig. 4.12, it can be seen that if 21 samples are arranged with $K = 3$ and $N = 7$, the proposed scheme offers a remarkable 6dB over the TWC, which is the best asymptotic method known thus

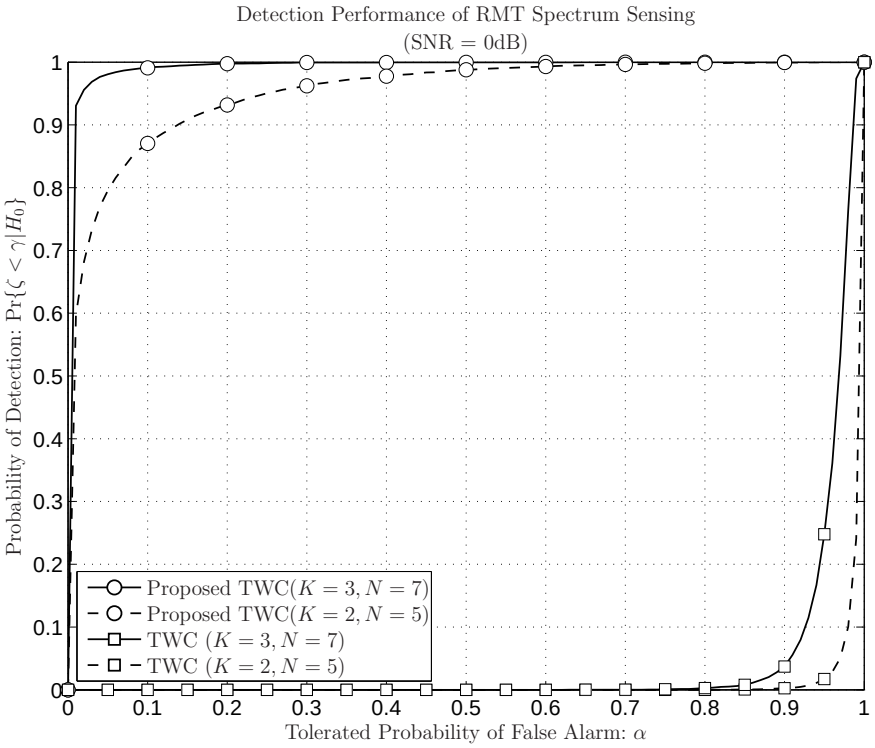

Figure 4.13: PD vs. PF. Detection performances of spectrum sensing algorithms.

far (to the best of our knowledge). An even larger gain of about 7dB is observed if only 10 samples is used, arranged with $K = 2$ and $N = 5$, although obviously the performance of all algorithms degrade as the total number of samples *per* test decreases.

Next, in Fig. 4.15, the algorithms are compared in terms of their Receiver Operating Characteristic curves. Again, the superiority of the proposed method over the asymptotic alternatives is evident. It is found in fact that with the Finite Random Matrix method, as little as 21 samples suffice to obtain a Probability of Detection of over 90%, with a negligible Probability of False-alarm.

To the best of our knowledge, there exists no Finite Random Matrix method we could compare the proposed algorithm to, except for our own earlier contribution [85], presented at Asilomar in 2010, which however has a limitation of admitting only arrangements with $K = 2$. There is, however, an alternative method based on the Anderson-Darling test [86], which however requires the calculation of a threshold through a far more complex process. Interestingly, our method seems to yield very similar results to the latter (compare for instance Fig. 4.15 against [86,

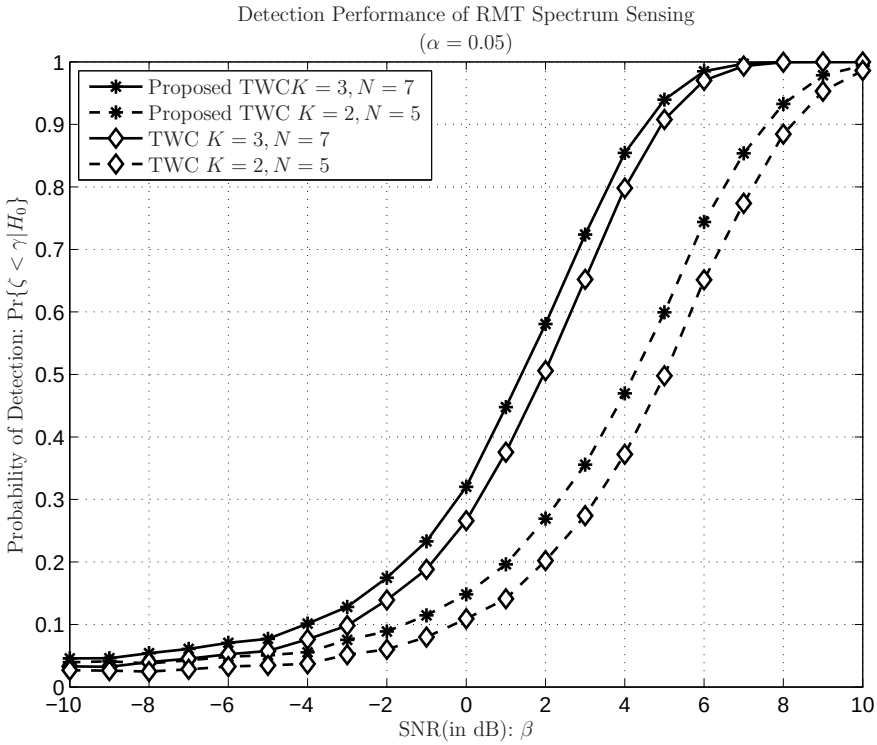

Figure 4.14: TWC PD vs. SNR. Detection performances of spectrum sensing algorithms.

Fig. 1]), which is an indication that the two techniques are equivalent[8]. The lower complexity of the FMT technique offered here, however, is to its advantage.

Furthermore, the FMT method has the potential of allowing the design of spectrum sensing algorithms operating on the distribution of the eigenvalues of Wishart matrices constructed in the *presence* of PU signal – *i.e*, $\mathcal{H}_1$ – as we have illustrated in [70]. A similar approach is rather unlikely under the Anderson-Darling framework [86] due to the prohibitive complexity of deriving corresponding distributions faced in that approach.

[8]A direct comparison will be offered at the Camera Ready version of the chapter.

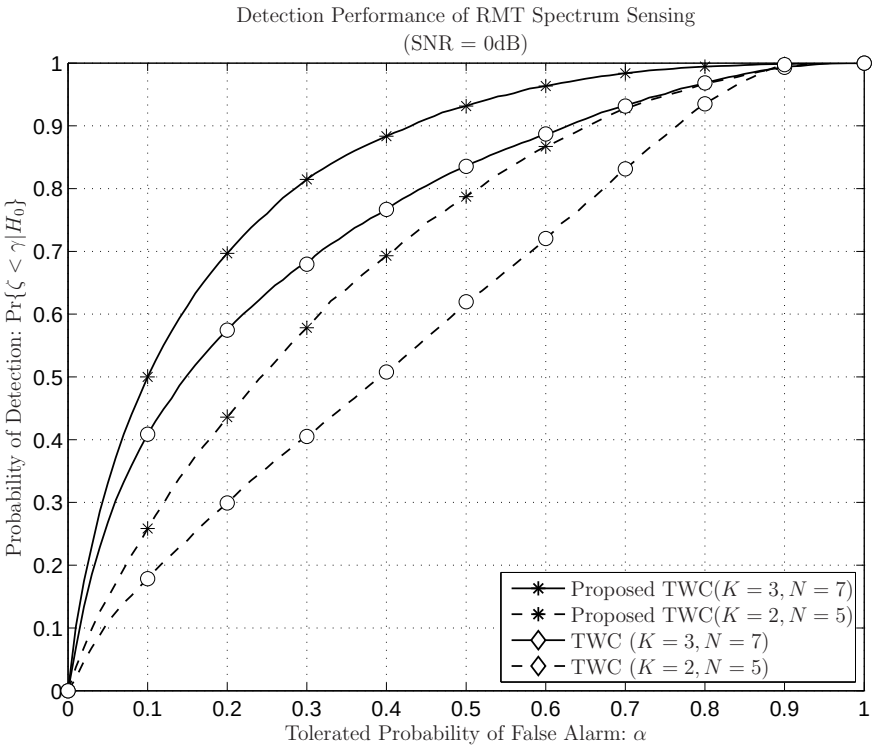

Figure 4.15: TWC PD vs. PF. Detection performances of spectrum sensing algorithms.

Table 4.5: Largest Eigenvalue Distributions

K	N	$F_{\lambda_1}(\lambda)$
2	2	$1+e^{-2\lambda}-2e^{-\lambda}-e^{-\lambda}\lambda^2$
	3	$1+e^{-2\lambda}-2e^{-\lambda}+2e^{-2\lambda}\lambda-2e^{-\lambda}\lambda+\frac{1}{2}e^{-2\lambda}\lambda^2+\frac{1}{2}e^{-\lambda}\lambda^2-\frac{1}{2}e^{-\lambda}\lambda^3$
	4	$1+e^{-2\lambda}-2e^{-\lambda}+2e^{-2\lambda}\lambda-2e^{-\lambda}\lambda+2e^{-2\lambda}\lambda^2-e^{-\lambda}\lambda^2+\frac{2}{3}e^{-2\lambda}\lambda^3+\frac{1}{3}e^{-\lambda}\lambda^3+\frac{1}{12}e^{-2\lambda}\lambda^4-\frac{1}{6}e^{-\lambda}\lambda^4$
	5	$1+e^{-2\lambda}-2e^{-\lambda}+2e^{-2\lambda}\lambda-2e^{-\lambda}\lambda+2e^{-2\lambda}\lambda^2-e^{-\lambda}\lambda^2+\frac{4}{3}e^{-2\lambda}\lambda^3-\frac{1}{3}e^{-\lambda}\lambda^3+\frac{11}{24}e^{-2\lambda}\lambda^4+\frac{1}{8}e^{-\lambda}\lambda^4+\frac{1}{12}e^{-2\lambda}\lambda^5-\frac{1}{24}e^{-\lambda}\lambda^5+\frac{1}{144}e^{-2\lambda}\lambda^6$
	6	$1+e^{-2\lambda}-2e^{-\lambda}+2e^{-2\lambda}\lambda-2e^{-\lambda}\lambda+2e^{-2\lambda}\lambda^2-e^{-\lambda}\lambda^2+\frac{4}{3}e^{-2\lambda}\lambda^3-\frac{1}{3}e^{-\lambda}\lambda^3+\frac{2}{3}e^{-2\lambda}\lambda^4-\frac{1}{12}e^{-\lambda}\lambda^4+\frac{13}{60}e^{-2\lambda}\lambda^5+\frac{1}{30}e^{-\lambda}\lambda^5+\frac{2}{45}e^{-2\lambda}\lambda^6-\frac{1}{120}e^{-\lambda}\lambda^6+\frac{1}{180}e^{-2\lambda}\lambda^7+\frac{e^{-2\lambda}\lambda^8}{2880}$
	7	$1+e^{-2\lambda}-2e^{-\lambda}+2e^{-2\lambda}\lambda-2e^{-\lambda}\lambda+2e^{-2\lambda}\lambda^2-e^{-\lambda}\lambda^2+\frac{4}{3}e^{-2\lambda}\lambda^3!-\frac{1}{3}e^{-\lambda}\lambda^3+\frac{2}{3}e^{-2\lambda}\lambda^4-\frac{1}{12}e^{-\lambda}\lambda^4+\frac{4}{15}e^{-2\lambda}\lambda^5-\frac{1}{60}e^{-\lambda}\lambda^5+\frac{19}{240}e^{-2\lambda}\lambda^6+\frac{1}{144}e^{-\lambda}\lambda^6+\frac{1}{60}e^{-2\lambda}\lambda^7-\frac{1}{720}e^{-\lambda}\lambda^7+\frac{7e^{-2\lambda}\lambda^8}{2880}+\frac{e^{-2\lambda}\lambda^9}{4320}+\frac{e^{-2\lambda}\lambda^{10}}{86400}$
3	3	$1-e^{-3\lambda}+3e^{-2\lambda}-3e^{-\lambda}+3e^{-2\lambda}\lambda^2-3e^{-\lambda}\lambda^2+e^{-2\lambda}\lambda^3+e^{-\lambda}\lambda^3+\frac{1}{4}e^{-2\lambda}\lambda^4-\frac{1}{4}e^{-\lambda}\lambda^4$
	4	$1-e^{-3\lambda}+3e^{-2\lambda}-3e^{-\lambda}-3e^{-3\lambda}\lambda+6e^{-2\lambda}\lambda-3e^{-\lambda}\lambda-\frac{3}{2}e^{-3\lambda}\lambda^2+\frac{3}{2}e^{-\lambda}\lambda^2-\frac{1}{6}e^{-3\lambda}\lambda^3+\frac{4}{3}e^{-2\lambda}\lambda^3-\frac{13}{6}e^{-\lambda}\lambda^3+\frac{11}{12}e^{-2\lambda}\lambda^4+\frac{7}{12}e^{-\lambda}\lambda^4+\frac{1}{6}e^{-2\lambda}\lambda^5-\frac{1}{12}e^{-\lambda}\lambda^5+\frac{1}{24}e^{-2\lambda}\lambda^6$
	5	$1-e^{-3\lambda}+3e^{-2\lambda}-3e^{-\lambda}-3e^{-3\lambda}\lambda+6e^{-2\lambda}\lambda-3e^{-\lambda}\lambda-\frac{9}{2}e^{-3\lambda}\lambda^2+6e^{-2\lambda}\lambda^2-\frac{3}{2}e^{-\lambda}\lambda^2-\frac{17}{6}e^{-3\lambda}\lambda^3+\frac{2}{3}e^{-2\lambda}\lambda^3+\frac{7}{6}e^{-\lambda}\lambda^3-\frac{7}{8}e^{-3\lambda}\lambda^4+\frac{1}{3}e^{-2\lambda}\lambda^4-\frac{23}{24}e^{-\lambda}\lambda^4-\frac{1}{8}e^{-3\lambda}\lambda^5+\frac{1}{3}e^{-2\lambda}\lambda^5+\frac{5}{24}e^{-\lambda}\lambda^5-\frac{1}{144}e^{-3\lambda}\lambda^6+\frac{1}{9}e^{-2\lambda}\lambda^6$ $-\frac{1}{48}e^{-\lambda}\lambda^6+\frac{1}{72}e^{-2\lambda}\lambda^7+\frac{1}{288}e^{-2\lambda}\lambda^8$
	6	$1-e^{-3\lambda}+3e^{-2\lambda}-3e^{-\lambda}-3e^{-3\lambda}\lambda+6e^{-2\lambda}\lambda-3e^{-\lambda}\lambda-\frac{9}{2}e^{-3\lambda}\lambda^2+6e^{-2\lambda}\lambda^2-\frac{3}{2}e^{-\lambda}\lambda^2-\frac{9}{2}e^{-3\lambda}\lambda^3+4e^{-2\lambda}\lambda^3-\frac{1}{2}e^{-\lambda}\lambda^3-\frac{11}{4}e^{-3\lambda}\lambda^4+\frac{3}{4}e^{-2\lambda}\lambda^4+\frac{1}{2}e^{-\lambda}\lambda^4-\frac{21}{20}e^{-3\lambda}\lambda^5+\frac{1}{10}e^{-2\lambda}\lambda^5-\frac{3}{10}e^{-\lambda}\lambda^5-\frac{61}{240}e^{-3\lambda}\lambda^6+\frac{3}{40}e^{-2\lambda}\lambda^6$ $+\frac{13}{240}e^{-\lambda}\lambda^6-\frac{3}{80}e^{-3\lambda}\lambda^7+\frac{1}{30}e^{-2\lambda}\lambda^7-\frac{1}{240}e^{-\lambda}\lambda^7-\frac{1}{320}e^{-3\lambda}\lambda^8+\frac{7}{960}e^{-2\lambda}\lambda^8-\frac{e^{-3\lambda}\lambda^9}{8640}+\frac{e^{-2\lambda}\lambda^9}{1440}+\frac{e^{-2\lambda}\lambda^{10}}{5760}$
	7	$1-e^{-3\lambda}+3e^{-2\lambda}-3e^{-\lambda}-3e^{-3\lambda}\lambda+6e^{-2\lambda}\lambda-3e^{-\lambda}\lambda-\frac{9}{2}e^{-3\lambda}\lambda^2+6e^{-2\lambda}\lambda^2-\frac{3}{2}e^{-\lambda}\lambda^2-\frac{9}{2}e^{-3\lambda}\lambda^3+4e^{-2\lambda}\lambda^3-\frac{1}{2}e^{-\lambda}\lambda^3-\frac{27}{8}e^{-3\lambda}\lambda^4+2e^{-2\lambda}\lambda^4-\frac{1}{8}e^{-\lambda}\lambda^4-\frac{37}{20}e^{-3\lambda}\lambda^5+\frac{9}{20}e^{-2\lambda}\lambda^5+\frac{3}{20}e^{-\lambda}\lambda^5-\frac{263}{360}e^{-3\lambda}\lambda^6+\frac{19}{360}e^{-2\lambda}\lambda^6$ $-\frac{13}{180}e^{-\lambda}\lambda^6-\frac{5}{24}e^{-3\lambda}\lambda^7+\frac{1}{72}e^{-2\lambda}\lambda^7+\frac{1}{90}e^{-\lambda}\lambda^7-\frac{41}{960}e^{-3\lambda}\lambda^8+\frac{19e^{-2\lambda}\lambda^8}{2880}-\frac{e^{-\lambda}\lambda^8}{1440}-\frac{53e^{-3\lambda}\lambda^9}{8640}+\frac{1}{540}e^{-2\lambda}\lambda^9-\frac{17e^{-3\lambda}\lambda^{10}}{28800}+\frac{13e^{-2\lambda}\lambda^{10}}{43200}-\frac{e^{-3\lambda}\lambda^{11}}{28800}+\frac{e^{-2\lambda}\lambda^{11}}{43200}-\frac{e^{-3\lambda}\lambda^{12}}{1036800}+\frac{e^{-2\lambda}\lambda^{12}}{172800}$
4	4	$1+e^{-4\lambda}-4e^{-3\lambda}+6e^{-2\lambda}-4e^{-\lambda}-6e^{-3\lambda}\lambda^2+12e^{-2\lambda}\lambda^2-6e^{-\lambda}\lambda^2-4e^{-3\lambda}\lambda^3+4e^{-\lambda}\lambda^3-\frac{11}{6}e^{-3\lambda}\lambda^4+\frac{2}{3}e^{-2\lambda}\lambda^4-\frac{11}{6}e^{-\lambda}\lambda^4-\frac{1}{3}e^{-3\lambda}\lambda^5+\frac{1}{3}e^{-\lambda}\lambda^5-\frac{1}{36}e^{-3\lambda}\lambda^6+\frac{2}{9}e^{-2\lambda}\lambda^6-\frac{1}{36}e^{-\lambda}\lambda^6+\frac{1}{144}e^{-2\lambda}\lambda^8$
	5	$1+e^{-4\lambda}-4e^{-3\lambda}+6e^{-2\lambda}-4e^{-\lambda}+4e^{-4\lambda}\lambda-12e^{-3\lambda}\lambda+12e^{-2\lambda}\lambda-4e^{-\lambda}\lambda+3e^{-4\lambda}\lambda^2-3e^{-3\lambda}\lambda^2-3e^{-2\lambda}\lambda^2+3e^{-\lambda}\lambda^2+\frac{2}{3}e^{-4\lambda}\lambda^3-3e^{-3\lambda}\lambda^3+8e^{-2\lambda}\lambda^3-\frac{17}{3}e^{-\lambda}\lambda^3+\frac{1}{24}e^{-4\lambda}\lambda^4-\frac{33}{8}e^{-3\lambda}\lambda^4+\frac{17}{8}e^{-2\lambda}\lambda^4+\frac{71}{24}e^{-\lambda}\lambda^4$ $-\frac{15}{8}e^{-3\lambda}\lambda^5-\frac{1}{4}e^{-2\lambda}\lambda^5-\frac{7}{8}e^{-\lambda}\lambda^5-\frac{97}{144}e^{-3\lambda}\lambda^6+\frac{2}{9}e^{-2\lambda}\lambda^6+\frac{17}{144}e^{-\lambda}\lambda^6-\frac{7}{48}e^{-3\lambda}\lambda^7-\frac{1}{18}e^{-2\lambda}\lambda^7-\frac{1}{144}e^{-\lambda}\lambda^7-\frac{5}{288}e^{-3\lambda}\lambda^8+\frac{1}{32}e^{-2\lambda}\lambda^8-\frac{1}{864}e^{-3\lambda}\lambda^9-\frac{1}{432}e^{-2\lambda}\lambda^9+\frac{e^{-2\lambda}\lambda^{10}}{1728}$
	6	$1+e^{-4\lambda}-4e^{-3\lambda}+6e^{-2\lambda}-4e^{-\lambda}+4e^{-4\lambda}\lambda-12e^{-3\lambda}\lambda+12e^{-2\lambda}\lambda-4e^{-\lambda}\lambda+8e^{-4\lambda}\lambda^2-18e^{-3\lambda}\lambda^2+12e^{-2\lambda}\lambda^2-2e^{-\lambda}\lambda^2+\frac{22}{3}e^{-4\lambda}\lambda^3-8e^{-3\lambda}\lambda^3-2e^{-2\lambda}\lambda^3+\frac{8}{3}e^{-\lambda}\lambda^3+\frac{43}{12}e^{-4\lambda}\lambda^4-\frac{9}{4}e^{-3\lambda}\lambda^4+\frac{11}{4}e^{-2\lambda}\lambda^4-\frac{37}{12}e^{-\lambda}\lambda^4$ $+\frac{29}{30}e^{-4\lambda}\lambda^5-\frac{33}{20}e^{-3\lambda}\lambda^5+\frac{7}{5}e^{-2\lambda}\lambda^5+\frac{77}{60}e^{-\lambda}\lambda^5+\frac{13}{90}e^{-4\lambda}\lambda^6-\frac{139}{120}e^{-3\lambda}\lambda^6+\frac{2}{15}e^{-2\lambda}\lambda^6-\frac{103}{360}e^{-\lambda}\lambda^6+\frac{1}{90}e^{-4\lambda}\lambda^7-\frac{17}{40}e^{-3\lambda}\lambda^7-\frac{1}{30}e^{-2\lambda}\lambda^7+\frac{11}{360}e^{-\lambda}\lambda^7+\frac{e^{-4\lambda}\lambda^8}{2880}-\frac{59}{480}e^{-3\lambda}\lambda^8+\frac{9}{320}e^{-2\lambda}\lambda^8$ $-\frac{1}{720}e^{-\lambda}\lambda^8-\frac{23}{864}e^{-3\lambda}\lambda^9-\frac{7}{864}e^{-2\lambda}\lambda^9-\frac{11e^{-3\lambda}\lambda^{10}}{2880}-\frac{e^{-3\lambda}\lambda^{11}}{2880}-\frac{e^{-2\lambda}\lambda^{11}}{4320}-\frac{e^{-3\lambda}\lambda^{12}}{51840}+\frac{e^{-2\lambda}\lambda^{12}}{34560}+\frac{11e^{-2\lambda}\lambda^{10}}{4320}$
	7	$1+e^{-4\lambda}-4e^{-3\lambda}+6e^{-2\lambda}-4e^{-\lambda}+4e^{-4\lambda}\lambda-12e^{-3\lambda}\lambda+12e^{-2\lambda}\lambda-4e^{-\lambda}\lambda+8e^{-4\lambda}\lambda^2-18e^{-3\lambda}\lambda^2+12e^{-2\lambda}\lambda^2-2e^{-\lambda}\lambda^2+\frac{32}{3}e^{-4\lambda}\lambda^3-18e^{-3\lambda}\lambda^3+8e^{-2\lambda}\lambda^3-\frac{2}{3}e^{-\lambda}\lambda^3+\frac{221}{24}e^{-4\lambda}\lambda^4-\frac{73}{8}e^{-3\lambda}\lambda^4-\frac{3}{8}e^{-2\lambda}\lambda^4+\frac{31}{24}e^{-\lambda}\lambda^4$ $+\frac{79}{15}e^{-4\lambda}\lambda^5-\frac{107}{40}e^{-3\lambda}\lambda^5+\frac{11}{20}e^{-2\lambda}\lambda^5-\frac{137}{120}e^{-\lambda}\lambda^5+\frac{739}{360}e^{-4\lambda}\lambda^6-\frac{181}{240}e^{-3\lambda}\lambda^6+\frac{19}{40}e^{-2\lambda}\lambda^6+\frac{283}{720}e^{-\lambda}\lambda^6+\frac{11}{20}e^{-4\lambda}\lambda^7-\frac{89}{240}e^{-3\lambda}\lambda^7+\frac{1}{160}e^{-\lambda}\lambda^8+\frac{1}{80}e^{-4\lambda}\lambda^9-\frac{239e^{-3\lambda}\lambda^9}{4320}-\frac{1}{480}e^{-2\lambda}\lambda^9-\frac{e^{-\lambda}\lambda^9}{4320}+\frac{43e^{-4\lambda}\lambda^{10}}{43200}$ $-\frac{293e^{-3\lambda}\lambda^{10}}{21600}+\frac{83e^{-2\lambda}\lambda^{10}}{43200}+\frac{e^{-4\lambda}\lambda^{11}}{21600}-\frac{59e^{-3\lambda}\lambda^{11}}{21600}-\frac{e^{-2\lambda}\lambda^{11}}{1800}+\frac{e^{-4\lambda}\lambda^{12}}{1036800}-\frac{433e^{-3\lambda}\lambda^{12}}{1036800}+\frac{67e^{-2\lambda}\lambda^{12}}{518400}-\frac{47e^{-3\lambda}\lambda^{13}}{1036800}-\frac{e^{-2\lambda}\lambda^{13}}{86400}-\frac{7e^{-3\lambda}\lambda^{14}}{2073600}+\frac{e^{-2\lambda}\lambda^{14}}{1036800}-\frac{e^{-3\lambda}\lambda^{15}}{6220800}$

Table 4.6: Smallest Eigenvalue Distributions

K	N	$F_{\lambda_K}(\lambda)$
2	2	$1-e^{-2\lambda}$
	3	$1-e^{-2\lambda}-2e^{-2\lambda}\lambda-\frac{1}{2}e^{-2\lambda}\lambda^2$
	4	$1-e^{-2\lambda}-2e^{-2\lambda}\lambda-2e^{-2\lambda}\lambda^2-\frac{2}{3}e^{-2\lambda}\lambda^3-\frac{2}{24}e^{-2\lambda}\lambda^4$
	5	$1-e^{-2\lambda}-2e^{-2\lambda}\lambda-2e^{-2\lambda}\lambda^2-\frac{4}{3}e^{-2\lambda}\lambda^3-\frac{11}{24}e^{-2\lambda}\lambda^4-\frac{5}{60}e^{-2\lambda}\lambda^5-\frac{10}{1440}e^{-2\lambda}\lambda^6$
	6	$1-e^{-2\lambda}-2e^{-2\lambda}\lambda-2e^{-2\lambda}\lambda^2-\frac{4}{3}e^{-2\lambda}\lambda^3-\frac{16}{24}e^{-2\lambda}\lambda^4-\frac{13}{60}e^{-2\lambda}\lambda^5-\frac{64}{1440}e^{-2\lambda}\lambda^6-\frac{1}{180}e^{-2\lambda}\lambda^7-\frac{1}{2880}e^{-2\lambda}\lambda^8$
	7	$1-e^{-2\lambda}-2e^{-2\lambda}\lambda-2e^{-2\lambda}\lambda^2-\frac{4}{3}e^{-2\lambda}\lambda^3-\frac{16}{24}e^{-2\lambda}\lambda^4-\frac{16}{60}e^{-2\lambda}\lambda^5-\frac{114}{1440}e^{-2\lambda}\lambda^6-\frac{3}{180}e^{-2\lambda}\lambda^7-\frac{7}{2880}e^{-2\lambda}\lambda^8-\frac{1}{4320}e^{-2\lambda}\lambda^9-\frac{1}{86400}e^{-2\lambda}\lambda^{10}$
3	3	$1-e^{-3\lambda}$
	4	$1-e^{-3\lambda}-3e^{-3\lambda}\lambda-\frac{3}{2}e^{-3\lambda}\lambda^2-\frac{1}{6}e^{-3\lambda}\lambda^3$
	5	$1-e^{-3\lambda}-3e^{-3\lambda}\lambda-\frac{9}{2}e^{-3\lambda}\lambda^2-\frac{17}{6}e^{-3\lambda}\lambda^3-\frac{7}{8}e^{-3\lambda}\lambda^4-\frac{5}{40}e^{-3\lambda}\lambda^5-\frac{10}{1440}e^{-3\lambda}\lambda^6$
	6	$1-e^{-3\lambda}-3e^{-3\lambda}\lambda-\frac{9}{2}e^{-3\lambda}\lambda^2-\frac{18}{6}e^{-3\lambda}\lambda^3-\frac{22}{8}e^{-3\lambda}\lambda^4-\frac{42}{40}e^{-3\lambda}\lambda^5-\frac{366}{1440}e^{-3\lambda}\lambda^6-\frac{9}{240}e^{-3\lambda}\lambda^7-\frac{3}{960}e^{-3\lambda}\lambda^8-\frac{1}{8640}e^{-3\lambda}\lambda^9$
	7	$1-e^{-3\lambda}-3e^{-3\lambda}\lambda-\frac{9}{2}e^{-3\lambda}\lambda^2-\frac{18}{6}e^{-3\lambda}\lambda^3-\frac{27}{8}e^{-3\lambda}\lambda^4-\frac{74}{40}e^{-3\lambda}\lambda^5-\frac{1052}{1440}e^{-3\lambda}\lambda^6-\frac{50}{240}e^{-3\lambda}\lambda^7-\frac{41}{960}e^{-3\lambda}\lambda^8-\frac{53}{8640}e^{-3\lambda}\lambda^9-\frac{17}{28800}e^{-3\lambda}\lambda^{10}-\frac{1}{28800}e^{-3\lambda}\lambda^{11}-\frac{1}{1036800}e^{-3\lambda}\lambda^{12}$
4	4	$1-e^{-4\lambda}$
	5	$1-e^{-4\lambda}-4e^{-4\lambda}\lambda-3e^{-4\lambda}\lambda^2-\frac{2}{3}e^{-4\lambda}\lambda^3-\frac{1}{24}e^{-4\lambda}\lambda^4$
	6	$1-e^{-4\lambda}-4e^{-4\lambda}\lambda-8e^{-4\lambda}\lambda^2-\frac{22}{3}e^{-4\lambda}\lambda^3-\frac{86}{24}e^{-4\lambda}\lambda^4-\frac{29}{30}e^{-4\lambda}\lambda^5-\frac{52}{360}e^{-4\lambda}\lambda^6-\frac{2}{180}e^{-4\lambda}\lambda^7-\frac{1}{2880}e^{-4\lambda}\lambda^8$
	7	$1-e^{-4\lambda}-4e^{-4\lambda}\lambda-8e^{-4\lambda}\lambda^2-\frac{32}{3}e^{-4\lambda}\lambda^3-\frac{221}{24}e^{-4\lambda}\lambda^4-\frac{158}{30}e^{-4\lambda}\lambda^5-\frac{739}{360}e^{-4\lambda}\lambda^6-\frac{99}{180}e^{-4\lambda}\lambda^7-\frac{291}{2880}e^{-4\lambda}\lambda^8-\frac{1}{80}e^{-4\lambda}\lambda^9-\frac{43}{43200}e^{-4\lambda}\lambda^{10}-\frac{1}{21600}e^{-4\lambda}\lambda^{11}-\frac{1}{1036800}e^{-4\lambda}\lambda^{12}$

4.5 Conclusions of this chapter

The author presented new blind spectrum sensing algorithms based on finite random matrix theory. The algorithm utilizes recently-derived *closed-form* and *exact* expressions for the CDF of the SCN of dual random Wishart matrices of finite size, both uncorrelated central and semi-correlated central (which approximates the non-central case). Based on these new models, hypothesis tests are formulated around both the hypothesis $\mathcal{H}_0$ that no PU signal is present, and the hypothesis $\mathcal{H}_1$ that a PU signal (random or constant) is present .

Similar to previous methods based on asymptotic RMT, the proposed algorithms admits for either a tolerated probability of false alarm α or a probability of miss-detection δ to be accounted for by design. Simple relationships between these two design parameters were also provided. It was shown, however, that the new finite-RMT algorithms not only outperforms known asymptotic-RMT alternatives, but also that the blind approach of employing $\mathcal{H}_0$ tests is the best choice overall (optimum at low SNR's or nearly optimum in the high SNR regime).

In passing, a comprehensive account of all random matrix-theoretical models relevant for the spectrum sensing applications if given, with several additional (albeit it small) offered.

Chapter 5

Overall Conclusions

In this dissertation, the author mainly discussed two kinds of signal detection schemes such as non-cooperative detection and cooperative detection, relevant to cognitive radio. Two non-cooperative detection schemes, low-complexity cyclostationarity feature detection scheme and dual-stage detection scheme, have been proposed to solve the coexistence issues between the UWB system and the IMT-Advanced system. Such coexistence model can be regarded as a practical cognitive radio prototype, in which the UWB system works as the secondary user system operating DAA mechanism to avoid the harmful interference to the INT-Advanced system being considered as the primary user system.

Low-complexity cyclostationarity feature detection scheme, discussing detailedly in Chapter 2, presents a low computational complexity scheme based on the conventional cyclostationarity feature detection scheme in order to reduce its heavy computational complexity under the condition that there is only a slight reduction on the detection performance.

This scheme is suitable for the detection of a localized SC-FDMA signal utilized in the uplink of IMT-Advanced system. The computational complexity of the proposed scheme is low, because that only one window width instead of all occupied spectrum interval will be searched for the possible cyclic-spectrums. On the other hand, the proposed scheme can also avoid the estimation of the cyclic-spectrums when the type of PU signal is unclear or the cyclic-spectrums are hard to estimate.

Simulation results indicate that the proposed scheme can make a tradeoff between detection performance and computational complexity. The low-complexity cyclostationarity feature detection also provides a substitute for the energy de-

tection when the later approach suffers from the noise uncertainty and cannot distinguish the target signal type.

Dual-stage detection scheme composed of coarse detection stage and refined detection stage is given in Chapter 3. This scheme utilizes both advantages of energy detection and cyclostationarity feature detection and tries to avoid their limitations. In this scheme, energy detection works as the coarse detection stage and the low-complexity cyclostationarity feature detection works as the refined detection stage, respectively.

In order to combine such two detection stages, the threshold factor for the probability of indefinite detection was first proposed and defined. The proposed scheme focuses on the integration of two different detection schemes with different complexities in order to reduce total computational complexity. A Single-carrier Frequency Division Multiple Access (SC-FDMA) uplink system operating in a TDD mode is utilized to evaluate the proposed detection scheme. Simulation results indicate that the proposed scheme can make a tradeoff between the detection performance and the computational complexity by setting the probability of indefinite detection.

Simulation results and theoretical analysis indicate that the proposed detection scheme can make a tradeoff between the detection performance and the computational complexity by setting varied the probability of indefinite detection parameter.

The author discussed the cooperative signal detection issues in Chapter 4, using random matrix theory. The author firstly includes the finite random matrix theory to solve the signal detection problem. Comparing with the conventional asymptotic random matrix theory schemes, our schemes can achieve better detection performance with less signal samples of the primary users. We also deduce exact extreme eigenvalue of the Wishart matrix and construct a signal detection scheme using the newly proposed exact extreme eigenvalue of the Wishart Matrix.

In particular, two algorithms are designed, with basis on the standard condition number distribution in the absence of PU signals and in the presence of PU signals, respectively.

Further attractive advantages of the new techniques are: *a*) due to the accuracy of the finite SCN distributions, superior performance is achieved under a finite number of samples, compared to asymptotic RMT-based alternatives; *b*) since ex-

pressions to model the SCN statistics both in the absence and presence of PU signal are used, the statistics of the spectrum sensing problem in question is completely characterized; and c) as a consequence of a) and b), accurate and simple analytical expressions for the receiver operating characteristic (ROC) – both in terms of the probability of detection as a function of the probability of false alarm (P_{D} *versus* P_{F}) and in terms of the probability of acquisition as a function of the probability of miss detection (P_{A} *versus* P_{M}) – are yielded. It is also shown that the proposed finite RMT-based algorithms outperforms all similar alternatives currently known in the literature, at a substantially lower complexity. In the process, several new results on the distributions of eigenvalues and SCNs of random Wishart Matrices are offered.

Bibliography

[1] I. F. Akyildiz, W.-Y. Lee, M. C. Vuran, and S. Mohanty, "Next generation/dynamic spectrum access/cognitive radio wireless networks: A survey," *Computer Networks*, vol. 50, no. 13, pp. 2127 – 2159, 2006.

[2] B. Wang and K. Liu, "Advances in cognitive radio networks: A survey," *Selected Topics in Signal Processing, IEEE Journal of*, vol. 5, no. 1, pp. 5 –23, feb. 2011.

[3] J. Mitola, "Cognitive radio: An integrated agent architecture for software defined radio," Ph.D. dissertation, KTH Royal Inst. of Technol., Stockholm, Sweden, 2000.

[4] S. Haykin, "Cognitive radio: Brain-empowered wireless communications," *IEEE J. Select. Areas Commun.*, vol. 23, no. 2, pp. 201 – 220, Feb. 2005.

[5] *Spectrum Sensing Interfaces and Data Structures for Dynamic Spectrum Access and other Advanced Radio Communication Systems*, IEEE P1900.6 IEEE DYSPAN Standards Committee, 3 2007.

[6] "Ieee 802.22 working group on wireless regional area networks." [Online]. Available: http://www.ieee802.org/22/

[7] "Software defined radio (sdr) forum." [Online]. Available: http://www.wirelessinnovation.org/mc/page.do;jsessionid=EAF4AF0117D46FABAB1BB95385B62B03.mc1?sitePageId=98428

[8] Q. Zhao and B. Sadler, "A survey of dynamic spectrum access," *Signal Processing Magazine, IEEE*, vol. 24, no. 3, pp. 79 –89, may 2007.

[9] *Technical characteristics of Detect-And-Avoid (DAA) mitigation techniques for SRD equipment using Ultra Wideband (UWB) technology*, ETSI TS 102

754 Version 1.2.1 ETSI Technical Specification. Electromagnetic compatibility and Radio spectrum Matters (ERM); Short Range Devices (SRD), 11 2008.

[10] *Technical Requirements for UWB DAA (Detect and Avoid) Devices to Ensure the Protection of Radiolocation Services in the Bands 3.1 - 3.4 GHz AND 8.5 - 9 GHz AND BWA Terminals in the Band 3.4 - 4.2 GHz*, Electronic Communications Committee (ECC) Std., 6 2008.

[11] "Ieee 802.19 wireless coexistence working group (wg)." [Online]. Available: http://www.ieee802.org/19/

[12] "The european computer manufacturers association (ecma)." [Online]. Available: http://www.ecma-international.org/default.htm

[13] S. Shetty and R. Aiello, "Detect and avoid (daa) techniques - enabler for worldwide ultrawideband regulations," in *Proc. Institution of Engineering and Technology Seminar Ultra Wideband Systems, Technologies and Applications*, 2006, pp. 21–29.

[14] A. Hashimoto, H. Yoshino, and H. Atarashi, "Roadmap of imt-advanced development," vol. 9, no. 4, pp. 80–88, 2008.

[15] M. TANNO, Y. KISHIYAMA, H. TAOKA, N. MIKI, K. HIGUCHI, and M. SAWAHASHI, "Layered ofdma and its radio access techniques for lte-advanced," *IEICE Transactions on Communications*, vol. E92.B, no. 5, pp. 1743–1750, 2009.

[16] *Feasibility study for Further Advancements for E-UTRA (LTE-Advanced)*, 3GPP TR 36.912 Version V9.2.0 3GPP. 3rd Generation Partnership Project; Technical Specification Group Radio Access Network, 3 2010.

[17] S. M. Mishra, S. T. Brink, and R. W. B. Fellow, "Detect and avoid: an ultra-wideband/wimax coexistence mechanism," *IEEE Communications Magazine*, vol. 45, pp. 68–75, 2007.

[18] *Base Station (BS) radio transmission and reception (Release 9).*, 3GPP TS 36.104 Version 9.3.0 3GPP. 3rd Generation Partnership Project; Technical Specification Group Radio Access Network; Evolved Universal Terrestrial Radio Access (E-UTRA);, 3 2010.

[19] *User Equipment (UE) radio transmission and reception (Release 9).*, 3GPP TS 36.101 Version 9.3.0 3GPP. 3rd Generation Partnership Project; Technical Specification Group Radio Access Network; Evolved Universal Terrestrial Radio Access (E-UTRA);, 3 2010.

[20] *Physical Channels and Modulation (Release 8)*, 3GPP TS 36.211 Version 8.7.0 3GPP. 3rd Generation Partnership Project; Technical Specification Group Radio Access Network; Evolved Universal Terrestrial Radio Access (E-UTRA), 5 2009.

[21] *Physical layer procedures (Release 8). (2009-09)*, 3GPP TS 36.213 Version 8.8.0 3GPP. 3rd Generation Partnership Project; Technical Specification Group Radio Access Network; Evolved Universal Terrestrial Radio Access (E-UTRA);, 9 2009.

[22] H. G. Myung, J. Lim, and D. J. Goodman, "Single carrier fdma for uplink wireless transmission," *Vehicular Technology Magazine, IEEE*, vol. 1, no. 3, pp. 30 –38, sept. 2006.

[23] "Draft final report of rf channel characterization," Joint Technical Committee of Committee T1 RlP1.4 and TIA TR46.3.3/TR45.4.4 on Wireless Access, Tech. Rep. JTC(AIR) /94.01.17-238R4, 1 1994.

[24] D. Cabric, "Experimental study of spectrum sensing based on energy detection and network cooperation," in *in Proc. of the ACM 1st International Workshop on Technology and Policy for Accessing Spectrum (TAPAS)*, 2006.

[25] Z. Quan, S. Cui, and A. H. Sayed, "Optimal linear cooperation for spectrum sensing in cognitive radio networks," vol. 2, no. 1, pp. 28–40, 2008.

[26] D. Cabric, A. Tkachenko, and R. Brodersen, "Spectrum sensing measurements of pilot, energy, and collaborative detection," in *Military Communications Conference, 2006. MILCOM 2006. IEEE*, oct. 2006, pp. 1 –7.

[27] W. Gardner, "Measurement of spectral correlation," *Acoustics, Speech and Signal Processing, IEEE Transactions on*, vol. 34, no. 5, pp. 1111 – 1123, oct 1986.

[28] ——, "Signal interception: a unifying theoretical framework for feature detection," *Communications, IEEE Transactions on*, vol. 36, no. 8, pp. 897 –906, aug 1988.

[29] A. Dandawate and G. Giannakis, "Statistical tests for presence of cyclostationarity," *Signal Processing, IEEE Transactions on*, vol. 42, no. 9, pp. 2355 –2369, sep 1994.

[30] M. Oner and F. Jondral, "Air interface recognition for a software radio system exploiting cyclostationarity," in *Proc. 15th IEEE Int. Symp. Personal, Indoor and Mobile Radio Communications PIMRC 2004*, vol. 3, 2004, pp. 1947–1951.

[31] A. Punchihewa, O. A. Dobre, Q. Zhang, S. Rajan, and R. Inkol, "The nth-order cyclostationarity of ofdm signals in time dispersive channels," in *Proc. 42nd Asilomar Conf. Signals, Systems and Computers*, 2008, pp. 574–580.

[32] J. Wang, T. Chen, and B. Huang, "Cyclo-period estimation for discrete-time cyclo-stationary signals," vol. 54, no. 1, pp. 83–94, 2006.

[33] D. Cabric, S. M. Mishra, and R. W. Brodersen, "Implementation issues in spectrum sensing for cognitive radios," in *Proc. Conf Signals, Systems and Computers Record of the Thirty-Eighth Asilomar Conf*, vol. 1, 2004, pp. 772–776.

[34] G. Ganesan and Y. Li, "Cooperative spectrum sensing in cognitive radio, part i: Two user networks," vol. 6, no. 6, pp. 2204–2213, 2007.

[35] J. Ma and Y. Li, "Soft combination and detection for cooperative spectrum sensing in cognitive radio networks," in *Proc. IEEE Global Telecommunications Conf. GLOBECOM '07*, 2007, pp. 3139–3143.

[36] Y. Zeng and Y.-C. Liang, "Eigenvalue-based sectrum sensing algorithms for cognitive radio," *IEEE Trans. Commun.*, vol. 57, no. 6, pp. 1784–1793, Jun. 2009.

[37] Y. DEMESSIE and et al., "Sensing techniques for cognitive radio - state of the art and trends," 4 2009. [Online]. Available: http://grouper.ieee.org/groups/scc41/6/documents/white_papers/P1900.6_WhitePaper_Sensing_final.pdf

[38] E. Peh and Y.-C. Liang, "Optimization for cooperative sensing in cognitive radio networks," in *Proc. IEEE Wireless Communications and Networking Conf. WCNC 2007*, 2007, pp. 27–32.

[39] W. Zhang, R. K. Mallik, and K. Ben Letaief, "Cooperative spectrum sensing optimization in cognitive radio networks," in *Proc. IEEE Int. Conf. Communications ICC '08*, pp. 3411–3415.

[40] R. Viswanathan and V. Aalo, "On counting rules in distributed detection," vol. 37, no. 5, pp. 772–775, 1989.

[41] L. S. Cardoso, M. Debbah, P. Bianchi, and J. Najim, "Cooperative spectrum sensing using random matrix theory," in *Proc. IEEE ISWPC*, 2008.

[42] F. Penna, R. Garello, and M. A. Spirito, "Cooperative spectrum sensing based on the limiting eigenvalue ratio distribution in Wishart matrices," *IEEE Commun. Lett.*, vol. 13, no. 7, pp. 507–509, 2009.

[43] F. Penna and R. Garello, "Theoretical performance analysis of eigenvalue-based detection," http://arxiv.org/abs/0907.1523.

[44] W. Zhang and Y. Sanada, "Low-complexity cyclostationarity feature detection scheme of localized sc-fdma uplink system for application to detect and avoid," *Wireless Personal Communications, Springer*, 2011.

[45] ——, "Dual-stage detection scheme for ultra-wideband detect and avoid," *IEICE Transactions*, vol. 94-A, no. 4, pp. 1124–1132, 2011.

[46] A. M. Tulino and S. Verdu, *Random Matrix Theory And Wireless Communications*, ser. Foundations and Trends in Communications and Information Theory. Now Publishers Inc, Jun. 28 2004.

[47] F. Götze and A. Tikhomirov, "Rate of convergence in probability to the marchenko-pastur law," *Bernoulli*, vol. 10, pp. 503–548, 2004.

[48] C. Tracy and H. Widom, "On orthogonal and sympletic matrix ensembles," *Communications of Mathematical Physics*, vol. 177, pp. 727–754, 1996.

[49] M. Dieng, "Distribution functions for edge eigenvalues in orthogonal and symplectic ensembles: Painlevé representations," Ph.D. dissertation, University of California, Davis, 2005.

[50] J. H. Curtiss, "On the distribution of the quotient of two chance variables," *The Annals of Mathematical Statistics*, vol. 12, no. 4, pp. 409–421, 1941.

[51] M. Matthaiou, M. R. Mckay, P. J. Smith, and J. A. Nossek, "On the condition number distribution of complex wishart matrices," vol. 58, no. 6, pp. 1705–1717, 2010.

[52] G. T. F. de Abreu, W. Zhang, , M. Inamori, and Y. Sanada, "Extreme eigenvalue distributions of finite random wishart matrices with application to spectrum sensing," in *Submitted to the IEEE* 45^{th} *Asilomar Conference on Signals, Systems and Computers*, 2011.

[53] R. Giuliano and F. Mazzenga, "On the coexistence of power-controlled ultrawide-band systems with umts, gps, dcs1800, and fixed wireless systems," vol. 54, no. 1, pp. 62–81, 2005.

[54] M. Schnell, I. D. Broeck, and U. Sorger, "A promising new wideband multiple-access scheme for future mobile communications systems," *European Transactions on Telecommunications*, vol. 10, no. 4, pp. 417–427, 1999.

[55] L. Luo and S. Roy, "A two-stage sensing technique for dynamic spectrum access," in *Proc. IEEE Int. Conf. Communications ICC '08*, 2008, pp. 4181–4185.

[56] C.-H. Hwang, G.-L. Lai, and S.-C. Chen, "Spectrum sensing in wideband ofdm cognitive radios," vol. 58, no. 2, pp. 709–719, 2010.

[57] C. Sun, W. Zhang, and K. B. Letaief, "Cooperative spectrum sensing for cognitive radios under bandwidth constraints," in *Proc. IEEE Wireless Communications and Networking Conf. WCNC 2007*, 2007, pp. 1–5.

[58] T. Yucek and H. Arslan, "A survey of spectrum sensing algorithms for cognitive radio applications," *IEEE Commun. Surveys and Tutorials*, vol. 11, no. 1, pp. 116 – 130, 2009.

[59] P. C. Pinto and M. Z. Win, "Communication in a Poisson field of interferers – part i: Interference distribution and error probability," *IEEE Trans. Wireless Commun.*, (to appear).

[60] A. Soshnikov, "A note on universality of the distribution of the largest eigenvalues in certain sample covariance matrices," *Journal of Statistical Physics*, vol. 108, no. 5-6, pp. 1033–1056, 2002.

[61] N. E. Karoui, "A rate of convergence result for the largest eigenvalue of complex white Wishart matrices," *The Annals of Probability*, vol. 34, no. 6, pp. 2077–2117, Nov. 2006.

[62] O. N. Feldheim and S. Sodin, "A universality result for the smallest eigenvalues of certain sample covariance matrices," *Geom. Funct. Anal.*, vol. 20, pp. 88–123, 2010.

[63] J. Baik, G. B. Arous, and S. Péché, "Phase transition of the largest eigenvalue for nonnull complex sample covariance matrices," *Ann. Probab*, vol. 33, no. 5, pp. 1643–1697, 2005.

[64] Z. Bai and J. Yao, "Central limit theorems for eigenvalues in a spiked population model," *Ann. Inst. H. Poincaré Probab. Statist.*, vol. 44, no. 3, pp. 447–474, 2008.

[65] M. Alamgir, M. Faulkner, C. P, and P. Smith, "Modified criterion of hypothesis testing for signal sensing in cognitive radio," in *Proc. IEEE International Conference on Cognitive Radio Oriented Wireless Networks and Communication (CrownCom'09)*, 2009, pp. 1 – 4.

[66] M. Kang and M.-S. Alouini, "Largest eigenvalue of complex wishart matrices and performance analysis of mimo mrc systems," vol. 21, no. 3, pp. 418–426, 2003.

[67] A. Maaref and S. Aissa, "Joint and marginal eigenvalue distributions of (non)central complex wishart matrices and pdf-based approach for characterizing the capacity statistics of mimo ricean and rayleigh fading channels," vol. 6, no. 10, pp. 3607–3619, 2007.

[68] C. S. Park and K. B. Lee, "Statistical multimode transmit antenna selection for limited feedback mimo systems," vol. 7, no. 11, pp. 4432–4438, 2008.

[69] P. A. Dighe, R. K. Mallik, and S. S. Jamuar, "Analysis of transmit-receive diversity in rayleigh fading," vol. 51, no. 4, pp. 694–703, 2003.

[70] W. Zhang, G. T. F. de Abreu, and Y. Sanada, "Spectrum sensing algorithms via finite random matrices," *IEEE Trans. Communications*, (to appear).

[71] D. Féral and S. Péché, "The largest eigenvalues of sample covariance matrices for a spiked population: diagonal case," *http://arxiv.org/abs/0812.2320v1*, 2008.

[72] C. G. Khatri, "Distribution of the largest or the smallest characteristic root under null hyperthesis concerning complex multivariate normal populations," *Ann. Math. Stat.*, vol. 35, pp. 1807–1810, Dec. 1964.

[73] B. V. Bronk, "Exponential ensembles for random matrices," *J. Math and Phys.*, vol. 6, pp. 228–237, 1965.

[74] H. Shin and J. H. Lee, "Capacity of multiple-antenna fading channels: Spatial fading correlation, double scattering, and keyhole," *IEEE Trans. Inform. Theory*, vol. 49, no. 10, pp. 2636–2646, Oct. 2003.

[75] G. Alfano, A. Lozano, A. M. Tulino, and S. Verdu, "Mutual information and eigenvalue distribution of mimo ricean channels," in *Proc. Int. Symp. Inf. Theory Applic. (ISITA)*, Parma. Italy, Oct. 2004.

[76] W. Y. Tan and R. P. Gupta, "On approximating the non-central Wishart distribution with Wishart distribution," *Commun. Stat. Theory Mehod*, vol. 12, pp. 2589–2600, 1983.

[77] A. T. James, "Distributions of matrix variates and latent roots derived from normal samples," *The Annals of Mathematical Statistics*, vol. 35, no. 2, pp. pp. 475–501, 1964.

[78] A. Edelman, "Eigenvalues and condition numbers of random matrices," Ph.D. dissertation, MIT, Cambridge, MA, May 1989.

[79] I. S. Gradshteyn and I. M. Ryzhik, *Table of Integrals, Series, and Products*, 6th ed. Academic Press, Jul. 2000.

[80] A. Papoulis and S. U. Pillai, *Probability, Random Variables and Stochastic Processes*, 4th ed. New York, NY: Mc-Graw-Hill, 2002.

[81] I. C. F. Ipsen and B. Nadler, "Refined perturbation bounds for eigenvalues of Hermitian and non-Hermitian matrices," *SIAM Journal on Matrix Analysis and Applications*, vol. 31, no. 1, pp. 40 – 53, Feb. 2009.

[82] T. Tao and V. Vu, "Random matrices: Universality of local eigenvalue statistics," *Acta Math.*, (to appear). Available at http://arxiv.org/abs/0906.0510.

[83] J. Baik and J. W. Silverstein, "Eigenvalues of large sample covariance matrices of spiked population models," *Journal of Multivariate Analysis*, vol. 97, pp. 1382–1408, 2006.

[84] A. Zanella, M. Chiani, and M. Win, "On the marginal distribution of the eigenvalues of wishart matrices," *IEEE Transactions on Communications*, vol. 57, no. 4, pp. 1050 – 1060, April 2009.

[85] G. Abreu, W. Zhang, and Y. Sanada, "Finite random matrices for blind spectrum sensing," in *Proc. IEEE* 44^{th} *Asilomar Conference on Signals, Systems and Computers*, 2010.

[86] H. Wang, E. hui Yang, Z. Zhao, and W. Zhang, "Spectrum sensing in cognitive radio using goodness of fit testing," *IEEE Trans. Commun.*, vol. 8, no. 11, pp. 5427 – 5430, Nov. 2009.

[87] V. A. Marchenko and L. A. Pastur, "Distributions of eigenvalues for some sets of random matrices." *Math USSR-Sbornik*, vol. 1, pp. 457–483, 1967.

Acknowledgements

I must firstly express my deep and sincere gratitude to my supervisor, Professor Yukitoshi Sanada, for his hard work, support, understanding, attention to details. Without everything he had done for me, I would not have been able to complete the PhD journey, which is really a long marathon match.

I would like to thank Prof. Sasase, Prof. Otsuki and Prof. Ikehara for their very constructive and helpful comments given in the revision of the thesis draft and the defenses.

Furthermore, I would also like to express my gratitude to my collaborator Prof. Abreu, who guided me to the magic world of random matrix theory.

I am very grateful to all colleagues in Sanada Laboratory. They are Ms. Inamori, Mr. Kizilirmak, Mr. Nishimura and so on. Thank you very much.

The financial support fromthe Ministry of Education, Culture, Sports, Science and Technology of Japan (MEXT) and Keio Leading-Edge Laboratory (KLL) are gratefully acknowledged.

Last but not least, I wish to express my loving thanks to my wife Chunhua Lin and my son Jiarun Zhang. They have lost too much during my study abroad. However, it was their love that encourage me to finish this work. My special gratitude is due to my parents, my brother, my sisters and their families for their support.

List of Achievements

Journal Publications

1. W. Zhang and Y. Sanada, "Dual-stage Detection Scheme for Ultra-Wideband Detect and Avoid," IEICE Trans. on Fundamentals, vol.E94-A, no.4, pp.1124-1132, April 2011.

2. W. Zhang and Y. Sanada, "Low-Complexity Cyclostationarity Detection Scheme of Localized SC-FDMA Uplink System for Application to Detect and Avoid," accepted to Wireless Personal Communications.

3. W. Zhang, G. Abreu, M. Inamori and Y. Sanada, "Spectrum Sensing Algorithms via Finite Random Matrices", Conditionally Accept (Major Revision), IEEE Trans. on Communications.

Conference Publications

1. W. Zhang and Y. Sanada, "Cyclostationarity Feature Matched Detection and Application to IFDMA System," in Proc. the Fourth International Conference on Cognitive Radio Oriented Wireless Networks and Communications, Hannover, Germany, June 2009.

2. W. Zhang and Y. Sanada, "Dual-stage Detection Scheme for Detect and Avoid," in Proc. 2010 IEEE International Conference on Ultra-Wideband, Nanjing, Sept. 2010.

3. W. Zhang , and Y. Sanada, "Low-Complexity Cyclostationarity Feature Detection Scheme of Localized SC-FDMA Uplink Signal for Detect and Avoid," in Proc. the 2010 International Symposium on Communications and Information Technologies, pp. 962-967, Tokyo, Oct. 2010.

4. W. Zhang , G. Abreu, M. Inamori and Y. Sanada, "On the Exact Distributions of Extreme Eigenvalues of Finite Random Wishart Matrices," accepted to the Communication Theory Workshop, Sitges, Spain, 2011

5. G. Abreu, W. Zhang , M. Inamori and Y. Sanada, "Finite Random Matrices for Blind Spectrum Sensing," in Proc. the 44th Annual Asilomar Conference on Signals, Systems, and Computers, Pacific Grove, Nov. 2010.

6. G. Abreu, W. Zhang , M. Inamori and Y. Sanada, "Spectrum Sensing Algorithms via Finite Random Matrix Theory," in Proc. IEEE International Conference on Communications, Kyoto, June 2011.

7. G. Abreu, W. Zhang , M. Inamori and Y. Sanada, "Extreme Eigenvalue Distributions of Finite Random Wishart Matrices with Application to Spectrum Sensing," Submitted to the 45th Annual Asilomar Conference on Signals, Systems, and Computers, Pacific Grove, Nov. 2011.

Technical Reports

1. W. Zhang and Y. Sanada, "Cyclostationarity Feature Detection to IFDMA Uplink System in Cognitive Radio Networks, " Technical Reports of IEICE, SR2009-17, May 2009

2. W. Zhang and Y. Sanada, "Low-complexity Cyclostationarity Detection Scheme of Localized SC-FDMA Uplink System and Application to Detection and Avoidance, " Technical Reports of IEICE, SR2009-85, Jan. 2010

3. W. Zhang and Y. Sanada, "Dual-stage Detection Scheme and Application for Ultra-wide Band Detect and Avoid, " Technical Reports of IEICE, SR2010-4, May 2010

4. W. Zhang, M. Inamori,Y. Sanada and G. Abreu, "Blind Spectrum Sensing Based on the Demmel Condition Number of Complex Wishart Matrices, " IEICE Society Conference 2010, BS9-4, Sept. 2010

Appendix
Asymptotic and Exact Random Matrix Theories

In this Appendix, the asymptotic random matrix theories utilized as the conventional cooperative signal detection schemes in [36, 41–43] and as the comparisons to the proposed schemes using exact random matrix theories are presented.

The author also puts the exact and finite random matrix theories utilized in the research.

Asymptotic Random Matrix Theories

Asymptotic Random Matrix Theories - The Marchenko-Pastur Model

The Marchenko-Pastur law [46], which models the asymptotic eigenspectrum of $\mathbf{W}$ under $\mathcal{H}_0$, can be concisely stated as follows.

Theorem 4 (Marchenko-Pastur PDF)**.**

Let $\lambda|_{\mathcal{H}_0}$ *denote any eigenvalue of* $\mathbf{W}$*, with* $\mathbf{H}$ *as in equation* (4.2a)*. Then,*

$$\lim_{\substack{(K,N)\to\infty \\ N/K=\rho>1}} \lambda|_{\mathcal{H}_0} \sim p_{\mathrm{MP}}(r;\rho) \triangleq \frac{\sqrt{-r^2+2(1+\rho)r-(1-\rho)^2}}{2\pi\cdot x}, \tag{A-1}$$

with $0 < (1-\sqrt{\rho})^2 < r < (1+\sqrt{\rho})^2$.

Proof: Due to Marchenko and Pastur, provided in [87].

Implicit in the statement of Theorem 4 is the fact that λ is lower bounded by $\lambda_{\mathrm{L}} \triangleq (1-\sqrt{\rho})^2$ and upper bounded by $\lambda_{\mathrm{U}} \triangleq (1+\sqrt{\rho})^2$. The Marchenko-Pastur law is known to converge at the rate $\mathcal{O}(K^{-1/2})$ [47], which proves sufficiently fast

to enable fairly accurate results to be derived in problems involving finite random matrices of large, but still reasonably-sized, matrices [46].

Hereafter the author will use the term *MP-variate* to refer to a variate following the Marchenko-Pastur Law. Notice also that, to the best of our knowledge, the Marchenko-Pastur CDF is not available with a closed-form in current literature.

Asymptotic Random Matrix Theories - The Tracy-Widom Model

Theorem 5 (Tracy-Widom PDF and CDF)**.**

Consider the centralized and normalized extreme eigenvalues of $\mathbf{W} \triangleq \mathbf{H}\cdot\mathbf{H}^{\dagger}$ *defined below, with* $\mathbf{H}$ *as in equation* (4.2a)*,*

$$\bar{\lambda}_K|_{\mathcal{H}_0} \triangleq \frac{\lambda_K - \lambda_{\mathrm{U}}}{\nu}, \tag{A-2}$$

$$\bar{\lambda}_1|_{\mathcal{H}_0} \triangleq \frac{\lambda_1 - \lambda_{\mathrm{L}}}{\mu}, \tag{A-3}$$

where

$$\nu \triangleq \frac{(\sqrt{N}+\sqrt{K})^{\frac{4}{3}}}{K\cdot\sqrt[6]{KN}}, \tag{A-4}$$

$$\mu \triangleq -\frac{(\sqrt{N}-\sqrt{K})^{\frac{4}{3}}}{K\cdot\sqrt[6]{KN}}. \tag{A-5}$$

For conciseness, let $\bar{\lambda}|_{\mathcal{H}_0}$ *denote either* $\bar{\lambda}_K|_{\mathcal{H}_0}$ *or* $\bar{\lambda}_1|_{\mathcal{H}_0}$*. Then*[1]

$$\lim_{\substack{(K,N)\to\infty \\ N/K=\rho>1}} \bar{\lambda}|_{\mathcal{H}_0} \sim p_{\mathrm{TW}}(r) \triangleq \frac{\mathrm{d}P_{\mathrm{TW}}(r)}{\mathrm{d}r}, \tag{A-6}$$

$$P_{\mathrm{TW}}(r) \triangleq \exp\left(-\int_r^{\infty}(x-r)q^2(x)\mathrm{d}x\right), \tag{A-7}$$

where $q^2(x)$ *is the Hastings-McLeod solution of the Painlevé equation of type II [48, 49].*

Proof: Given in [60] for the largest, and [62] for the smallest eigenvalues, respectively.

[1] For real Wishart matrices, a similar result holds, where $P_{\mathrm{TW}}(r) \triangleq \exp\left(-\frac{1}{2}\int_r^{\infty} q(x)\mathrm{d}x\right)\exp\left(-\int_r^{\infty}(x-r)q^2(x)\mathrm{d}x\right)$.

Asymptotic Random Matrix Theories - The Tracy-Widom-Curtiss Model

Theorem 6 (Tracy-Widom-Curtiss PDF)**.**

Let $\xi_K|_{\mathcal{H}_0}$ *denote the SCN of* $\mathbf{W} \triangleq \mathbf{H} \cdot \mathbf{H}^{\dagger}$*, with* $\mathbf{H}$ *constructed in the absence PU signals as indicated by equation* (4.2a)*. Denote the largest and smallest eigenvalues of* $\mathbf{W}$ *by* $\lambda_K|_{\mathcal{H}_0}$ *and* $\lambda_1|_{\mathcal{H}_0}$ *respectively, and the SCN by* $\xi_K|_{\mathcal{H}_0} \triangleq \frac{\lambda_K|_{\mathcal{H}_0}}{\lambda_1|_{\mathcal{H}_0}}$*. Then*

$$\xi_K|_{\mathcal{H}_0} \sim p_{\text{TWC}}(r;\mu,\nu,\lambda_L,\lambda_U) \triangleq \frac{-1}{\mu\cdot\nu}\int_0^{\infty} x p_{\text{TW}}\left(\frac{r\cdot x-\lambda_U}{\nu}\right)p_{\text{TW}}\left(\frac{x-\lambda_L}{\mu}\right)\,\mathrm{d}x. \quad \text{(A-8)}$$

where $p_{\text{TW}}(r)$ *is as in equation, i.e., obtained by derivation of equation* (A-6)*).*

Proof: The result follows from [50, Eq. (3.2)].

For Hypothesis Testing purposes the CDF is desirable, the following result is thus in order.

Corollary 7 (Tracy-Widom-Curtiss CDF)**.**

$$P_{\text{TWC}}(r;\mu,\nu,\lambda_L,\lambda_U) = \int_{\frac{\lambda_L}{\mu}}^{\infty} p_{\text{TW}}(-x)\cdot P_{\text{TW}}\left(\frac{r\cdot(\lambda_L-\mu\cdot x)-\lambda_U}{\nu}\right)\,\mathrm{d}x. \quad \text{(A-9)}$$

Proof: By definition (integration) of equation (A-8) we obtain, after interchanging the order of integration and rearranging

$$P_{\text{TWC}}(r;\mu,\nu,\lambda_L,\lambda_U) = \frac{-1}{\mu}\int_0^{\infty} p_{\text{TW}}\left(\frac{x-\lambda_L}{\mu}\right)\cdot\left[\int_{-\infty}^{r}\frac{x}{\nu}\cdot p_{\text{TW}}\left(\frac{y\cdot x-\lambda_U}{\nu}\right)\cdot\mathrm{d}y\right]\,\mathrm{d}x. \quad \text{(A-10)}$$

Under the change of variables $y \to \frac{y\cdot x-\lambda_U}{\nu} \triangleq z$, the integral within brackets reduces to $\int_{-\infty}^{\frac{r\cdot x-\lambda_U}{\nu}} p_{\text{TW}}(z)\,\mathrm{d}z = P_{\text{TW}}\left(\frac{r\cdot x-\lambda_U}{\nu}\right)$ Substituting this result into equation (A-10) yields

$$P_{\text{TWC}}(r;\mu,\nu,\lambda_L,\lambda_U) = \frac{-1}{\mu}\int_0^{\infty} p_{\text{TW}}\left(\frac{x-\lambda_L}{\mu}\right)\cdot P_{\text{TW}}\left(\frac{r\cdot x-\lambda_U}{\nu}\right)\,\mathrm{d}x. \quad \text{(A-11)}$$

Through another change of variables $\frac{x-\lambda_L}{-\mu} \to w$ and under the fact that $\mu < 0$, we finally arrive at equation (A-9).

Exact Random Matrix Theories

Exact Finite Random Matrix Theories - The Eigenvalue Distribution Model

The exact distribution of eigenvalues of uncorrelated central Wishart matrix has been presented in [73] and [74].

Lemma 8 (Bronk-Shin-Lee PDF)**.**

Let $\lambda|_{\mathcal{H}_0}$ *denote any eigenvalue of* $\mathbf{W}$*, with* $\mathbf{H}$ *as in equation* (4.2a)*. Then,*

$$\lambda|_{\mathcal{H}_0} \sim p_{\text{BSL}}(r; K, N) \triangleq \frac{1}{K} \sum_{k=0}^{K-1} \frac{k! \cdot r^{N-K} \cdot e^{-r}}{(N-K+k)!} [L_k^{N-K}(r)]^2, \tag{A-12}$$

where $L_a^b(x)$ *is the Laguerre polynomial of order* a*,*

$$L_a^b(x) = \sum_{l=0}^{a} (-1)^l \cdot \binom{a+b}{a-l} \cdot \frac{x^l}{l!}. \tag{A-13}$$

Proof: Found in [73] and [74].

Lemma 9 (Scaled Bronk-Shin-Lee PDF)**.**

Let $\lambda|_{\mathcal{H}_1^r}$ *denote any eigenvalue of* $\mathbf{W}$*, with* $\mathbf{H}$ *as in equation* (4.2b) *and* $\mathbf{H}_s \sim \mathcal{N}_{\mathbb{C}^{K\times N}}(0, \beta)$*. Then,*

$$\lambda|_{\mathcal{H}_1^r} \sim p_{\text{BS}}^{(s)}(r; K, N, \beta) \triangleq \frac{1}{1+\beta} \cdot p_{\text{BSL}}\left(\frac{r}{1+\beta}; K, N\right). \tag{A-14}$$

Proof: Follows immediately under arguments similar to those in the proof.

Lemma 10 (Extended Alfano PDF)**.**

Let $\lambda|_{\mathcal{H}_1^c}$ *denote any eigenvalue of* $\mathbf{W}$*, with* $\mathbf{H}$ *as in equation* (4.2b) *and a* $\mathbf{H}_s = s \cdot \mathbf{1}_{K\times N}$*, where* $\mathbf{1}_{K\times N}$ *is a matrix whose elements are all* 1*'s, while* s *is an*

unknown complex constant with $|s| = 1$. *Then,*

$$\lambda\big|_{\mathcal{H}_1^c} \sim p_{\text{A}}(r; K, N, \beta, \boldsymbol{\phi}) \triangleq \frac{\exp(-\phi_K)}{K\cdot((N-K)!)^K}\cdot\frac{\exp((\beta+1)\cdot r)}{r}\times$$
$$\sum_{k=1}^{K}\frac{((\beta+1)\cdot r)^{N-K+k}}{\phi_K^{k-1}\prod_{l=0}^{K-2} l!}\cdot\left[\frac{{}_0F_1(N-K+1,(\beta+1)\cdot\phi_K\cdot r)}{C_{K,k}^{-1}}+\sum_{i=1}^{K-1}\frac{r^{i-1}}{\langle N-K+1\rangle_{i-1}}\cdot C_{i,k}\right],$$

where $\boldsymbol{\phi} = \{\phi_1, \cdots, \phi_K\}$ *is the vector of squared singular values vector of* $\mathbf{H}_s$ *in ascending order,* ${}_0F_1(\cdot)$ *is the confluent hypergeometric function, the function* $\langle x\rangle_y \triangleq \frac{(x+y-1)!}{(x-1)!}$, *and* $C_{i,j}$ *is the* (i,j)*-th cofactor of* $K\times K$ *matrix* $\mathbf{A}$, *whose* (ℓ,k)*-th elements are defined as*

$$a_{\ell,k} \triangleq \begin{cases} \dfrac{(N-K+k+\ell-2)!}{[N-K+1]_{\ell-1}} & \text{if } 1\leqslant\ell\leqslant K-1, \quad \text{(A-15a)} \\ \dfrac{{}_0F_1(N-K+k,N-K+1,\phi_\ell)}{((N-K+k-1)!)^{-1}} & \text{if } \ell = K. \quad \text{(A-15b)} \end{cases}$$

Proof: Given in [75].